**Synthesis and Characterization of Nanostructured Conducting Polymers and Their Composites with Noble Metal Nanoparticles**

by

Selcuk Poyraz

A thesis submitted to the Graduate Faculty of
Auburn University
in partial fulfillment of the
requirements for the Degree of
Master of Science

Auburn, Alabama
December 13, 2010

Keywords: conducting polymers, noble metal nanoparticles, composite nanostructures

Copyright 2010 by Selcuk Poyraz

Approved by

Xinyu Zhang, Chair, Assistant Professor of Polymer and Fiber Engineering
Peter Schwartz, Professor of Polymer and Fiber Engineering
Sabit Adanur, Professor of Polymer and Fiber Engineering
Maria Lujan Auad, Assistant Professor of Polymer and Fiber Engineering

## Abstract

Conducting polymers and noble metals were combined in one nanostructure to produce materials with academic and industrial interest gathering properties. Novel, facile, one-step and seeding-template-assisted oxidative polymerization reactions of pyrrole were conducted to synthesize such nanocomposites made up of Polypyrrole (PPy) nanofibers decorated by the noble metal (Au, Pt) nanoparticles. Enhanced sensing properties and catalytic capability were meant to be provided in a 2-D nanocomposite matrix. As the reaction media, four different noble metal salts' aqueous electrolyte solutions were used. AuCl, $PtCl_2$, $PtCl_4$ and $HAuCl_4$ salts were, individually, dissolved in water to prepare these solutions. They eliminated the use of oxidative agents like ammonium peroxydisulfate and also large amounts of in/soluble templates like zeolites, opals and surfactants by both acting as the dopant and the oxidant for pyrrole. Vanadium pentoxide ($V_2O_5$) sol-gel nanofibers were assisting, as the seeding-template, to ensure fibrillar morphology during the reactions.

The goal of this study was to build a substantial background for the futuristic industrial applications, i.e., fuel-cell membranes of such nanocomposites by utilizing the knowledge obtained from the chemical analysis and the instrumental characterizations.

To control, investigate, improve and characterize several properties of conducting polymer based nanocomposites and to determine the effects of the electrolyte concentration besides the other reaction parameters on the final product morphology and properties, the above mentioned project was undertaken in details throughout the Master's degree.

Acknowledgments

The author would like to express his thanks to his advisor and mentor, Dr. Xinyu Zhang, for his time, guidance, and judicious advice. The author also expresses his gratitude to all his committee members for their suggestions.

The author is owed special thanks to his research group partner, Zhen Liu, for his collaboration, guidance, and precious advice. Appreciation is also owed to another previous research group partner, Johannes Bär, for his valuable contributions during his summer internship. Thanks to the Department of Polymer and Fiber Engineering for welcoming environment. The author would like to thank the Turkish Ministry of Education for the aid in sponsoring him during his studies.

The author finally would like to express his most sincere thanks to his parents, Kemalettin and Alime, and his big sister, Seval, for their sincere love. The author's appreciation from the bottom of his heart also goes to his fiancée, Tuba, for her ongoing encouragement and love. The author also expresses his gratitude to all his friends in Polymer and Fiber Engineering Department and in Auburn, for providing him ongoing support throughout these two years. He also would like to express his infinite appreciation to God for bestowing him skills and ability to think.

Table of Contents

List of Tables

List of Figures

# CHAPTER 1

# LITERATURE REVIEW

## 1.1 Introduction

No more than 40 years ago all carbon based polymers[1], polyethylene, polypropylene, e.g., which are essentially made up of σ-bonds[2], have traditionally been considered as insulators[2] (due to the lack of mobility of created charge through given polymer backbone chains). According to this manner, most of the polymer applications have focused on this insulating property[2]. Because of their light weight[2], greater ease of processability[2] and shaping, polymers (plastics) started to shape humans' lives[3] in a very short time by a continuous and rapid replacement over metals in various areas of applications, which eventually and often remarked in those days as "from buckets to rockets"[2].

By virtue of the common respect for the insulating property and wide utilization of polymers (plastics) by electric industry as inactive packaging and insulating material[1] especially for electricity and telephone wires' coating, at that time, the idea of making polymers to conduct electricity was generally considered to be absurd[1]. However, this minute inspiration has been the major driving force behind most of the research trials to design polymers that could fit the electronic applications with their conducting property[3].

Throughout the time, starting from this very narrow perspective[1], in 1958 Natta et al. was succeeded to synthesize polyacetylene in a black powder form, much like charcoal[2], as the first

conducting polymer prototype exhibiting conductivity (due to the presence of extended π-bond conjugation that confers charge carrying property along the polymer backbone chain[2]) values between $7x10^{-11}$ to $7x10^{-3}$ S/cm (semi-conductor level)[1]. The conductivity range of the resulting polymer was mainly depending upon how it was processed and/or manipulated[1].

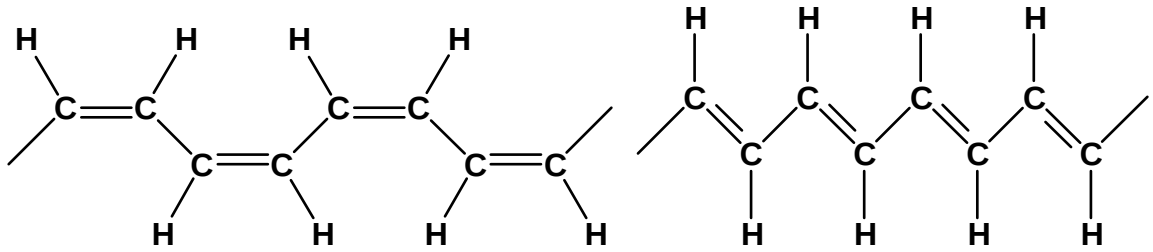

Figure 1 Cis- and trans- polyacetylene

This discovery was remained as a laboratory curiosity[2] for the following nine years until one postgraduate student of Hideki Shirakawa at the Tokyo Institute of Technology[1] serendipitously[2], obtained, a lustrous metallic thin film that exactly looks like aluminum foil[2], while trying to synthesize polyacetylene in 1967[1]. Because of misusing 1000 times more of Ziegler-Natta ($AlEt_3$ – $Ti(OBu^n)_4$) catalyst[3], this attempt was ended up with a shiny film like this. The film's conductivity range was in semi-conductor level exhibiting similar values of conductivity to the best of the former black powders[1]. During the couple of years after this attempt, a tidal wave of renewed and amplified interest[3] in conducting polymers had enticed many scientists and industrialists[3] for new developments.

Figure 2 Free-standing polyacetylene film

Conducting polymer research made its major resurgence[2] in the late 70's after a trans-pacific collaboration[2] of scientists Hideki Shirakawa, Alan G. MacDiarmid and Alan J. Heeger. At that time, chemist scientists Shirakawa and MacDiarmid were focused on an ongoing research about the conductivity improvement of polyacetylene through a process named "doping" which was also parallel to the terminology used by semi-conductor physicist Alan J. Heeger[2].

Eventually, they were able to increase the conductivity of polyacetylene by almost ten orders of magnitude[2] between $10^{-7}$ to $10^{3}$ S/cm. In further steps, they doped (either oxidizing or reducing the polymer to create charge carriers) polyacetylene films by halogens[3], iodine ($I_2$)[1] or arsenic pentafluoride ($AsF_5$)[1] which cause a dramatic increase in conductivity of polyacetylene ranging between $10^{4}$ to $10^{5}$ S/cm (compared to copper = $10^{6}$ S/cm)[2].

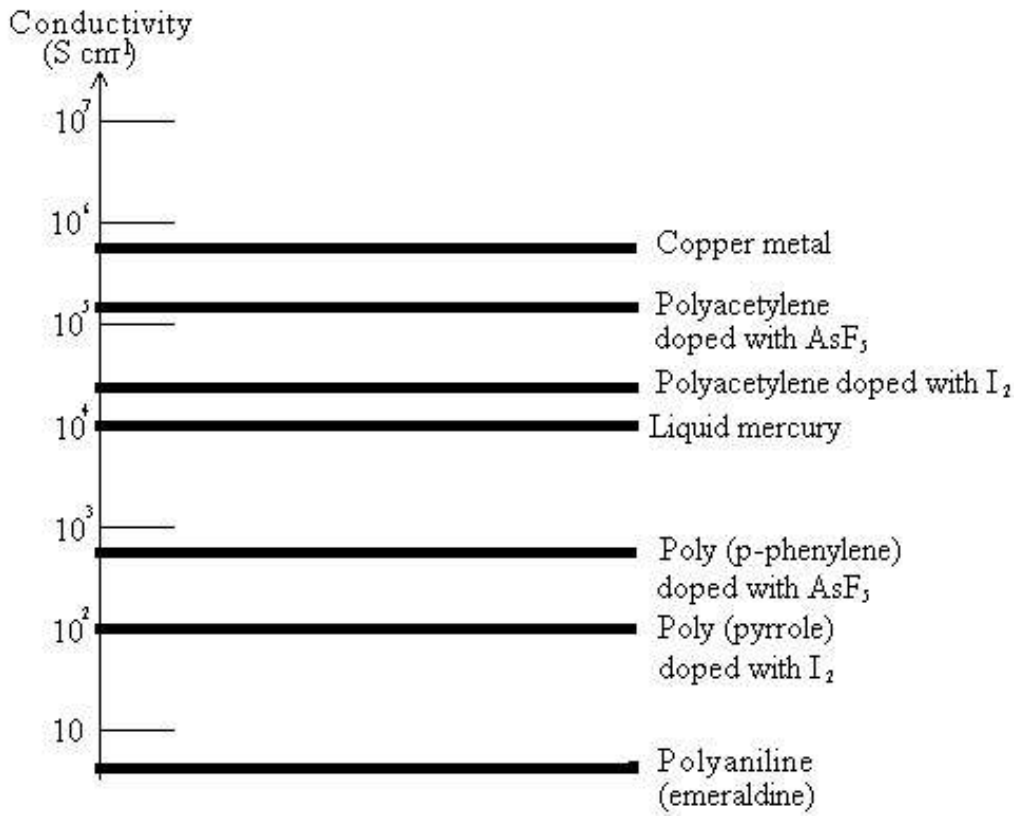


Figure 3 Logarithmic conductivity levels of some metals and conducting polymers[1]

Pioneered by the discovery of doped polyacetylene in the late 70's a new branch of polymer family known as intrinsically conducting polymers[1], electro active polymers[1] or plastronics[3] were invented like this and became a very popular field for both academic and the industrial sides[3] to catalyze many new and interesting applications[3]. The intrinsic conducting property and the traditional ease of processing and/or fitting into complex multi-polymer designs[3] are the main reasons that make this newly popularizing polymer family very promising for future applications.

Table 1 Number of journal articles published annually related to conducting polymers[8]

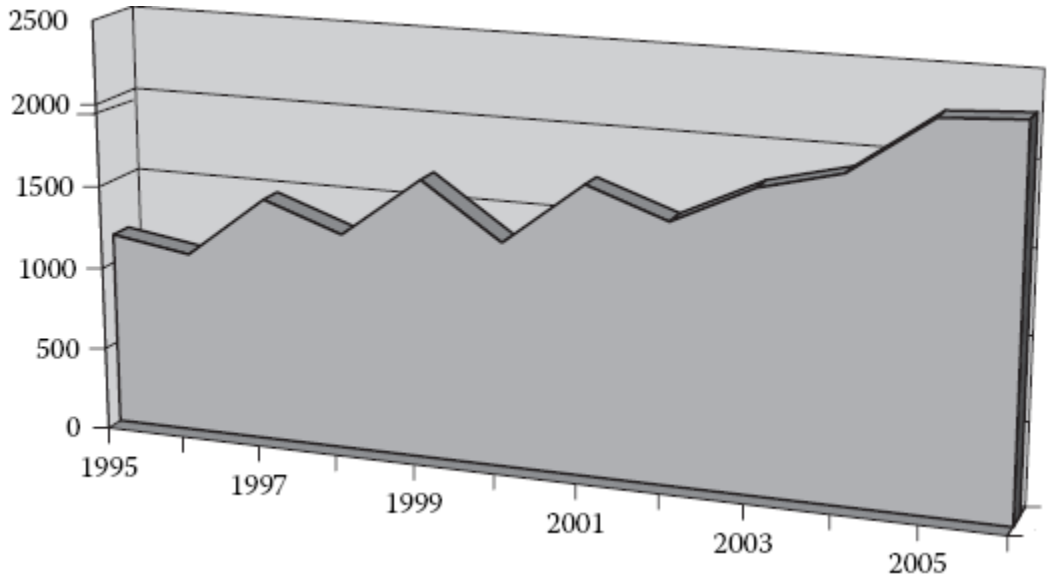


Table 2 Scientific papers published on conducting polymers categorized into main topics[8]

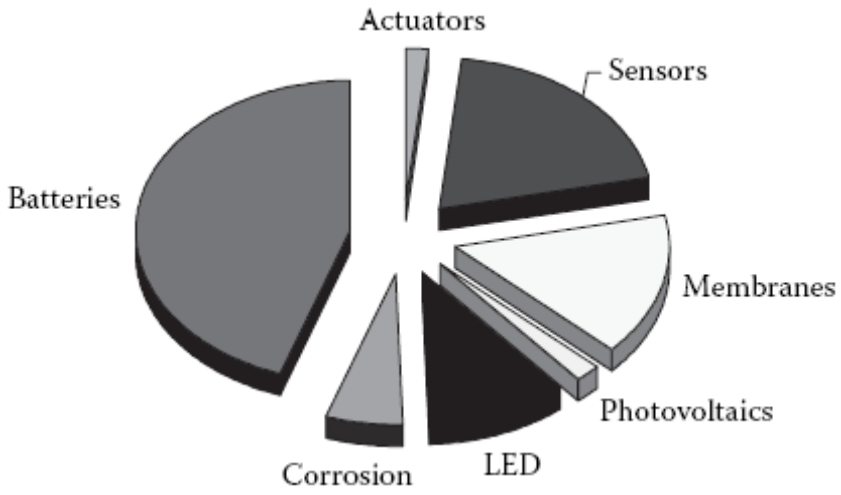

Figure 4 Y2K Nobel laureates: Alan J. Heeger, Alan G. MacDiarmid and Hideki Shirakawa

Having an extended π-bond conjugation along their backbone chain[2] can be considered both advantageous in terms of providing intrinsic electron conducting characteristic and disadvantageous due to having strong inter-chain interactions and finally ending up with insoluble and infusible characteristics[2], for these polymers. Throughout the time, the early and common problems related with exhibiting unstable characteristics in doped form and the poor solubility of intrinsically conducting polymers were almost surmounted by different chemical intuitions (by lateral substituent attachment)[1] and/or experimentation[2]. After those so-called modifications were made in conducting polymer structures, their properties (especially conductivity) did not change negatively at all[2].

Although this polymer family branch is in its infancy[1], like the plastics industry in the 30's or 50's, they have myriad and very significant potential areas of use[1] such as solar cells, fuel cell membranes[4], organic vapor sensors[4], organic light emitting diodes (OLEDs), capacitors[4] and building blocks for nanoelectronic devices[4].

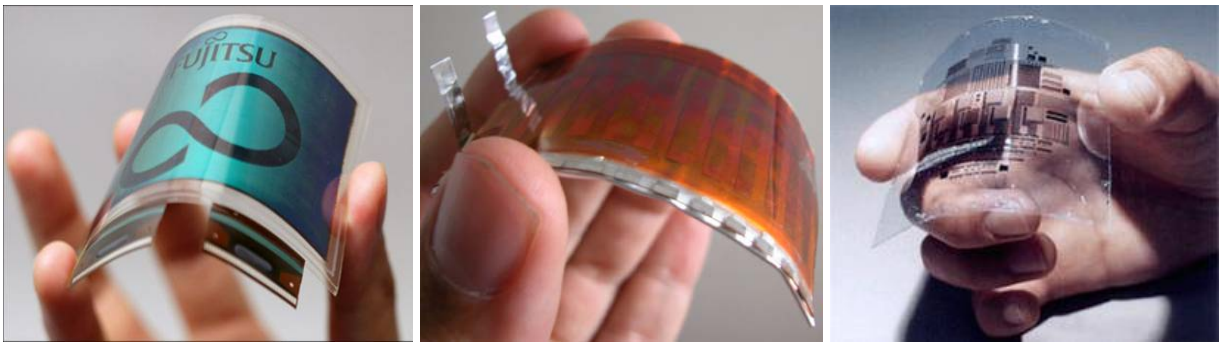


Figure 5 Different applications of conducting polymers as flexible OLED display, solar cell and organic thin-film transistor

That is to say, one should not be considered as a daydreamer due to imagining that one day in close future we will all go to the beach, carrying our table sized, solar-powered, foldable OLED display with us to read on-line newspaper, surf the net or watch TV while we are simply sitting down on it[3].

Table 3 Comparison of metals, plastics and conducting polymers in different ways[5]

| | **Metals** | **Plastics** | **Conducting Polymers** |
|---|---|---|---|
| **Electrical property** | Conductors | Insulators | Conductors |
| **Processability** | Difficult | Easy | Easy |
| **Optical property** | Colorful/shining | Colorless | Colorful/shining |
| **Others** | Hard/tough | Soft/flexible | Soft/flexible |

## 1.2 Types of Electronic Conducting Polymers (ECPs)

The following paragraphs of this section of thesis are mainly focused on giving information about different types of conducting polymers. Therefore, the major well-known members of electronic conducting polymer family such as polyacetylene, polypyrrole (PPy), polyaniline (PANI), polythiophene (PTh) with its soluble derivative poly (3-hexylthiophene) (P3HTh) and poly (3, 4-ethylenedioxythiophene) (PEDOT), are explained from different points of view; including their history of invention and methods of synthesis, their structural and molecular properties and the intrinsic conduction mechanism that they exhibit during their applications in a simple and straightforward way.

### 1.2.1 Polyacetylene

Polyacetylene has been the main subject of innumerable conducting polymer studies so far[3], due to having a longer history of invention (the first reports about this polymer dates back to the late middle of last century[3]). This polymer possesses the simplest conjugated molecular framework[2]. That is why polyacetylene has been regarded as the starting point for a variety of research studies, especially by physics and chemistry[2], with an emphasis on understanding the conducting polymers and their conduction mechanisms[2].

Polyacetylene yields precipitates in a form of black, air sensitive (poor environmental stability[2]), infusible and insoluble powders[3], which can not be further processed out of its reaction media after its polymerization reaction conducted by using Ziegler-Natta catalyst [$AlEt_3$ – $Ti(OPr)_4$][3].

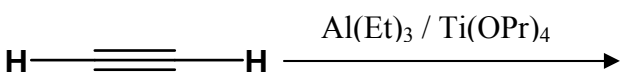


Black colored, infusible, insoluble, environmentally unstable polyacetylene powders

Figure 6 Polyacetylene synthesis by using Ziegler-Natta catalyst[3]

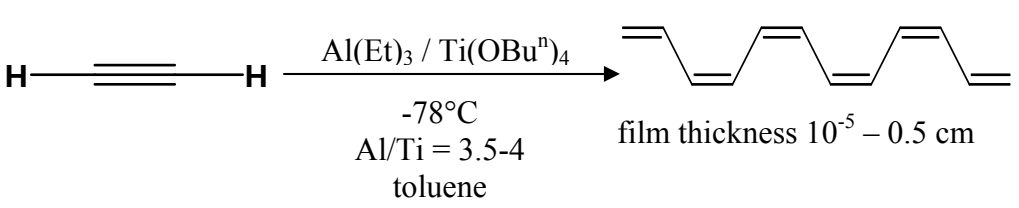


Free-standing, conducting polyacetylene film (with cis-characteristics)

Figure 7 Free-standing polyacetylene film syntheses with cis- characteristics by using Ziegler-Natta catalyst and $AsF_5$ as dopant[3]

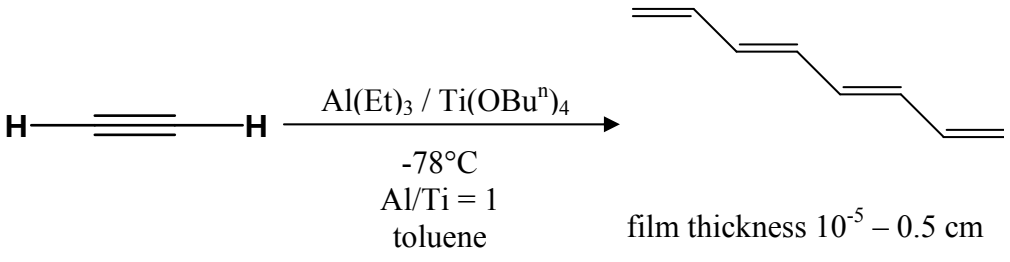


Free-standing, conducting polyacetylene film (with trans-characteristics)

Figure 8 Free-standing, conducting polyacetylene film syntheses with trans- characteristics by using Ziegler-Natta catalyst and $AsF_5$ as dopant[3]

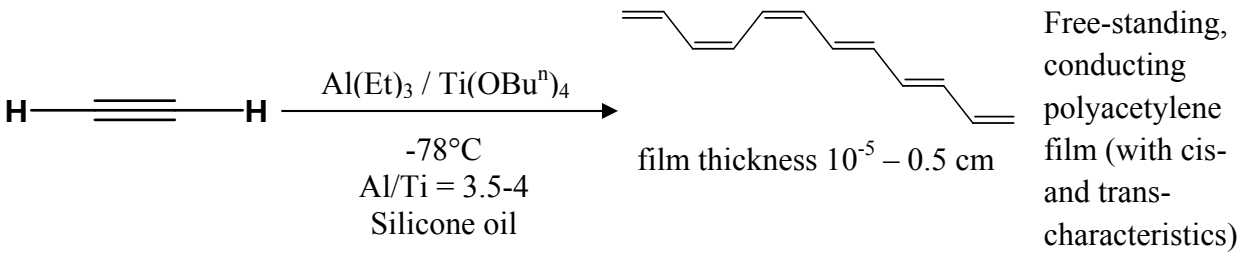


Figure 9 Free-standing polyacetylene film syntheses with cis-/trans- characteristics by using Ziegler-Natta catalyst and $AsF_5$ as dopant[3]

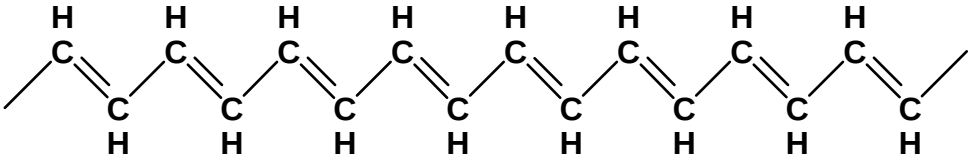

Figure 10 Chemical structure of as-produced trans-polyacetylene[5]

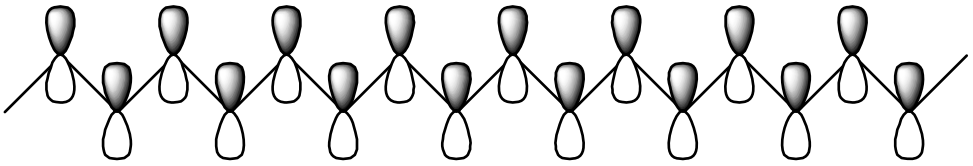

Figure 11 A different illustration of the chemical structure of trans-polyacetylene[5]

Further polymerization attempts for polyacetylene synthesis were mainly focused on "doping process" which were conducted by utilizing halogens[3], iodine ($I_2$)[1] or arsenic pentafluoride ($AsF_5$)[1] as the dopant for classical Ziegler-Natta [$AlEt_3 – Ti(OBu^n)_4$][3] catalyst reaction. As a result of doping process it became possible to produce free-standing, conducting polyacetylene films of up to 0.5 cm thickness[3].

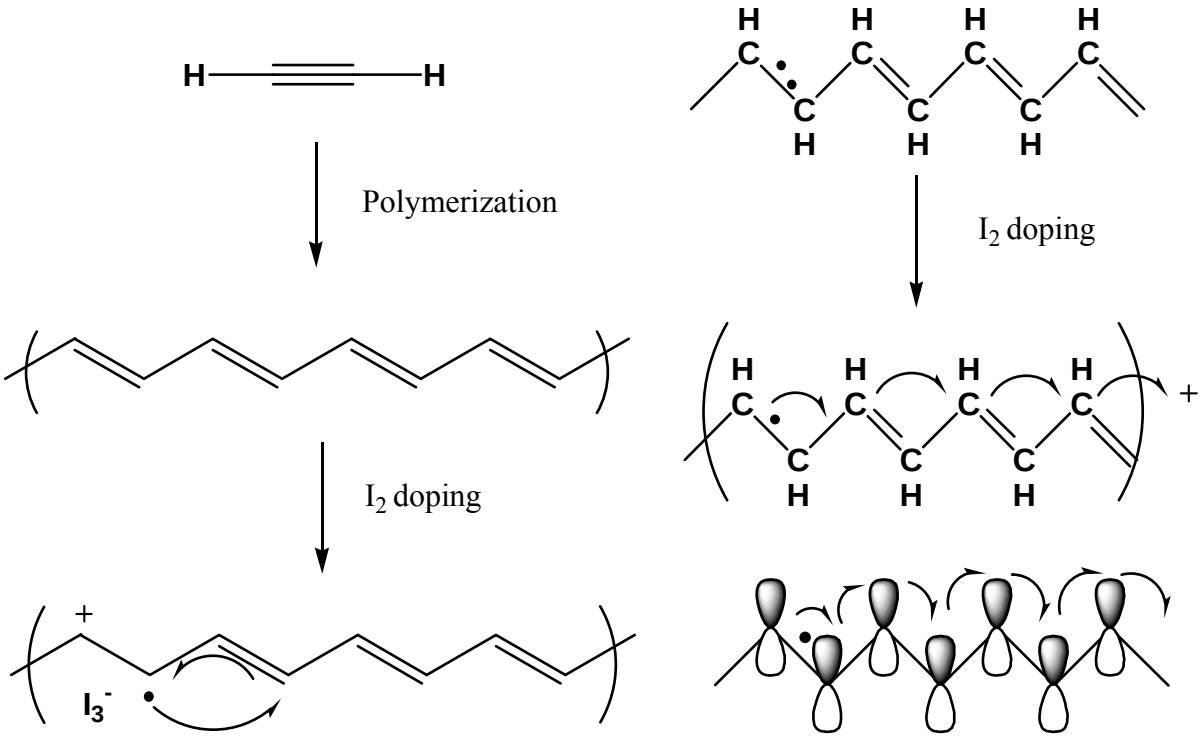


Figure 12 Iodine doping process of polyacetylene[5]

Previous study reports also claimed that when iodine ($I_2$) is utilized as the dopant it makes possible to elevate the conductivity level of final polymers of up to $10^5$ S/cm and allows producing stretchable polyacetylene films[3]. During this process, halogen iodine atoms ($I_2$) first of all attack to the one of the double bonds in polyacetylene backbone chain, then break it and easily grab one electron ($I_3^-$) and make the other electron free (create charge) to hop along the adjacent double bonds in polymer backbone chain by simply delocalizing its position with the subsequent double bond. It is possible to obtain polyacetylene molecules with different morphologies such as powder, gel, spongy mass or film by simply changing the similar reaction conditions[3].

Extended π-bond conjugated structure renders the polyacetylene insoluble, infusible and environmentally unstable due to the strong intermolecular chain interactions, albeit provides a

nice pathway for created charges better than similar type of structures. Possessing this kind of inherently insoluble and insoluble structure[2] coupled with poor environmental stability[3] makes polyacetylene rather unattractive for technological applications[2] and imposes a barrier in front of the processability of this polymer[3]. Throughout the time, considerable amount of research effort has been spent to obtain processable polyacetylene structures[3] by following different methods like transformation of similar structured polymers, dehydrohalogenation of poly(vinyl chloride) (PVC), e.g., and/or utilization of thermally convertible metal prepolymers/precursors[3] (ROMP).

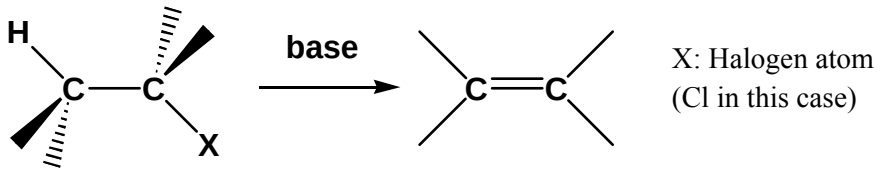


Figure 13 Dehydrohalogenation reaction for polyacetylene synthesis

Drawbacks of the dehydrohalogenation reaction are; (i) short conjugated chain length yield, (ii) crosslink formation, and (iii) defection threat in polymer structure[3]. Advantages of the ROMP method are; (i) continuous solid polyacetylene film yield, (ii) controllable morphology range of polyacetylene from amorphous to crystalline, and (iii) stretchable film formation during or prior to conversion by heat[3]. As a matter of fact, none of the polyacetylene products obtained through these two reactions, so far, was able to exhibit better conductivity results than that of doped polyacetylene itself[3]. This situation, is the work underway to be solved, can be explained by; (i) the reduction of conjugated chain length, and (ii) the steric repulsions between adjacent side groups which causes polymer chains to twist during or at the end of the reactions[3], for the final products. Today, ongoing research activities are still focused on to synthesize soluble, easily processable and highly conducting polyacetylene structures.

## 1.3 Intrinsically Conducting Polymers (ICPs)

During the last few decades, conducting polymers have been gathering a great interest of academia and industry by providing the opportunity of combining the electrical properties of a semiconductor and metals with the traditional advantages of conventional polymers such as easy and low cost preparation and fabrication in the same structure[6]. Other three major advantages of these polymers are their flexibility, environmental stability and chemical inertness[6].

As it was mentioned earlier, intrinsic electronic conductivity of these polymers arises from the extended conjugated π-bond structure along their backbone chain[6]. It should be kept in mind that conjugated organic molecules can exhibit semiconductor properties[6] and since the conducting property originates from the inherent (extended conjugated π-bond) structure of these polymers, they are called as intrinsically conducting polymers[6]. These polymers cannot be considered apart from the polyacetylene. However, they can be specified into four major polymer families, namely, polyaniline (PANI), polythiophene (PTh) with its soluble derivative poly (3-hexylthiophene) (P3HTh), poly (3, 4-ethylenedioxythiophene) (PEDOT) and polypyrrole (PPy) in terms of being the technologically relevant front runners[2].

Intrinsically conducting polymers can be synthesized through different types of polymerization reactions such as chemical oxidative polymerization, electrochemical polymerization, photochemical polymerization, plasma polymerization and organic synthesis[4].

The method we followed in our study was the chemical oxidative polymerization. For this type of reactions, oxidants like ammonium peroxydisulfate ($(NH_4)_2S_2O_8$), hydrogen peroxide ($H_2O_2$), ferric chloride ($FeCl_3$), potassium permanganate ($KMnO_4$), potassium dichromate ($K_2Cr_2O_7$) and potassium perchlorate ($KClO_4$)…etc.[5] are utilized to oxidize the monomer. The oxidation potential of these materials, which is mainly determined by the active group in their

molecule, is the key point for their selection and preference for the suitable polymerization reactions.

In this study, to eliminate the use of those toxic oxidative agents and to be able to directly deposit the noble metal nanoparticles onto the conducting polymer nanostructures, different noble metal salts with oxidation properties such as AuCl, $PtCl_2$, $PtCl_4$ and $HAuCl_4.3H_2O$ were utilized to obtain "polypyrrole (PPy) nanofiber/Au or Pt nanoparticle" composites.

### 1.3.1 Polyaniline (PANI)

Polyaniline was invented by a German chemist, Carl Julius Fritzsche, in 1840[7]. He first obtained a colorless oil from indigo and called it aniline due to the similarity of these two materials in appearance and then oxidized this oil to polyaniline (PANI)[7]. Since this invention, polyaniline has attracted lots of scientists' attention and made them to investigate this polymer largely from different points of view.

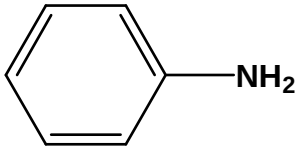


Figure 14 Chemical structure of the aniline monomer

To obtain polyaniline from the aniline monomer, the most widely employed synthetic routes are the chemical oxidative polymerization and the electrochemical (constant voltage, constant current, sweeping voltage methods) polymerization[3]. Besides these two routes; the interfacial polymerization, electro spinning, seeding polymerization and the template polymerization methods are also commonly used to produce nanostructured polyaniline[7].

Chemical oxidative polymerization (radical cationic) reaction of aniline is usually conducted in acidic medium with a suitable oxidizing agent such as APS ($(NH_4)_2S_2O_8$) and proceeds to form polyaniline. As-produced polyaniline can be rendered electrically conducting by an additional acid treatment (doping) after its polymerization reaction.

Polyaniline has a rather unique polymeric structure which is mainly composed of sequentially alternating benzene rings and nitrogen atoms[2]. The existence of nitrogen atoms as imine (in $sp^2$ hybridized state) or amine (in $sp^3$ hybridized state) forms[2], and their relative proportion in the overall polymer backbone chain determines the resulting structure and the different properties of polyaniline.

There are four well-known forms of polyaniline available in the literature according to their reduced/oxidized repeating unit proportions[2]. Different oxidation states of polyaniline can be obtained by using previously mentioned oxidants like iodine ($I_2$), but the resulting conductivity of these structures is less than that are obtained by acid doping[3].

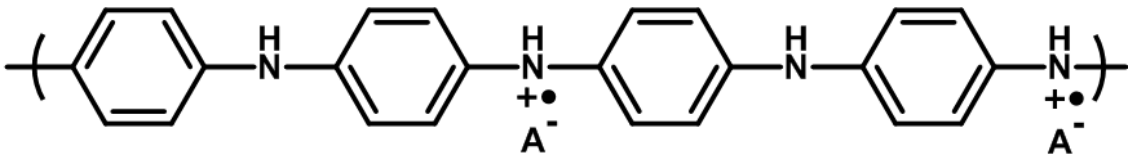


Figure 15 Chemical structure of polyaniline (PANI)[5]

Leucoemeraldine is the fully reduced state of polyaniline. This type of polyaniline has a pale brown color and does not exhibit conducting property[2]. The emeraldine state of polyaniline does not have conducting property either and can be differentiated with its blue color. On the other hand, the only electronic conducting state of polyaniline is the protonated emeraldine form which has partially oxidized/reduced structure. Conductive property of this state originates from

the protonated charge carriers that are generated after the acid treatment of the emeraldine form (reversible reaction by base treatment)[2]. This state of polyaniline has a dark green color, a versatile solid structure that is insoluble, infusible and intractable[7] in organic solvents and a conductivity value between 2-10 S/cm. In contrast to this form, emeraldine polyaniline can be dissolved in N-methyl pyrrolidone (NMP) or dimethyl sulfoxide (DMSO) solvents and has a processable characteristic with a conductivity value of $10^{-10}$ S/cm[7].The fully oxidized state of polyaniline with its pink/purple color is called pernigraniline. In contrast to the most of the similar polyaromatics, pernigraniline state of the polyaniline does not exhibit conducting property like the others do[3] in its fully oxidized state.

Conductivity of the polymer is mainly affected by the impurities (water and dopant content) in its structure[3]. For example, completely dry polymers exhibit five times less conductivity than the ones containing some water in their structure. Similarly, polymers with more dopant content have higher conductivity than the pure ones[3].

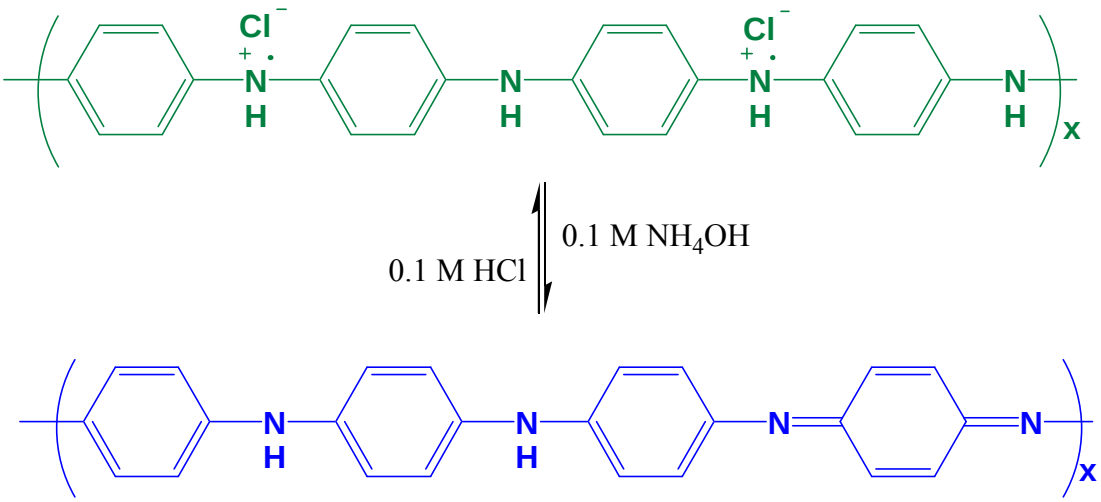


Figure 16 Protonic acid and base treatments of polyaniline between its emeraldine forms[7]

Polyaniline itself has some unique properties such as wide and controllable range of conductivity, yielding intrinsic fibrillar morphology, and melt or solution processable property that are superior to other conducting polymers[7]. This polymer can be used as the conductive compound for different blends with conventional polymers like polystyrene[7]. Also polyaniline plays an important role as the processing aid material by providing conductivity for its various reactions[7]. Another important application area of polyaniline is the use of this polymer to produce colored or transparency conductive products[7].

### 1.3.2 Polythiophene (PTh) and Poly (3-hexylthiophene) (P3HTh)

The earliest research studies about the synthesis and/or the different properties of polythiophene are dating back to thirty years ago. This polymer can be prepared through similar synthetic approaches as those (chemical oxidative polymerization, electrochemical polymerization…etc.) described for polyaniline[3].

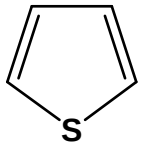


Figure 17 Chemical structure of the thiophene monomer

Polymerization reaction of thiophene takes place by following almost the same way of polyaniline and finally, polythiophene structure is obtained by the coupling of chains propagated during the reaction and the loss of two protons from their structure at each step. In further steps polythiophene can be doped by using different acids or dopants like $FeCl_3$ to render the polymer electrically conducting. This polymer also has a rigid polymer backbone structure that can not be dissolved in organic solvents like many other linear polyaromatic compounds[3].

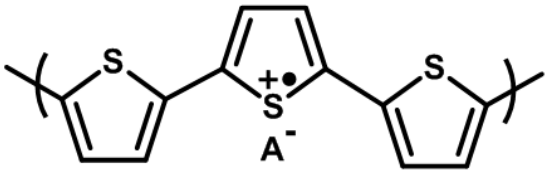


Figure 18 Chemical structure of polythiophene (PTh)[5]

However, by lateral substitution group attachments at the 3-position (prevents the crystallization of conjugated polymer backbone chain), solubility and the processability of the structure can be enhanced[7] and a more soluble form of this polymer, namely, poly(3-hexylthiophene) (P3HTh) with its long alkyl side chain groups can be obtained[2].

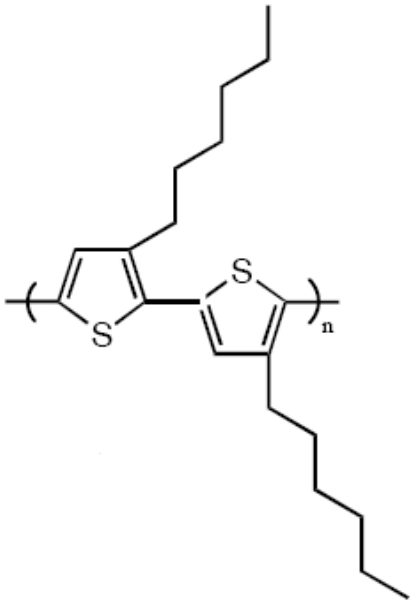


Figure 19 Chemical structure of soluble poly(3-hexylthiophene) (P3HTh)[2]

Electrochemical polymerization method is also commonly utilized for thiophene to prepare thin conducting films with controlled thicknesses[3]. Likewise the other conducting polymers[7] polythiophene (PTh) also have various popular and interesting areas of use such as

light emitting diodes, corrosion protection of metals, non-linear optical devices, sensors for volatile organic materials and organic solar cells.

### 1.3.3 Poly (3, 4-ethylenedioxythiophene) (PEDOT)

One of the most popular members of the conducting polymer family is PEDOT with its uniquely combined conductive and optical properties that have been largely investigated in recent years by the academia and intentionally by the different areas of industry to build a better knowledge for the future studies and applications of this polymer like organic light emitting diodes, flat panel displays and as semiconductor for organic transistors.

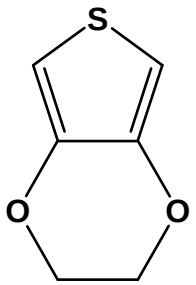


Figure 20 Chemical structure of the ethylenedioxythiophene monomer

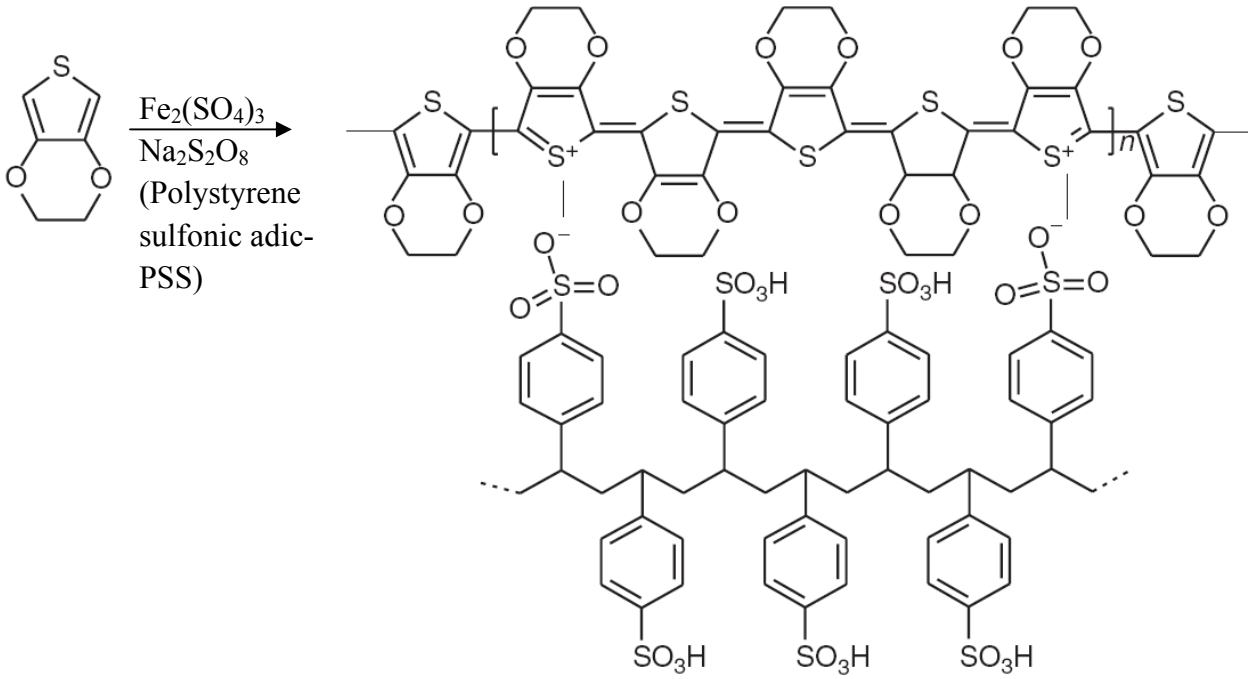


Figure 21 Oxidative polymerization of EDOT in the presence of PSS[7]

Chemical oxidative polymerization is the most commonly used method to synthesize this polymer out of EDOT[7]. A well-known polymerization reaction takes place in the presence of EDOT monomer, polystyrene sulfonic acid (PSS) and a suitable oxidant like iron(III)sulfate ($Fe_2(SO_4)_3$) by resulting a polymer complex of two ionomers called PEDOT:PSS.

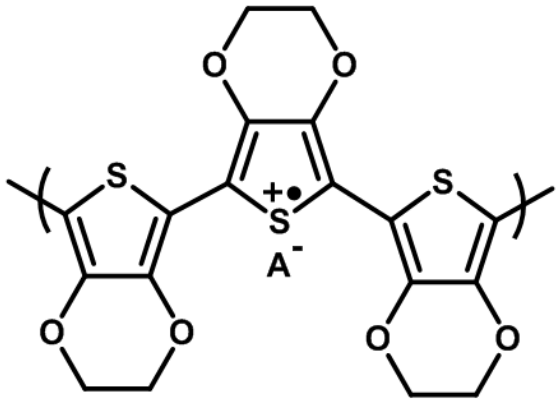


Figure 22 Chemical structure of poly (3, 4-ethylenedioxythiophene) (PEDOT)[5]

This final polymer mixture is one of the most popular industrial outcomes of PEDOT which is utilized for different applications mentioned above. Excellent transparent and optical properties in hand, PEDOT also exhibit good electrical conductivity (due to its low band gap) within its environmentally stable structure. Unfortunately this polymer is also insoluble in organic solvents like its big brothers, which makes it hard to process during its revolutionary applications.

### 1.3.4 Polypyrrole (PPy)

Polypyrrole is one of the most widely studied members of intrinsic conducting polymer family in different areas of science and industry. The first solid information about the conductivity level of iodine doped, chemically oxidized polypyrrole is dating back to 1963 (DE Weiss et.al.)[7].

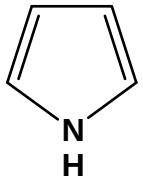


Figure 23 Chemical structure of the pyrrole monomer

With this information in hand, polypyrrole can be considered as the first derivative of polyacetylene that exhibits a high level of conductivity. Throughout the time polypyrrole research has been extended to the very different parts of chemistry and polymer science to gain a deeper knowledge and to improve different properties of this polymer for further applications.

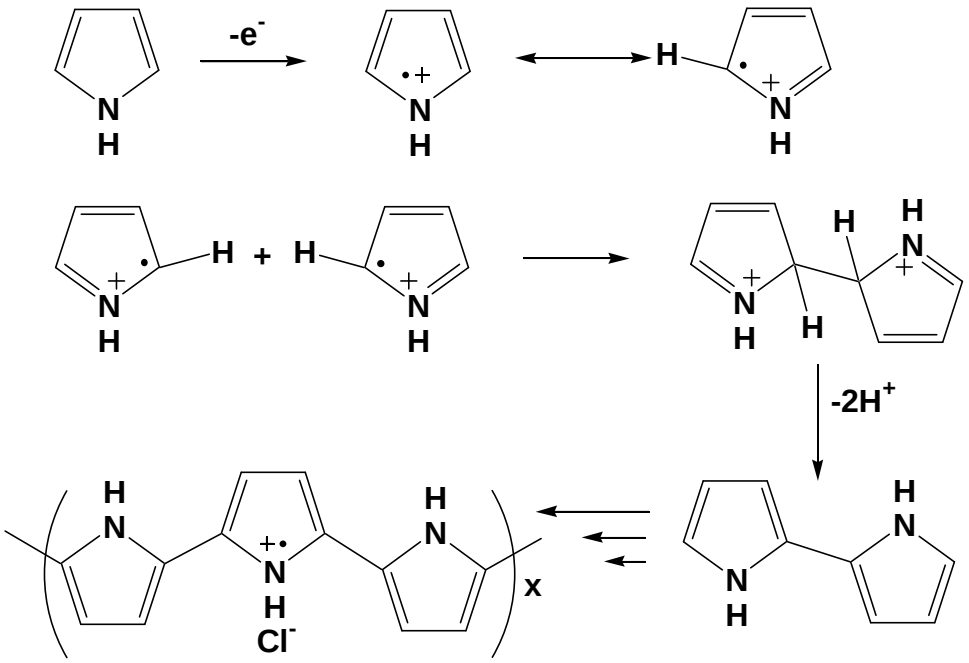


Figure 24 Chemical oxidative polymerization and doping process of pyrrole[7]

The most common methods applied to synthesize polypyrrole are the chemical oxidative polymerization with doping, electrochemical polymerization, plasma polymerization and the organic synthesis. Chemical oxidative polymerization of pyrrole monomer is very similar to that of thiophene[3] with one distinct difference that should be kept in mind during the reaction which related to the reactive nitrogen-hydrogen bond[3]. Due to this reactive bond in its structure, protection of amine is required to prevent undesired side reactions to take place such as crosslinking[3].

General mechanism of the oxidative polymerization of pyrrole can be briefly explained in the following way. Formation of cationic free radicals after the loss of an electron from the monomer structure is followed by the coupling of active resonance structures in different positions during the reaction (oxidation of monomer, radical-radical coupling). These already

coupled structures finally form the polypyrrole chain at the end of the polymerization reaction (deprotonation, re-aromatization and chain propagation).

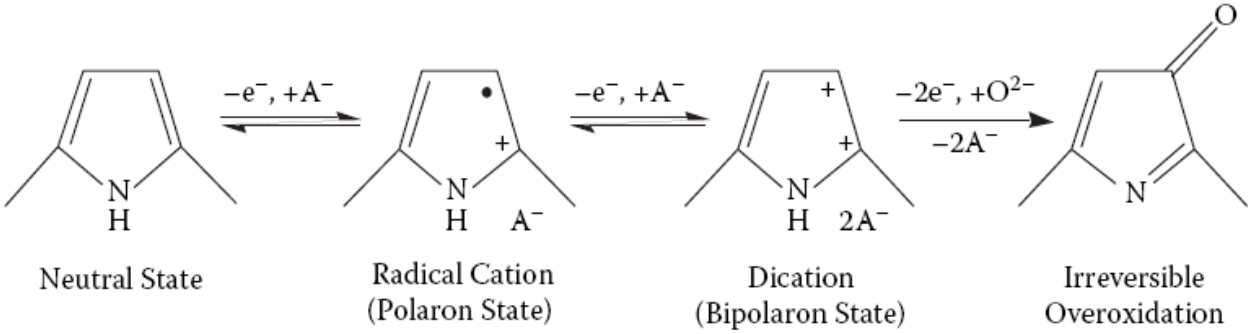


Figure 25 Oxidation states of pyrrole[8]

The traditional conjugated π-bond backbone structure of polypyrrole usually is not enough to possess significant conductivity on its own[9]. The conductivity level of this polymer can remarkably be changed from an insulating level to a metallic one through the doping process[9]. That is why the partial charge extraction (doping) process is required and can be explained for this polymer in the following way.

Again, first of all, an electron is removed from the polymer backbone by yielding a radical and a spinless positive charge[1]. Next, the newly formed cation and the radical are coupled to each other by local resonance[1]. During coupling, quinoid-like sequential rings are also formed and utilized to provide higher energy of distortion than the remaining part of the chain[1]. The created lattice distortion is usually extended over four pyrrole rings (charged site) and when they coupled with a radical, this structure is called polaron[1]. As a result, further oxidation of the polaron yields a new spinless defect called bipolaron having a lower energy than two distinct polarons[1]. At higher doping levels, polarons are eventually replaced by bipolarons[1]. For a heavily doped polypyrrole it is suggested that the upper and lower bipolarons merge to the valence and

conduction bands respectively to produce partially filled bands and provide metallic-like conductivity for the final polymer[1].

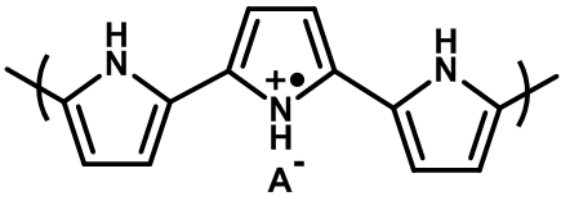


Figure 26 Chemical structure of polypyrrole (PPy)[5]

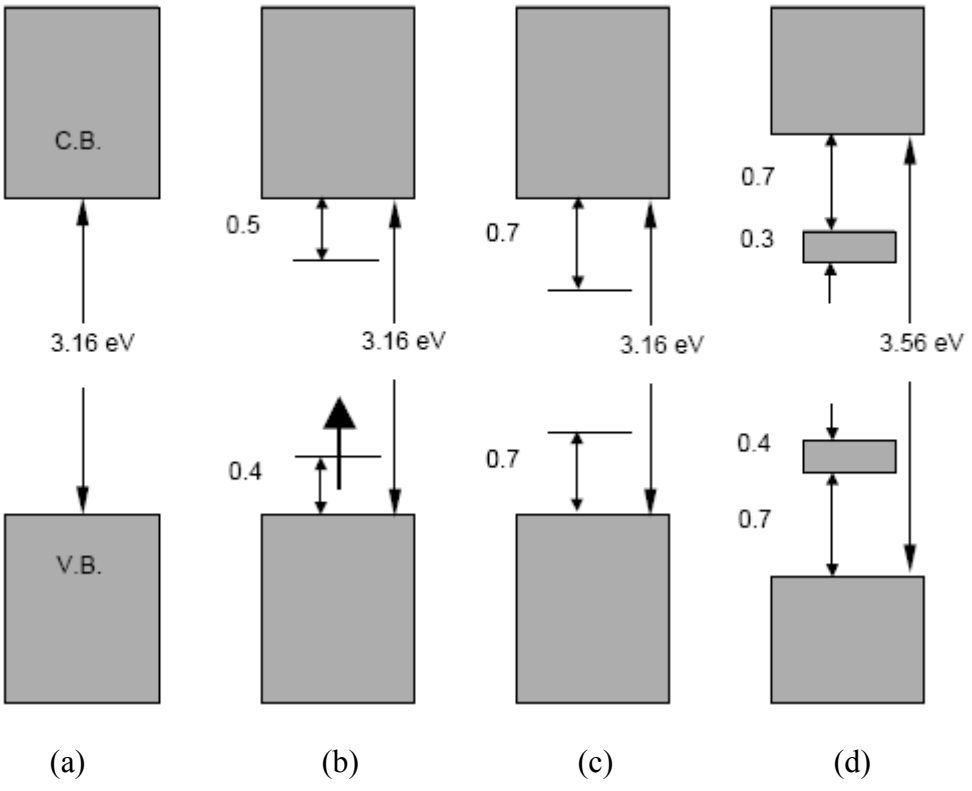


Figure 27 Electronic energy diagrams for (a) neutral, (b) polaron, (c) bipolaron and (d) fully doped polyprrole (C.B.: conduction band, V.B.: valence band)[9]

Polypyrrole also has an insoluble and intractable conjugated polymer backbone chain similar to the other members of this family. However, in different reports so far it has been reported that it is possible to synthesize soluble polypyrrole structures by using alcohol or organic solvent soluble dopants with long alkyl chains like sodium bis(2-ethylhexyl) sulfosuccinate ($C_{20}H_{37}NaO_7S$)[8].

Exhibiting conductivity values[5] between 10-50 S/cm polypyrrole has been verily utilized in different types of scientific/industrial applications such as electrodes for rechargeable batteries and supercapacitors, electromagnetic shielding materials, actuators, electrochromic devices and membranes, corrosion protecting materials and fuel-cell membranes[7]. It is also possible to process different kinds of conventional polymers with polypyrrole while they are still in solution or melt forms[8].

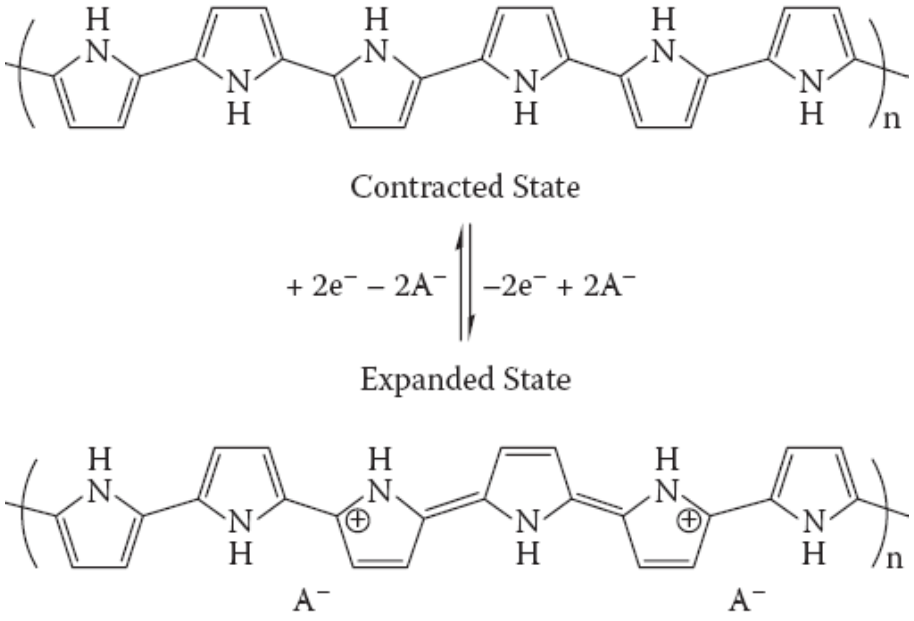


Figure 28 Reduced (top) and the oxidized (bottom) states of polypyrrole[8]

Due to providing unique and tunable physicochemical and conductivity properties as well as better environmental stability and advantageous higher surface area for various applications, nanostructured polypyrrole has also gained a great prominence throughout the different studies[4, 10-12] so far and became one of the major inspirations of this study too.

Table 4 Different attributes of ICPs[1]

| **Conducting Polymer** | **Conductivity (1/Ω.cm)** | **Stability (doped state)** | **Processability** |
|---|---|---|---|
| **Polyacetylene** | $10^3$ - $10^5$ | Poor | Limited |
| **Polyaniline** | 1-10 | Good | Good |
| **Polythiophene** | 10-50 | Good | Excellent |
| **Poly(3, 4-ethylenedioxythiophene)** | 10-50 | Good | Excellent |
| **Polypyrrole** | 10-50 | Good | Good |

### 1.4 Theory of Conductivity and the Conduction Mechanism of Conducting Polymers

The electronic conducting property and conduction mechanism of these polymers have been the key point and/or major inspiration for both their first discovery and for many researches on conducting polymers throughout the time. As it was mentioned frequently in various points of this study, also, the electronic conductivity is the most important property of conducting polymers than any others they possess. This very significant property of conducting polymers can be explained in a simple and straightforward way by the HOMO-LUMO (band gap) theory[5].

According to this theory, to obtain higher conductivity in organic semiconductors; longer, conjugated π-bond backbone structure is required. Therefore, lower energy will be enough for charges to move through the bands with less energy difference. In other words, the energy difference between the lowest unoccupied molecular orbital (conduction band) and the highest occupied molecular orbital (valence band) will be lower as the conjugated π-bond structure gets longer for these polymers.

The intrinsic conjugated polymer backbone structure, which provides a pathway for free charges to move through the polymer backbone chain by a sequential delocalization with π-bonds (hopping) under an applied electric field or during the doping process, is the main reason of conducting property of these polymers. Then it becomes possible to claim that the overall conducting property depends on two components; (i) intrachain mobility, which corresponds to the charge transfer along the polymer backbone chain and (ii) interchain mobility which involves the hopping or tunneling of the created charge from a bond to neighboring bonds[9].

The final conductivity of a polymer is controlled by the combination of these two types[9] of mobility. Conformational and chemical defects (distorted conjugated structure) in polymer backbone, which should be kept in mind and taken care of during polymerization, can restrict the intrachain mobility[9]. Therefore, to be able to achieve higher electrical conductivities in conducting polymers the mobility of the charge carriers should be improved[9] through the effectively controlled polymerizations of these structures.

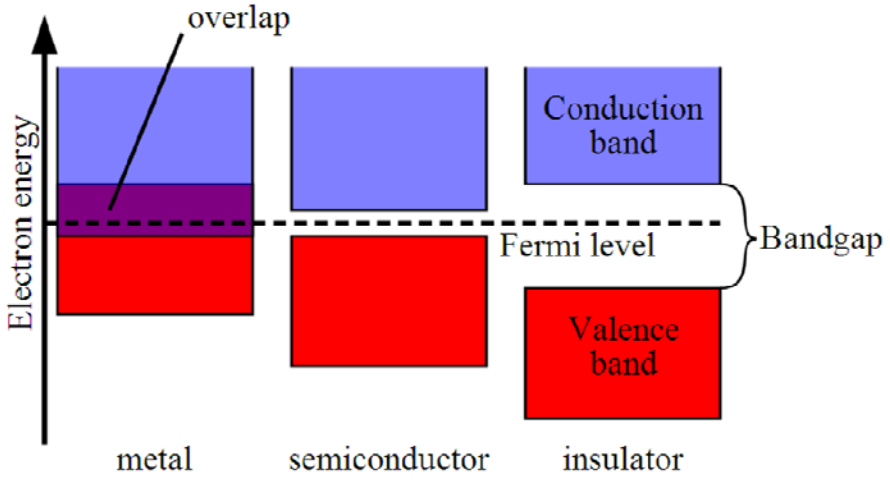


Figure 29 Electronic band structures of different materials[5]

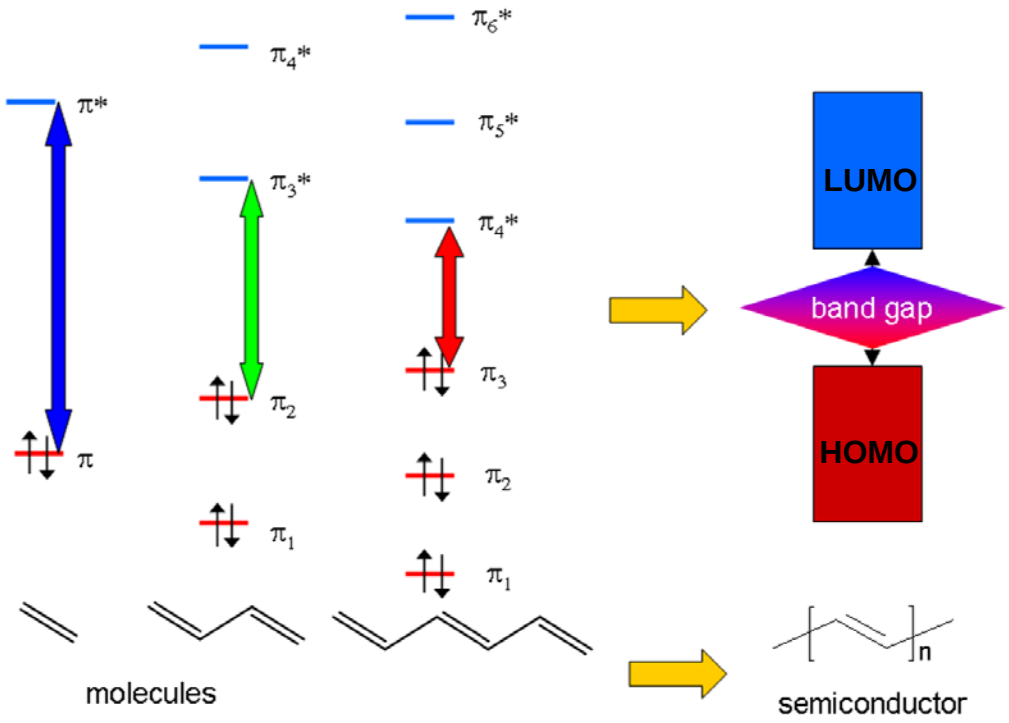


Figure 30 HOMO-LUMO theory in organic semiconductor polymers[5]

# CHAPTER 2

# SYNTHESIS OF CONDUCTING POLYMER/NOBLE METAL PARTICLE NANOCOMPOSITES

## 2.1 Introduction

Since MacDiarmid and his co-workers' first successfully synthesis of the highly conductive polyacetylene film through iodine ($I_2$) doping process[2] in 1977, studies focused on the intrinsically conducting polymers has shown a tremendous increase during the last few decades. Owing to their relatively easy preparation, high levels of conductivity, tunable physicochemical properties and morphologies with good environmental stability[13], the synthesis of intrinsically conducting polymers and their nano-sized composites, which are playing vital roles (by providing higher surface area and superior electron transfer performances) in determining material properties[12] that are obtained through various academic and industrial applications, has received a wide-spread interest[10] throughout the time. Most of the potential scientific and commercial applications like nanoelectronics[12] devices, light emitting diodes[10], volatile organic gas sensors[14], biosensors[14], capacitors[14] and catalysts[14] e.g. of the nano-sized versions of conducting polymers are highly benefiting these unique properties that they intrinsically provide.

In particular, due to its uniqueness among the intrinsically conducting polymers[13] with its high conductivity at physiological pH[11], easy preparation[12], environmentally stable structure[12]

and promising potential for future applications[12] polypyrrole (PPy) was selected to be synthesized in its nanofiber form for this study. Despite several methods that have been developed or utilized to synthesize polypyrrole with different properties and morphologies, the shape-depending synthesis and properties of this polymer was rarely discussed[12].

Overall reports, so far, indicate the need of different kinds of "seed templates" to ensure the synthesis and growth of nanofiber formed polypyrrole[12]. Fibrillar growth is an intrinsic property of another conducting polymer polyaniline (PANI)[12]. It has been proved that an added seed template into the reaction media orchestrates[11] the synthetic route along the pre-existing pathways of polyaniline, however, in polypyrrole system these pathways have to be induced by using either seed templates that are self-reactive toward the pyrrole monomer or those that can be rendered reactive[12], if not, PPy with only spherical morphology can be obtained[12].

The bulk synthesis of PPy nanofibers, directly from its monomer, having fiber diameters in nanoscale has been reported as a challenge for several studies that attempted to try and achieve this within the pores of different in/soluble templates such as zeolite, alumina or on the surface of nanostructured templates[11]. Some previous methods like surfactant-mediated synthesis, interfacial synthesis and nanofiber seeding…etc.[11] were, again, successful in the synthesis of PANI nanofibers, however, they were only able to yield nanofibrous or granular powders of PPy[11]. The only observation of PPy nanofibers or nanotubes could be possible when the large organic dopant anions such as naphthalene sulfonic acid were used during reactions[11]. These so-called nanofibers or tubes were seemingly formed as a result of the solution aggregation of the dopant anions and presented a wide range of diameters changing between 50-2000nm[11].

As an attempt to surmount this key synthetic challenge in the control of nanofibrillar morphology of polypyrrole, in this study, a novel "seeding approach" that utilizes an oxidative-

reactive and degradable[13] seeding template (vanadium pentoxide, $V_2O_5$ sol-gel nanofibers) which can chemically react with the pyrrole monomers prior to the addition of oxidant[11], was described.

The reaction that takes place on the surface of the fibrillar $V_2O_5$ seeding templates enables to manage the evolution of bulk nanofibrillar morphology before the oxidant is subsequently added to the reaction media[11]. It is not possible to obtain any fibrillar morphology if a passive or an inert seed is used for such reactions[11]. Unlike the previously described template directed methods[11] only a catalytic amount of seeding template was used for this study[11]. Other than $V_2O_5$, a variety of in/organic and biological seeding templates such as ~50nm diameter polyaniline nanofibers[15], ~20nm diameter single-wall carbon nanotube (SWCNT) bundles obtained from HiPco route[15] and ~12nm diameter nanofibrous hexapeptide (a seed in the polymerization of Alzheimer's disease tau protein)[15]…etc. were also utilized for similar type of reactions in previous studies.

As it was postulated in a former study that[15] regardless of the diversity in different synthetic approaches about this topic, the remarkable change in polymer morphology is originating from a mechanism explained as; polymeric nanostructures presenting at the very early stages of a polymerization reaction can direct the bulk formation of similar nanostructures. In this study, also consistent with the above mechanism, bulk polypyrrole nanofibers which were obtained through a polymerization reaction was seeded at the very early stages by a very small amount of nanofibers (independently from their chemical nature), were instantiated[15].

In short, nanofibrillar morphology can only be observed in such systems which the seeding template used must; (i) itself provide nanofibrillar morphology and (ii) also be oxidative-reactive with the monomer[11].

Potential advantages of incorporating noble metal nanoparticles into conducting polymers have gained great prominence in recent years; with most of these can be considered initial reports focusing on gold[10]. In a previous study, gold nanoparticles were modified with flourophores to generate an effective route for improved optoelectronic applications[10]. Other than that in another study a significant problem of charge recombination, which often restricts the charge separation performances in donor-acceptor systems, was overcame with the presence of gold nanocores which can quench the excited states of polymer and remarkably enhance the overall performance[10]. It was mentioned in one previous work that the use of gold nanoparticles was also improved the performance of light emitting diodes and efficient memory devices[12] with the power conversion efficiency of solar cells[10] and the sensitivity of chemical sensors[12].

Recently, benefits of using aqueous solutions of noble metal salts as the growth media for conducting polymers have also attracted increasing attention[10]. Utilization of this kind of solutions is (one of the key points of this study) getting increasingly preferable over volatile molecular solvents for wide-spread synthetic and device applications[10] because of providing advantageous properties like eliminating the production of toxic vapors during reactions, improving the performance and lifetimes of conducting polymers that are used as supporting surfaces, eliminating the use of toxic oxidative agents like APS [$(NH_4)_2S_2O_8$] or in/soluble templates that are used for conventional oxidative polymerization of conducting polymers, and allowing to work at potentials that were previously prohibited by the smaller electrochemical window of molecular solvent/electrolyte systems[10].

The synthesis and characterization of nanocomposites of intrinsically conducting polymers with the noble metal nanoparticles was the main topic and the goal of this study by reason of its cruciality that originates from the potential that was readily provided by combining

two frontier technologies in one structure to yield materials with great academic and industrial interest gathering properties[10], which would be fuelling a drive towards promising future applications[10].

Via a novel, facile and one-step chemical oxidative polymerization reaction, which was assisted by self-degrading, self-oxidative-reactive seeding template $V_2O_5$ sol-gel nanofibers, of pyrrole monomers, conducting polymer (polypyrrole-PPy) nanofibers containing noble metal (Au or Pt) nanoparticles that were in-situ deposited through a spontaneous redox reaction with PPy[12], were synthesized. During the following paragraphs of this chapter the experimental method, that was followed for this novel approach, in different concentrated variant aqueous solutions of the previously mentioned noble metal salts such as AuCl, $PtCl_2$, $PtCl_4$ and $HAuCl_4.3H_2O$ without the need for any toxic oxidative agents, in/soluble templates and/or capping agents, was explained in details.

## 2.2 Experimental Section

### 2.2.1 Materials

*For polypyrrole fiber, granule, nanocomposite and carbon nanotube (CNT) synthesis;* pyrrole (98+%), gold (I) chloride (AuCl)Au 84.2% min., platinum (II) chloride ($PtCl_2$) 98%, hydrogen tetrachloroaurate (III) hydrate ($HAuCl_4.3H_2O$) Au 49% min., platinum (IV) chloride ($PtCl_4$) Pt 57.9% min. and ammonium peroxydisulfate (APS $(NH_4)_2S_2O_8$) 98% were all purchased from Alfa Aesar and used as received.

Also, ammonium metavanadate ($NH_4VO_3$) 99.5% from ACROS ORGANICS and DOWEX® MARATHON (H) ion-exchange resin from Sigma Aldrich were purchased to prepare $V_2O_5$ sol-gel nanofibers within Deionized (DI) water, according to a process which was

explained earlier[11] (in 160mL DI water + 0.8g $NH_4VO_3$ + 8g Dowex resin were mixed together without shaking or magnetic stirring).

*For the purification of final polymeric and nanocomposite structures;* acetone (BDH®) $(CH_3)_2CO$ was purchased from VWR and used with DI water.

*For the electrochemical (cyclic voltametry, CV) and different characterization applications of polymeric and nanocomposite structures of PPy;* potassium hydroxide (KOH) pellets from SPECTRUM, methanol (BDH®) $CH_3OH$ from VWR, ethyl alcohol pure 200 proof ($CH_3CH_2OH$) from EMD, graphite rods (6.15mm diameter, 152mm length and 99.9995% metal basis) from Alfa Aesar and colloidal graphite (isopropanol base) as EM science brand product from VWR were all purchased and used without further purification.

### 2.2.2 Synthesis Methods

#### 2.2.2.1 Synthesis of Polypyrrole (PPy) Granules and Fibers

Two different PPy structures having granular and fibrillar morphologies were prepared as control samples for the nanocomposite structures whose preparation will be explained in the following parts of this section.

Granular PPy preparation can be explained as; in 60mL DI water, 1mL of pyrrole was gently added under magnetic stirring. This mixture was stirred for the following 5-10min. to obtain a better dispersion of pyrrole in DI water. At the end, 1.15g of APS was added into the solution by changing its color from light yellow to black with the spontaneous formation of PPy structures dispersed into the solution.

Fibrillar PPy preparation can be explained as; in 60mL of DI water, 1mL of $V_2O_5$ sol-gel nanofibers was firstly added under magnetic stirring. The addition of 1mL pyrrole monomers into this solution should be completed in 20-60sec. after $V_2O_5$, to initiate and maintain the

fibrillar structure formation for resulting PPy molecules. Finally, 1.15g of APS was added into the reaction media, by changing its greenish yellow color to black, to initiate the polymerization of pyrrole. Both solutions were magnetic stirred for the following 4-5 hours to obtain better polymerization of so-called structures.

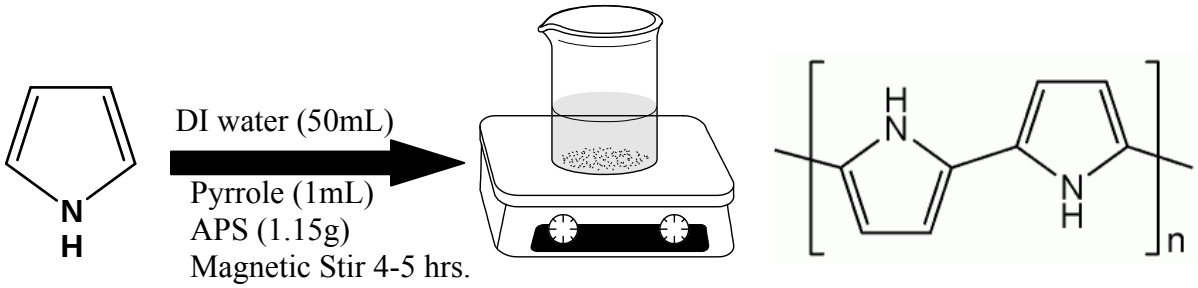


Figure 31 PPy granule synthesis

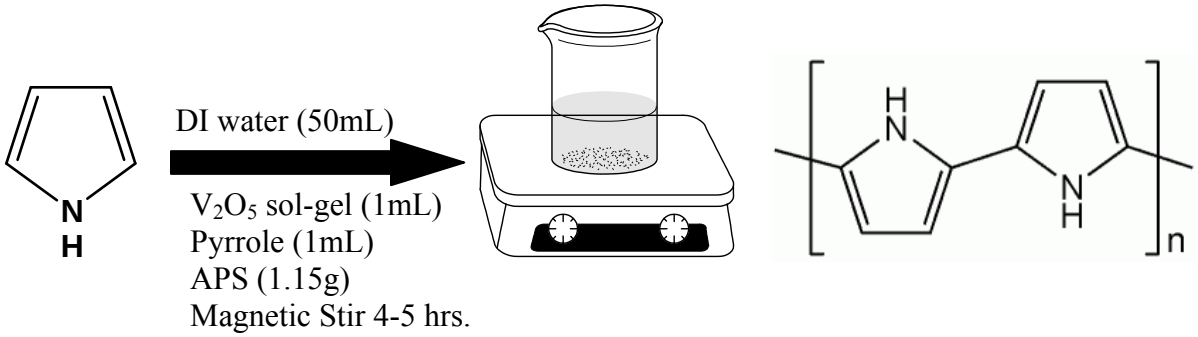


Figure 32 PPy fiber synthesis

### 2.2.2.2 Preparation of Standard Aqueous Noble Metal Salt Solutions

The standard concentration was 0.02M for the aqueous electrolyte solutions of different metal salts. 0.001mole of each noble metal salt (0.266g of $PtCl_2$, 0.337g of $PtCl_4$, 0.232g of AuCl and 0.394g of $HAuCl_4.3H_2O$) were weighed and then dissolved in 50mL of DI water in

individual beakers under continuous magnetic stirring to obtain better homogeneity. The solution color was changed from transparent to light yellow, yellow, dark yellow and pale brown (after AuCl, $HAuCl_4.3H_2O$, $PtCl_4$ and $PtCl_2$ additions, respectively) in each beaker with the dissolved noble metal salts' particles floating into it.

These standard solutions were later used to prepare control electrolyte solutions of same salts with different concentrations (0.01M and 0.005M) to unveil the effect of concentration on the final product morphology and other properties. The control electrolyte solutions' preparation can be explained as; 25mL of 0.02M electrolyte solution was diluted in 25mL of DI water to obtain 0.01M concentration, and 12.5mL of 0.02M solution was diluted in 37.5mL DI water to obtain 0.005M concentration to obtain same amounts (50mL).

**2.2.2.3 Synthesis of Polypyrrole (PPy) Nanofiber/Noble Metal Nanoparticle Composites**

To the best of our knowledge, this type of one step, self-oxidative-reactive and self-degrading seeding template ($V_2O_5$ sol-gel nanofibers) assisted oxidative polymerization of pyrrole monomers, was the first attempt that has ever been made to obtain nanocomposites composed of nanofiber shaped conducting polymers (PPy) that were decorated with noble metal nanoparticles (Au, Pt).

The method followed can be simply explained as; 1mL of $V_2O_5$ sol-gel nanofibers was gently added into the readily prepared, different concentrated aqueous noble metal salt electrolyte solutions (reaction media) under magnetic stirring by changing the solution color into greenish yellow. Here, one key point that should be kept in mind is about the length of the time gap between the sequential addition of $V_2O_5$ and the pyrrole monomer, which should be very small. In order to initiate and maintain the nanofiber formation for the resulting polymer structures, the addition of monomer to the reaction media should be completed within 20-60sec.

after the $V_2O_5$. Next, 0.1mL of pyrrole monomers were added subsequently to the reaction media by obeying the above mentioned rule. The solution color was spontaneously darkened and turned into black with the formation and dispersion of black precipitates of PPy into the reaction media as a result of oxidation and/or polymerization of pyrrole initiated by the noble metal salts. The reaction solution was magnetic stirred for the following 24 hours for better distribution of conducting polymer nanocomposites and noble metal nanoparticles among them.

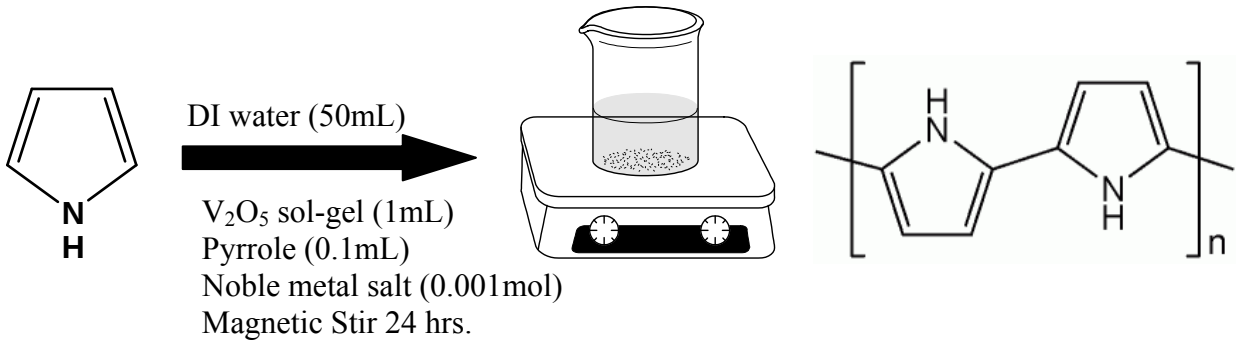


Figure 33 PPy nanofiber/noble metal nanoparticle composite synthesis

**2.2.2.4 Purification of As-prepared Samples**

At the end of the specific polymerization times (4-5 hours for PPy granule and fiber and 24 hours for the nanocomposite samples) all different types of reaction solutions containing the black precipitates of polymeric structures and/or nanocomposites were gone through the same purification process. Each and every prepared sample was washed and suction filtered, in a Whatman 70mm diameter filter paper equipped[16] Buchner funnel, which was attached to a water respirator, by using copious amounts of DI water (3x100mL) -to remove the residual monomers and its water soluble decomposition by products with the oxidant- and Acetone (3x100mL) -to remove low molecular weight organic intermediates and oligomers[17]- from the system and to

facilitate the drying process of the as-prepared samples with the quick evaporation of acetone. The wet dark blue or dark brown precipitates were allowed air drying (5-10min.) inside the funnel until there was no more liquid left to suck from the filter paper.

Next, the filter paper was taken out of the funnel and stored at standard laboratory conditions overnight for a complete evaporation and drying. At the following day, dried precipitates of polymeric structures and nanocomposites were finally collected from the filter paper surface, then weighed and stored in different glass vials with correct labeling for further characterization steps. The average yields of PPy fiber and granules were both ~0.41g and the average yields of the nanocomposites obtained from different electrolyte solutions were summarized in the following table.

Table 5 Amounts of the nanocomposite yields obtained from different noble metal salt solutions

| | **0.02M** | **0.01M** | **0.005M** |
|---|---|---|---|
| **AuCl/PPy** | 0.0698g | 0.0431g | 0.0061g |
| **$HAuCl_4.3H_2O$/PPy** | 0.2975g | 0.1685g | 0.0421g |
| **$PtCl_2$/PPy** | 0.2032g | 0.0811g | 0.0336g |
| **$PtCl_4$/PPy** | 0.2425g | 0.1663g | 0.0741g |

### 2.2.3 Preparation of Electrolytes for the Cyclic Voltammetry (CV) Applications and Electrochemical Characterization

For the electrochemical methanol ($CH_3OH$) oxidation reaction, catalyzed by the noble metal particles in as-prepared nanocomposites, through cyclic voltammetry (CV) of readily prepared PPy fiber and nanocomposite samples with noble metal nanoparticles, 1M aqueous

KOH solution was prepared by first of all weighing ~56.1g (1mol) of KOH pellets, then dissolving them into 1L volumetric flask filled with DI water under magnetic stirring. 80mL of KOH+$CH_3OH$ solution was prepared by mixing 76mL of 1M aq. KOH + 4mL methanol respectively in same beaker and used as the electrolyte for the electrochemical application and characterizations of above mentioned samples.

### 2.2.4 Preparation of Electrodes for the Cyclic Voltammetry (CV) Applications

Besides these electrolytes, graphite rods and colloidal graphite were utilized to prepare electrodes for so-called applications. Graphite rods were modified to decrease the amount of surface and material amount interacting with the alligator clips and the electrolyte solutions. At the effective tips of the graphite rods (working electrode) which were placed into the electrolyte, colloidal graphite was applied to be able to paste as-prepared polymeric and nanocomposite samples. Another pure graphite rod with sharpened tips was used as counter electrode vs. SCE (saturated calomel electrode -a saturated solution of potassium chloride [KCl] in water linked to the electrolyte via a porous salt bridge[35]), which were readily prepared by Zhen Liu, used as the reference electrode.

### 2.2.5 Microwave Initiated Carbonization of Nanocomposite Samples

The major goal of this subsection was to investigate another novel nanoengineering technique, which had already been proposed for a different, previous research study[18], to convert conductive polymer nanocomposite surfaces decorated with noble metal nanoparticles into carbon nanocomposites (CNCs).

Higher surface area of CNCs provides remarkable advantages for the processability and the applications of the material. That is why these kinds of carbon nanocomposites are widely utilized as the composite additive to enhance the several properties and also the conductivity of

different structures. Despite these superior merits, this research has also some challenges in terms of the areas of design, synthesis and instrumentation.

Various conventional techniques that require high temperature and high energy density for extended periods of time and also the use of inorganic templates, were commonly used to obtain nanocarbon products. The main common challenges of these conventional production methods and nanocarbon material itself can be summarized as; (i) the requirement of an inert gas protection, complicated instrumentation, long periods of high energy density, insoluble template use (and additional removal steps for these templates) (ii) and the lack of capability for the bulk synthesis of such structures from lab scale to industrial level.

As an attempt to address the challenges mentioned so far; a novel and high scale production capable microwave approach[18] was developed to synthesize CNC materials. By using microwave irradiation such composite materials with tunable and beneficial properties like catalysis ability, can be manufactured by remaining their original morphologies.

Before the performance of this novel technique to the nanocomposite materials, the interactions between microwave irradiation and different types of (conductor, insulator) materials should be understood carefully. Here, the key property of different materials which plays a vital role to understand this interaction is the conductivity. The experimental data up to date indicates that materials within moderate conductivity (intrinsically conducting polymers) levels from $10^{-5}$ to 10Ω.m can be heated more efficiently than insulating or highly conductive materials.

Another important property that affects the performance of the microwave treatment is the dimensions of the material. Since, in most cases, good and thick conductors are readily able to reflect the microwave irradiation and thin ones have a lot less capabilities; nanostructured

conducting polymers with moderate conductivity can absorb microwave energy in a very efficient way which makes them promising outcomes of the rapid CNC production applications[18]. In view of the fact that a huge amount of heat can be generated by microwave treatment of conducting polymers, they can readily be used as sacrificial precursor matrixes to support their conversion to CNCs.

This novel method to produce CNCs requires more simplified setups than conventional ones. Basically, a microwave oven and glass vials are more than enough to conduct this energy efficient method that eliminates especially the cumbersome template removal step of the conventional approaches. The cost of resulting CNCs from this method is also much lower than any other existing approaches. The production volume of CNCs can be readily scaled up to large amounts, which is required for the applications in different areas, such as the infrastructure and composite materials' production due to their high demand every year.

For this application 50mg or 100mg of each polymeric and nanocomposite structure was prepared in solid state and placed into glass vials. As-prepared solid samples were exposed to microwave irradiation for a very short time (30s to 1min.; depending on the reactivity of the material) at, usually, highest energy level (1250W) to convert their PPy nanofiber matrixes into CNCs. During microwave irradiation, the conducting polymer matrix absorbs the energy, and its temperature increases rapidly (continuous flames and sparks were observed during applications) which was high enough to convert PPy nanofiber molecules into carbon.

As-prepared PPy nanofibers decorated with Au/Pt nanoparticles


Carbon nanocomposites decorated with Au/Pt nanoparticles (with remained nanofiber morphology)

Figure 34 Microwave initiated carbonization mechanism of nanocomposites

Care should be taken, in case of explosion of glass vials due to the rapid increase of temperature and pressure inside them, during the applications. Finally, CNC samples exhibiting similar fibrillar morphology were collected and stored carefully for further characterization studies. To investigate the morphology and other property changes, after microwave treatment, of selected nanocomposite samples various characterization tests were applied and the obtained results were discussed in the following chapter of this study.

### 2.2.6 Instruments and Characterization Methods

*Thermogravimetric Analysis (TGA);* a TA Instruments TGA Q500 thermogravimetric analyzer was used to characterize the thermal properties of PPy structures with different morphologies (PPy fibers/granules and nanocomposites decorated with different noble metal nanoparticles and CNT samples obtained from microwave treatment). ~5mg of each sample was exposed to thermal heating under pressurized air, from room temperature to 800°C at 10°C/min rate.

*Scanning Electron Microscopy (SEM);* a Zeiss EVO 50 variable pressure scanning electron microscope with digital imaging and EDS, was used to characterize the morphological properties of very small pieces of above mentioned samples. An EMS 550X auto sputter coating

device with carbon coating attachment was also utilized for gold sputtering of samples, which were readily prepared on carbon tape mounted sample holders, before testing them at SEM.

*Transmission Electron Microscopy (TEM);* a Zeiss EM 10C 10CR transmission electron microscope was used for a more detailed morphological characterization. Different nanocomposite samples were dispersed homogenously in ethyl alcohol, then transferred (~5µL) onto a carbon coated aluminum Formvar grid and left drying at standard laboratory conditions before TEM testing.

*Electrochemical Cyclic Voltammetry (CV);* voltammetric data of four different samples (PPy fiber, PPy/$PtCl_2$ 0.02M, PPy/$PtCl_2$ 0.01M, PPy/$PtCl_2$ 0.005M and microwaved PPy/$PtCl_2$ 0.01M) were recorded at standard laboratory conditions by an Arbin electrochemical instrument (Arbin-010 MITS Pro 4-BT 2000). Tests were conducted by applying -0.8V to 0.4V vs. SCE at 20mV/s to the so-called samples coated electrodes in KOH+$CH_3OH$ electrolyte, according to the way described earlier.

*Fourier Transform Infrared (FT-IR) Spectroscopy;* all the IR Transmittance spectra were recorded by a Thermo Fischer Scientific NICOLET 6700 FT-IR instrument. This device uses an attenuated total reflectance (ATR) module that collects IR spectra independently from sample size and without any further sample preparation requirement for solid and liquid samples, between wave number ranges of 400$cm^{-1}$ to 4000$cm^{-1}$.

*Elemental Analysis;* weight %s of C, N, O, Cl, V, Au, Pt elements within each as-prepared nanocomposite were measured by Oxford Instruments, INCA EDX instrument to verify and determine the exact chemical formulas of the sample products obtained.

*4-Probe Conductivity Measurement;* was performed by following a linear four probe method that was described in a previous study[19] of our group. Four probes were connected to

Agilent Technologies 34980 multifunctional switch & measure unit which was applying an adjusted potential to the sample that was interacting with the four probes. As-prepared nanocomposites and different morphology PPy structures were initially and individually pressed under 3500psi in a mold cavity to form a thin film, and then four probes were touched onto this thin film to measure the specific resistance. Measurement results and calculations about the conductivity values of each sample were given and explained in the following chapter.

# CHAPTER 3

# RESULTS AND DISCUSSIONS

## 3.1 Introduction

A novel, facile, one-step chemical oxidative polymerization of pyrrole monomers, which was assisted by self-degrading and oxidative-reactive seeding templates ($V_2O_5$ sol-gel nanofibers), to synthesize nanostructured composite materials that were composed of conducting polymer (PPy) nanofibers decorated with in-situ deposited noble metal (Au, Pt) nanoparticles, was described in details. Besides this novel method, conventional syntheses of conducting polymers (PPy) with different morphologies (fiber, granule) were also explained as the control mechanisms.

All different samples obtained through these experiments were characterized through different perspectives by using various polymer characterization techniques to build a substantial knowledge for the promising future applications of these structures. Characterization results collected during the tests and applications mentioned at the previous chapter of so-called polymeric structures were discussed in a detailed and comprehensive manner along the following sections of this chapter.

Inspired from a previously described "nanofiber seeding" approach[15] this method's novelty originates from its "in/soluble template and toxic, inorganic oxidative agent free" synthesis route that utilizes various aqueous noble metal salt solutions as the reaction media and

the oxidative agent with self-degrading, oxidative-reactive $V_2O_5$ sol-gel nanofibers as the seeding template. It was also postulated, according to the previously inspired "nanofiber seeding" approach, in this study that the underlying reason of conducting polymer nanofiber formation was mainly due to the addition of nanofiber seeding templates ($V_2O_5$ sol-gel in both cases) at the very early stages of the chemical oxidative reaction of pyrrole monomers. This early addition before the oxidant was considered to be the reason to initiate and guarantee the bulk formation of similar morphology structures during the polymerization reaction as a result of a surface interaction (pre-polymerization) between pyrrole and the seeding template. That is why this approach was called "nanofiber seeding"[17].

### 3.2 Different Characterization and Application Results and Discussions

#### 3.2.1 SEM Characterization Results

Different morphology conducting PPy structures (granules and fibers) were initially characterized by SEM to verify and prove the success of above mentioned, seeding-template-assisted ($V_2O_5$ sol-gel nanofibers) chemical oxidative polymerization approach in aqueous media.

In PPy granule sample's SEM image below, the characteristic spherical formation of PPy molecule aggregates was clearly been exhibited. By the initial addition of $V_2O_5$ sol-gel nanofibers, before the pyrrole monomers and oxidant, to the reaction media let this chemical to generate and maintain the formation of similar structures like itself through a spontaneous pre-polymerization that took place at the interface created between these nanofibers and pyrrole monomers. Thus, when the oxidant, APS, was added to the reaction solution it could initiate the formation of PPy fibers through a rapid oxidation polymerization reaction which was already assisted by $V_2O_5$ sol-gel nanofibers. PPy fibers that were obtained through a same kind of

polymerization reaction, exhibiting the dominant fibrillar morphology through its overall matrix structure, could clearly be observed from the second SEM image below.

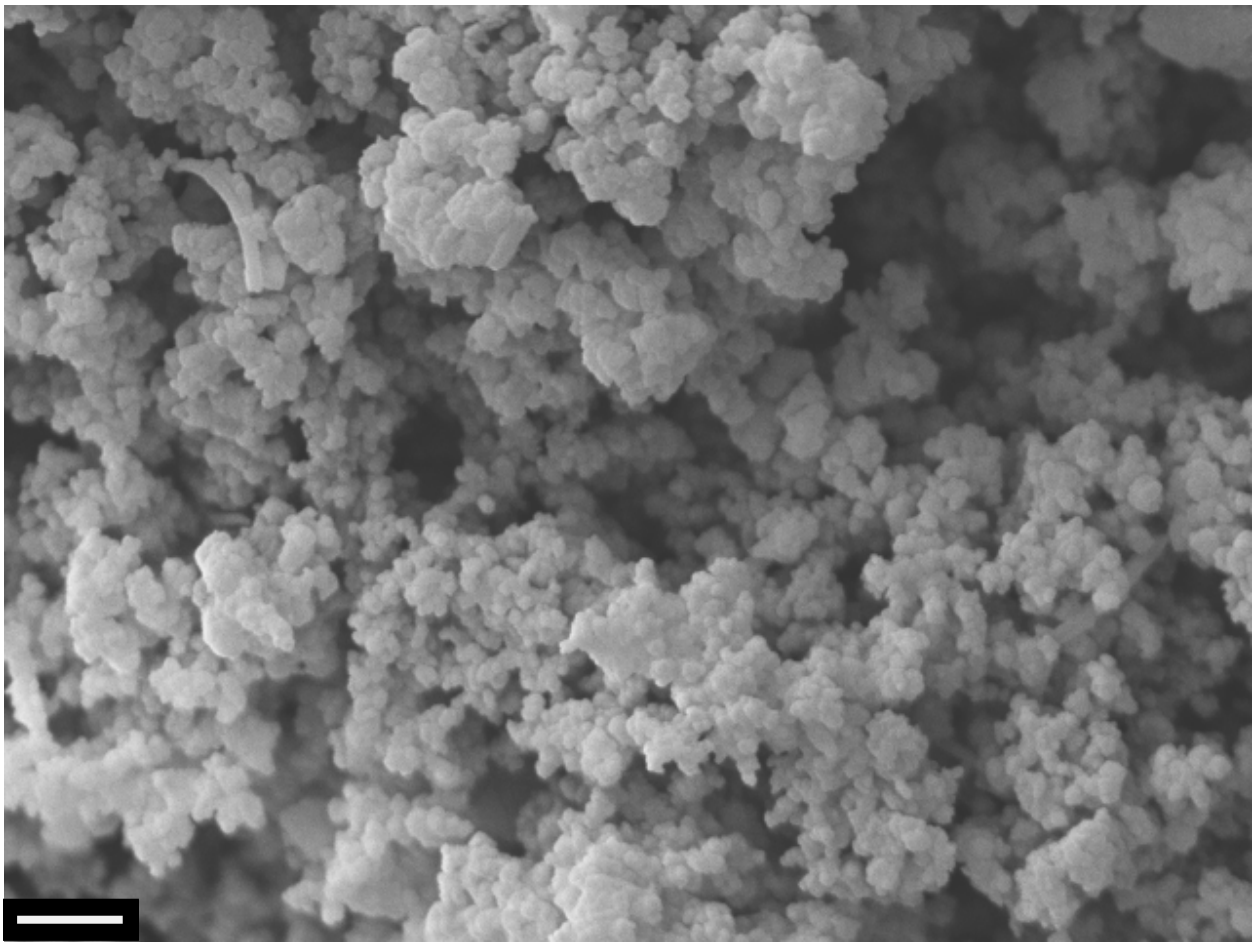

Figure 35 SEM image of PPy granule (scale bar: 2μm)

In conclusion, the success of early mentioned novel, one-step, seeding-template-assisted oxidative polymerization reaction of pyrrole monomers under the control of $V_2O_5$ sol-gel nanofibers has simply been verified through the morphological analysis of same polymers' differently shaped structures, by SEM. By the initial addition of so-called seeding templates to

the reaction media before the monomer and oxidative agent, similar morphology (fibrillar) polymeric structure formations were offered and guaranteed through this approach.

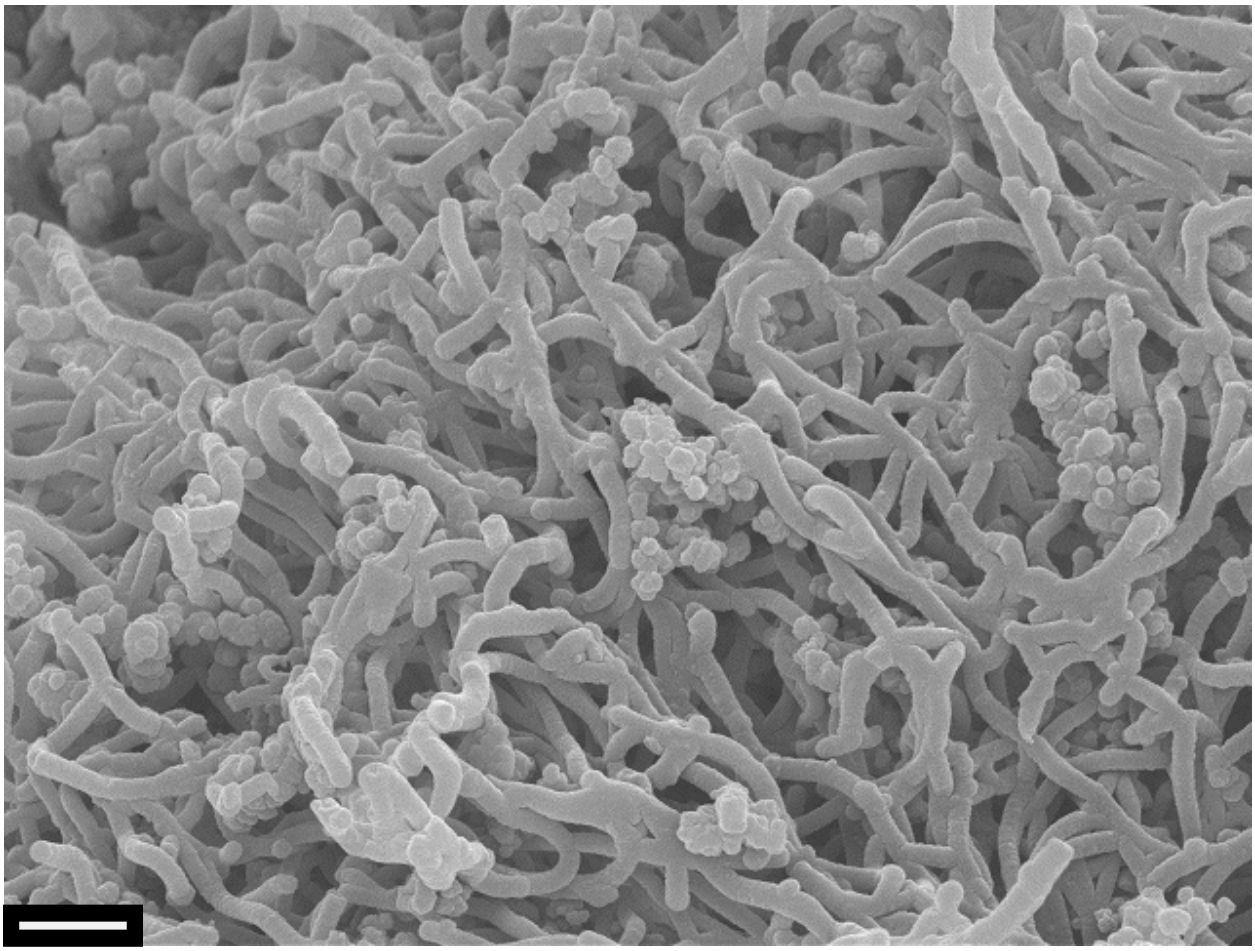

Figure 36 SEM image of PPy fiber (scale bar: 1μm)

As it can clearly be seen from the following SEM images of as prepared nanocomposite samples below, the method followed to obtain nanocomposites (PPy nanofibers that were decorated with noble metal nanoparticles) was also successful. Ten different measurements taken from the arbitrary points of each and every SEM image of nanocomposite structures clearly

proved that there was a very high yield of uniform diameter conducting polymer nanofibers with well dispersed, different sized noble metal nanoparticle particle aggregates among them.

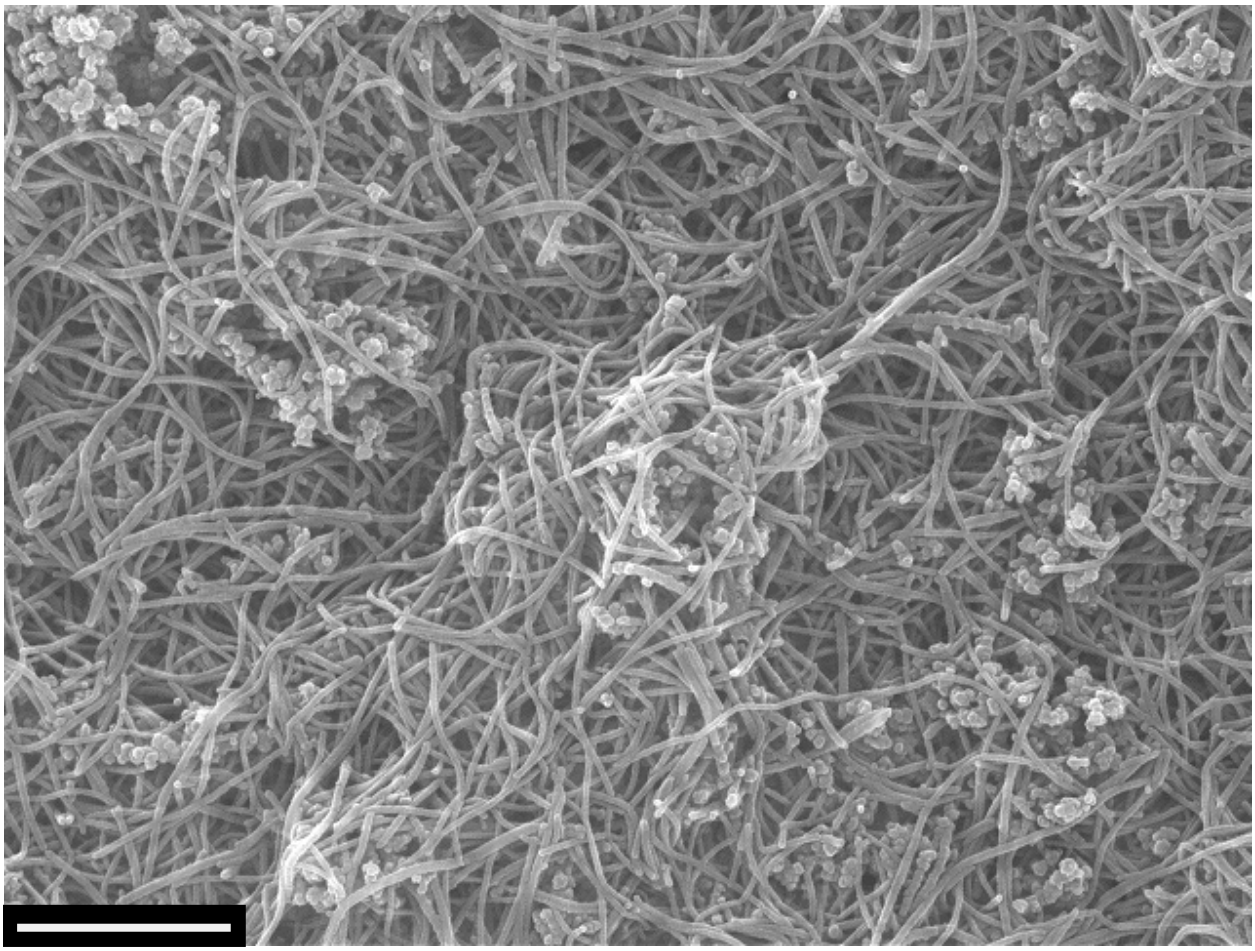

Figure 37 SEM image of PPy/AuCl (0.02M) nanocomposite (scale bar: 1μm)

For the nanocomposites obtained from different concentrated AuCl salt solutions (0.02M, 0.01M and 0.005M) the SEM images were indicating uniformly dispersed and smooth conducting polymer nanofibers having average diameters of 50nm, 50nm and 55nm, respectively. Aggregations of mostly spherical noble metal nanoparticles having several hundred nm average sizes (580nm, 255nm, and 677.5nm, respectively) could also clearly be observed

from those images. The aggregation and dispersion of the noble metal nanoparticles was more uniform at nanocomposite samples obtained from 0.02M solution, but more obvious and dominant at samples obtained from 0.005M solution.

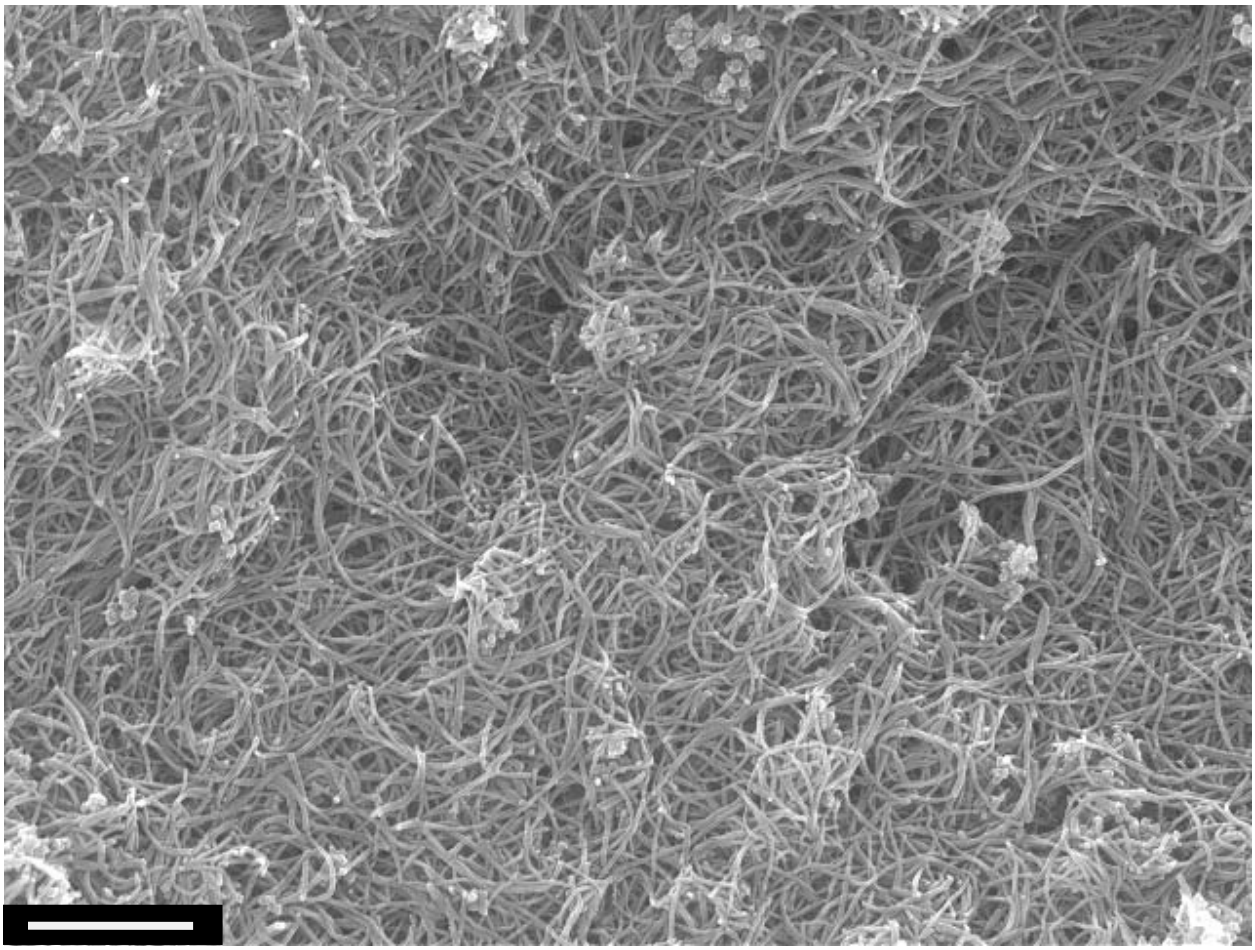

Figure 38 SEM image of PPy/AuCl (0.01M) nanocomposite (scale bar: 1μm)

This was probably related with the changing reaction solution concentrations. Fewer amounts of the noble metal particle nuclei that were ubiquitous in the lowest concentrated noble metal salt solution could not be dispersed and induced through conducting polymer nanofibers during the polymerization reaction. The interactions between different concentrated noble metal

salt solutions and conducting polymer nanofibers could clearly be observed from different SEM images below, according to the final morphologies of the nanocomposite structures.

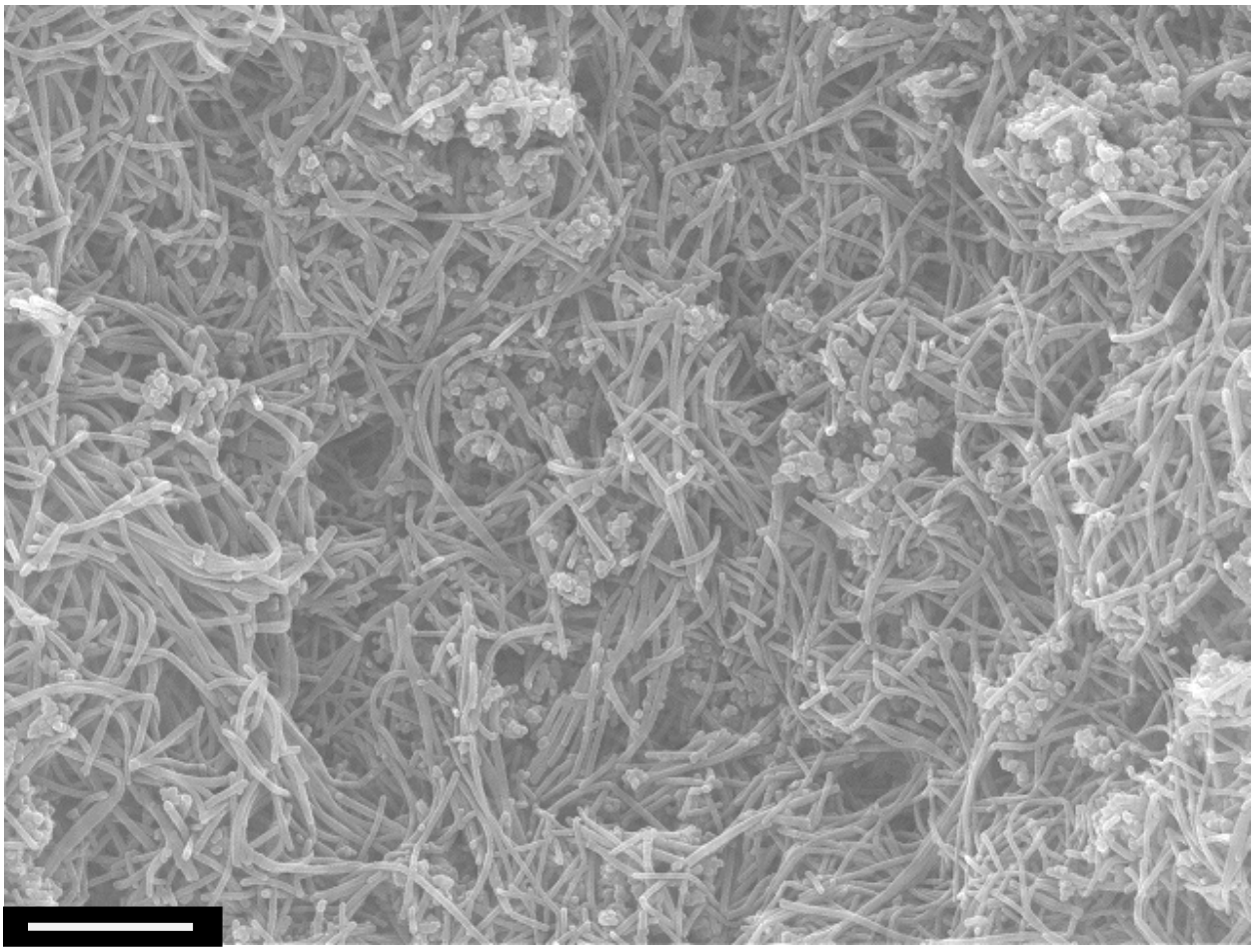

Figure 39 SEM image of PPy/AuCl (0.005M) nanocomposite (scale bar: 1μm)

Reactions in higher concentrated solutions tend to produce longer, thinner and smoother nanofibers of PPy. In such reactions, the resulting PPy nanofibers were utilized to fabricate noble metal nanoparticles via in-situ deposition[12]. Thus, if the solution concentration is higher, then it becomes easier to form nanofibers (with the higher oxidation potential of the solution) that can manipulate the dispersion and dimensions of the metal nanoparticles and their aggregates.

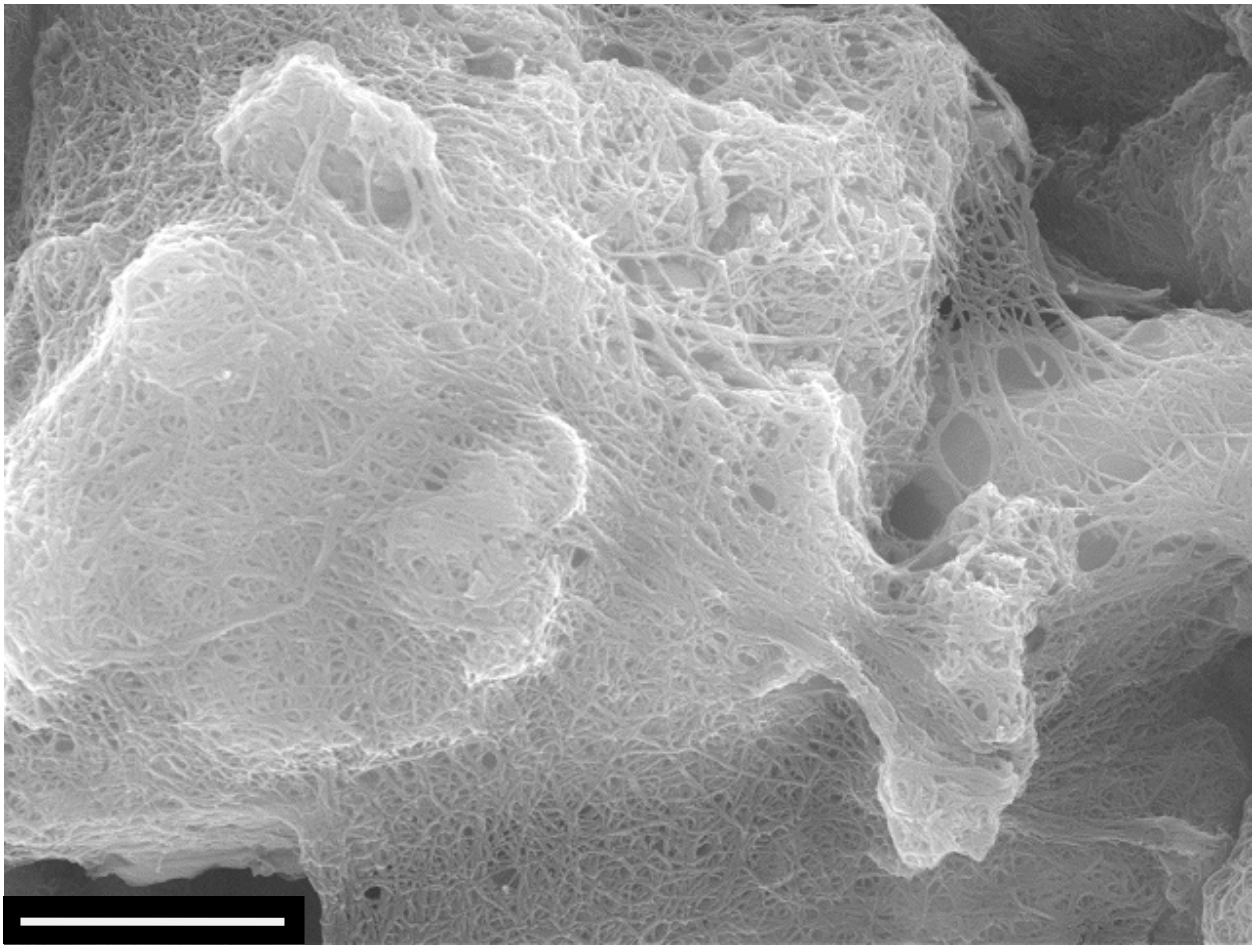

Figure 40 SEM image of PPy/$HAuCl_4$ (0.02M) nanocomposite (scale bar: 1μm)

In contrast, when a lower concentrated noble metal salt solution was used for polymerization then the resulting nanofibers became shorter in length, thicker in diameter and less effective for manipulating the dispersion and dimensions of the noble metal nanoparticles.

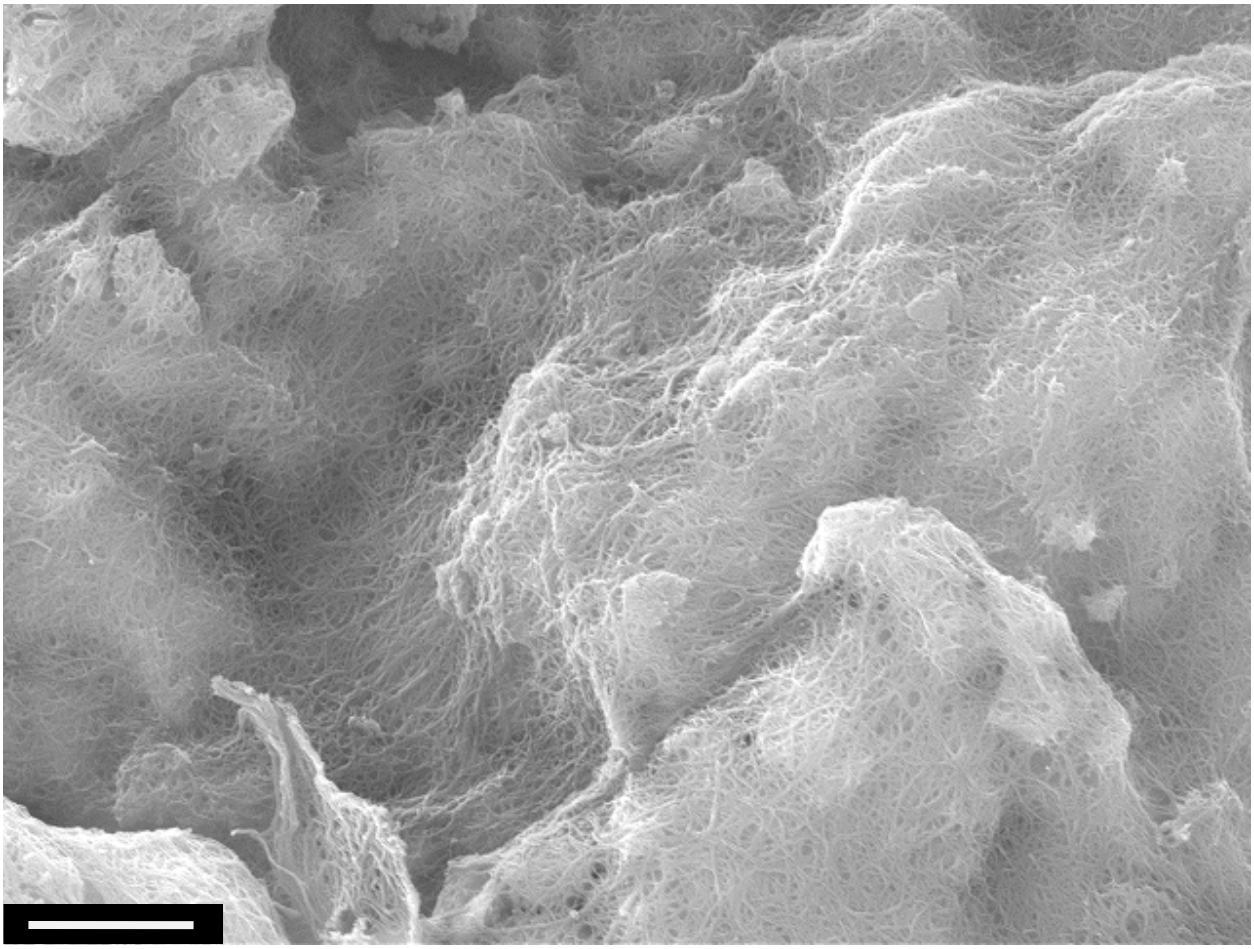

Figure 41 SEM image of PPy/$HAuCl_4$ (0.01M) nanocomposite (scale bar: 1μm)

Nanocomposites obtained from different concentrated $HAuCl_4.3H_2O$ salt solutions were exhibiting unique stereoscopic[12] web-like structures. These structures were obtained a result of a uniform nanofiber dispersion that was coating the surface of the aggregated noble metal nanoparticles. It was really hard to point these aggregates within the nanocomposite structures. They could barely be located by just visualizing their irregular solid morphologies under the web-like nanofibers.

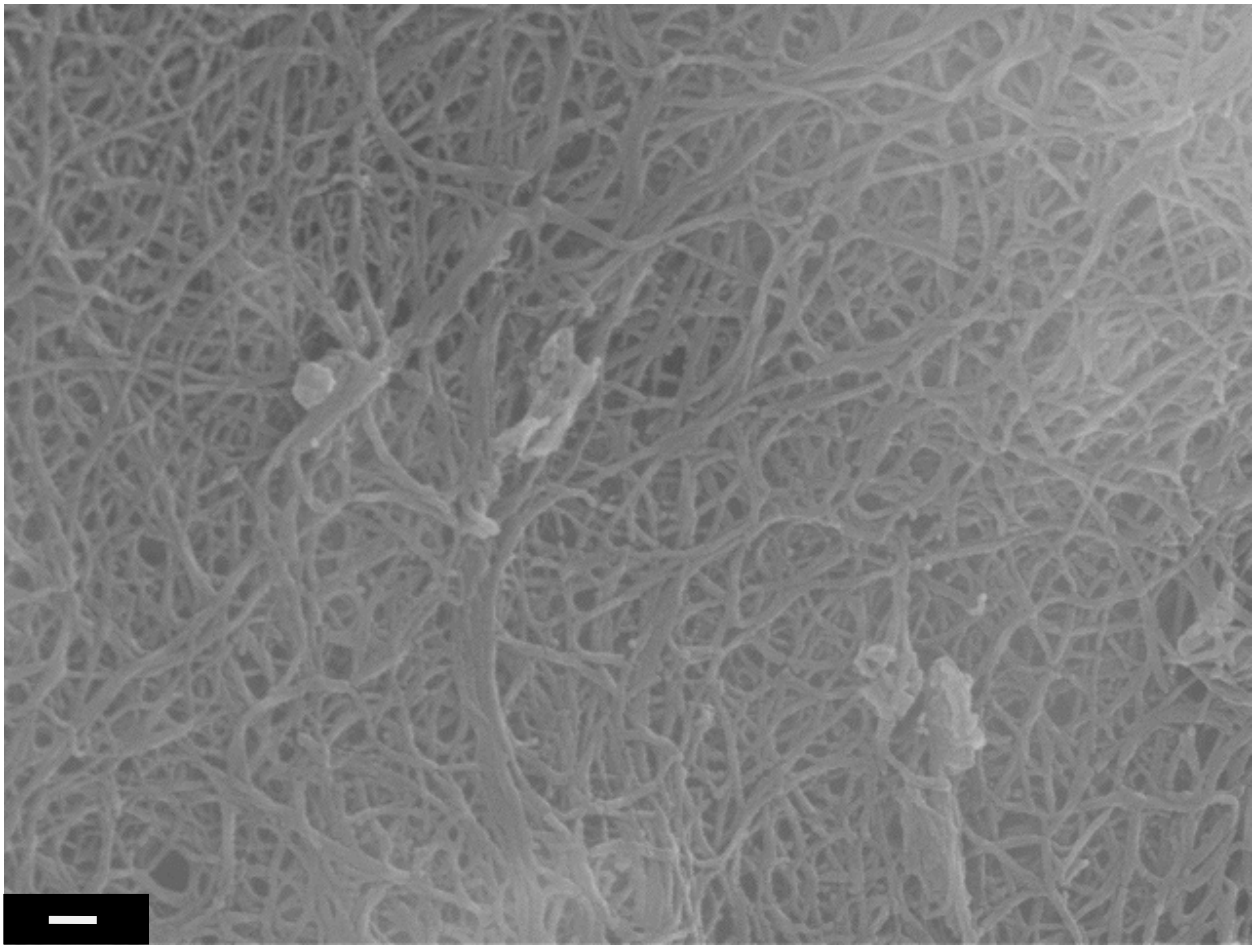

Figure 42 SEM image of PPy/$HAuCl_4$ (0.005M) nanocomposite (scale bar: 100nm)

The same, uniform fiber diameter dispersion was also dominant for these nanocomposites like in PPy/AuCl ones. According to the arbitrary measurements taken from the SEM images of these nanostructures; average nanofiber diameters were 27nm, 25nm and 23nm for the metal salt solution concentrations of 0.02M, 0.01M and 0.005M, respectively.

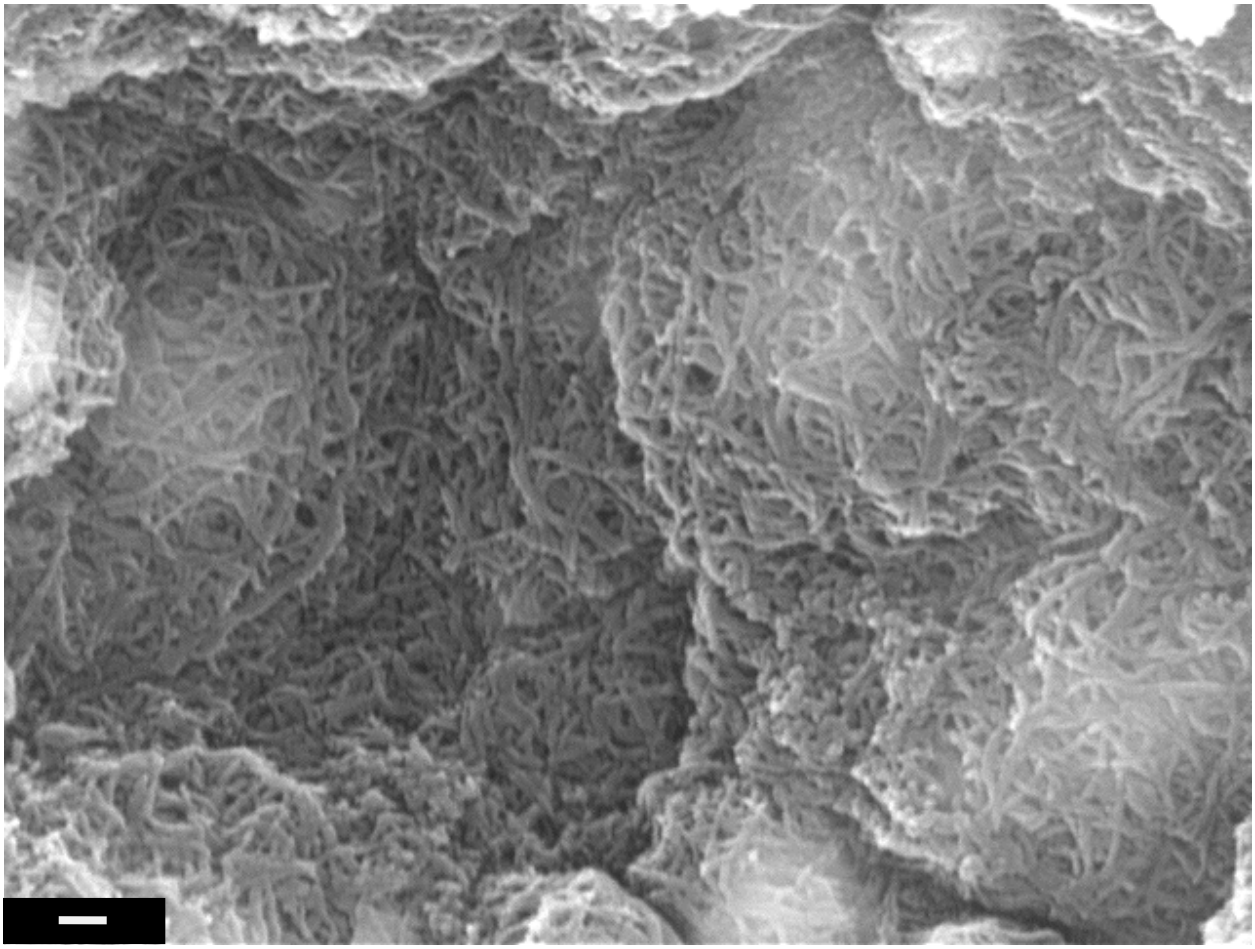

Figure 43 SEM image of PPy/$PtCl_2$ (0.02M) nanocomposite (scale bar: 100nm)

As the solution concentration was decreased, obtained nanofiber diameters were also decreased by remaining their web-like structures for these nanocomposites. Then it became much easier to locate the noble metal nanoparticle aggregates within the nanocomposite structures.

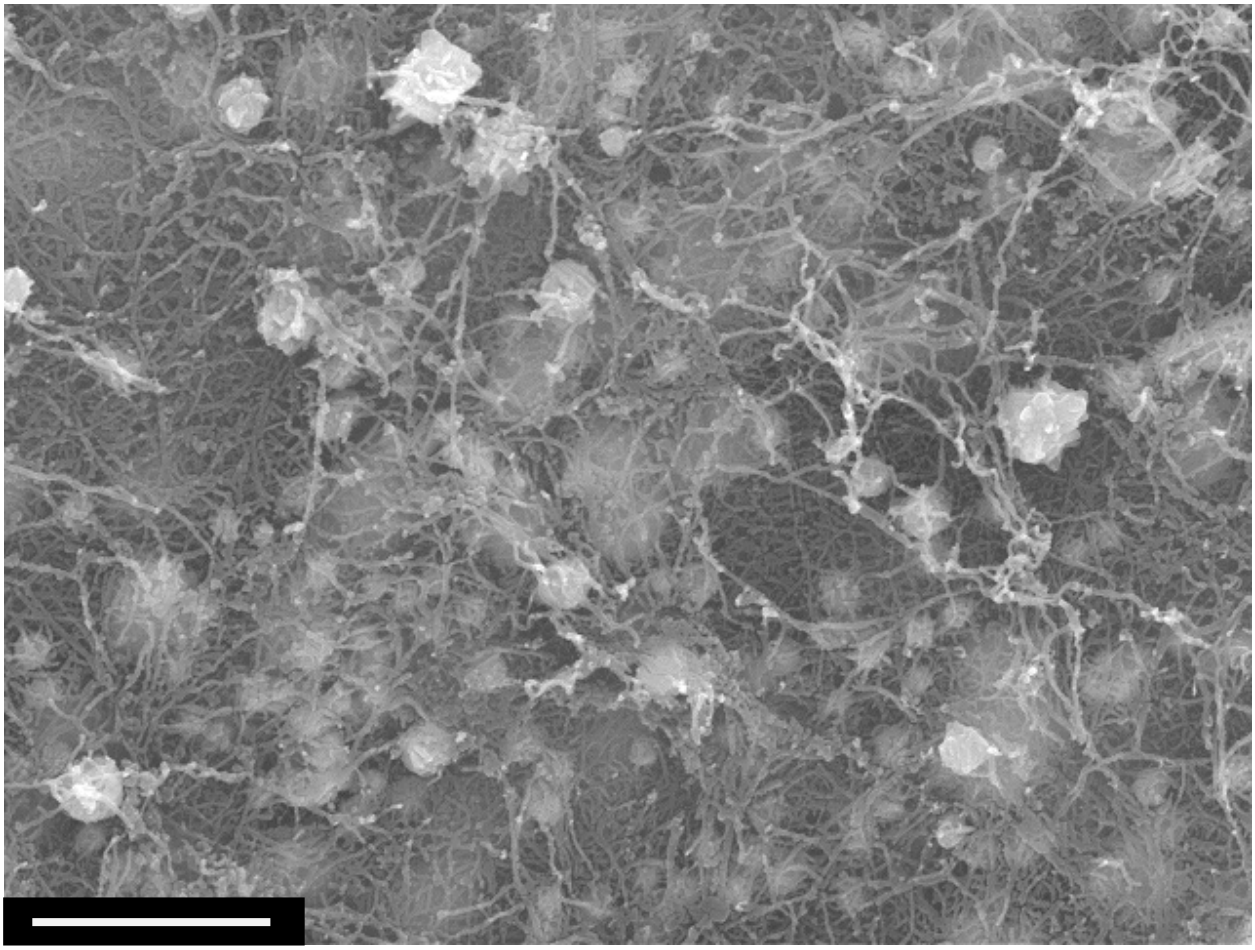

Figure 44 SEM image of PPy/$PtCl_2$ (0.01M) nanocomposite (scale bar: 1μm)

The dispersion of noble metal nanoparticle aggregates were seemed to be more uniform in nanocomposite structures obtained from less concentrated solutions. The average sizes of such structures were 507nm, 446nm and 193nm, respectively for the samples from 0.02M, 0.01M and 0.005M noble metal salt solutions.

In contrast to its higher concentrated versions, it was possible to easily observe a fewer amount of aggregated noble metal nanoparticles in the nanocomposite structure obtained from 0.005M noble metal salt solution which was also exhibiting an obvious, uniform and traditional web-like nanofiber formation.

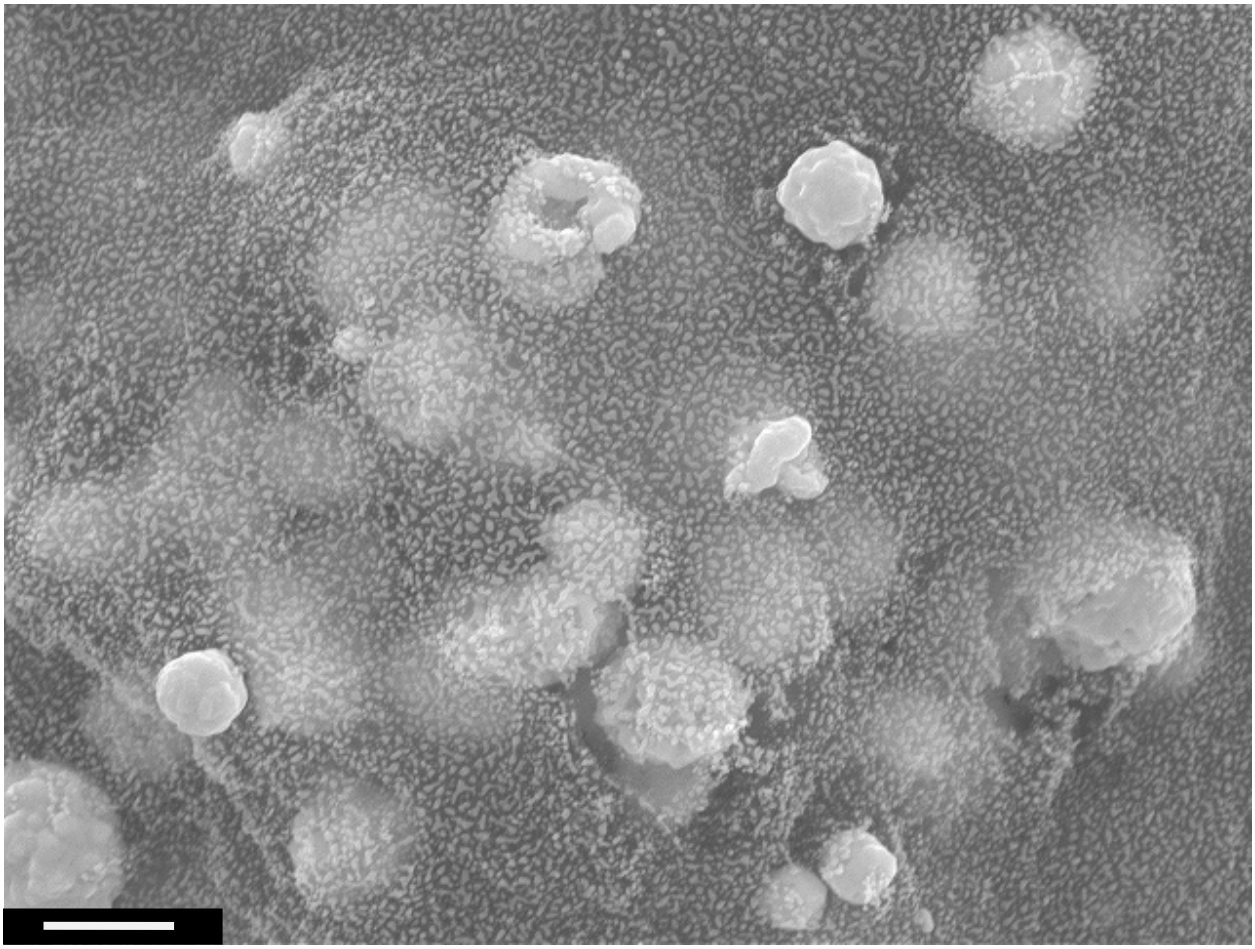

Figure 45 SEM image of PPy/$PtCl_2$ (0.005M) nanocomposite (scale bar: 1μm)

Here, according to a general phenomenon, one key property that determined the final morphology of the conducting polymer nanofibers and aggregated noble metal nanoparticles was the reduction/oxidation potential relationship of both sides.

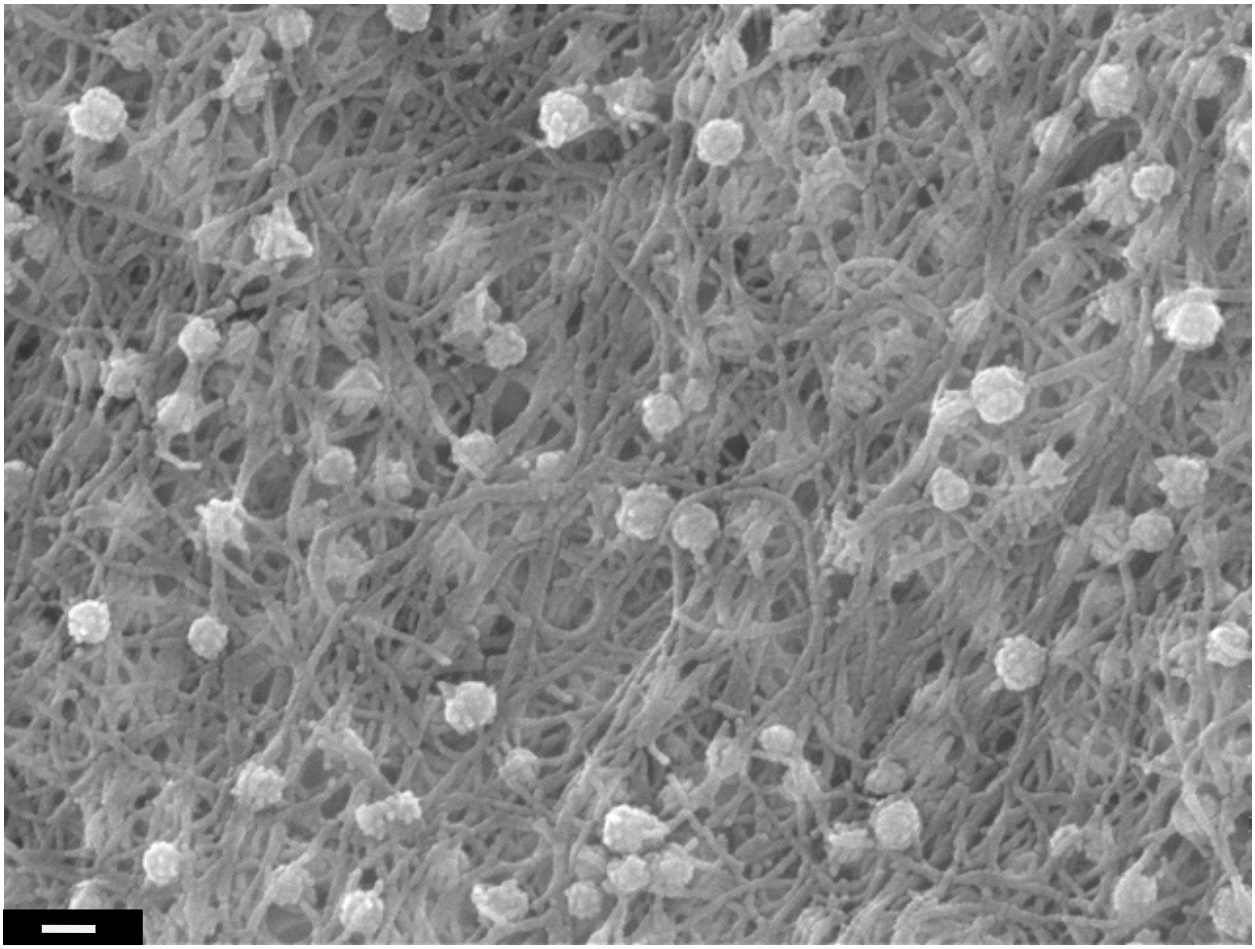

Figure 46 SEM image of PPy/$PtCl_4$ (0.02M) nanocomposite (scale bar: 100nm)

The oxidation potential provided by the noble metal salts was utilized to initiate the polymerization of pyrrole. Likewise, the reduction potential provided by the conducting polymer (PPy) supplies the necessary electrons to reduce the noble metal ions to particles, through a nucleation reaction. Therefore, the redox potential of the conducting polymer must be negative of the standard potential of the noble metal complex[14] or vice versa.

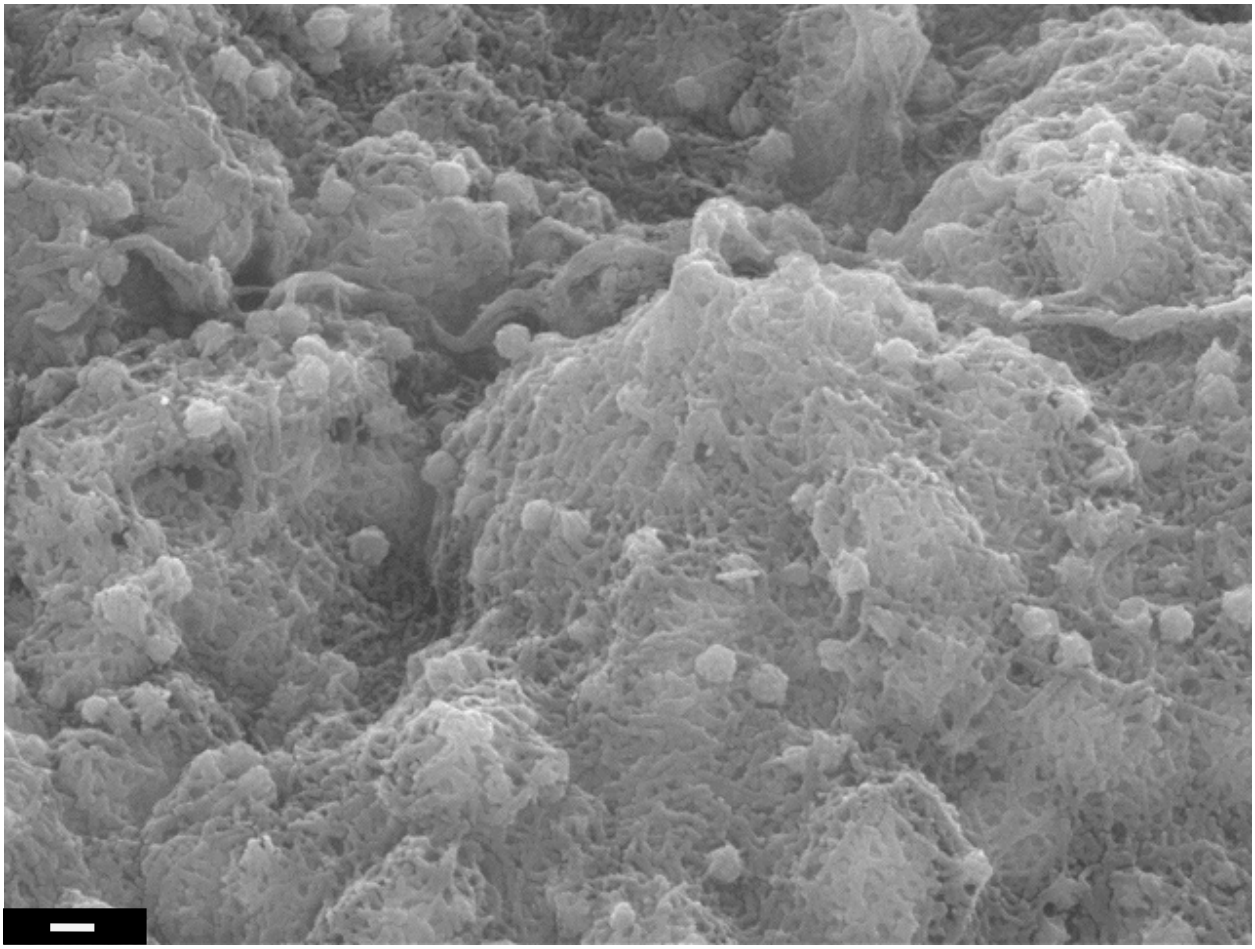

Figure 47 SEM image of PPy/$PtCl_4$ (0.01M) nanocomposite (scale bar: 100nm)

Similarly to the previous structures, PPy/$PtCl_2$ nanocomposites were also exhibiting a very dense nanofiber formation and hardly defined noble metal nanoparticle aggregations (almost impossible to locate). For the highest concentrated noble metal salt solution, the nanocomposite sample obtained was composed of obvious -but not uniform- and irregularly shaped nanofibers that were covering the hidden noble metal nanoparticles whose surface could barely be seen as silhouettes by shining brighter than the nanocomposite matrix.

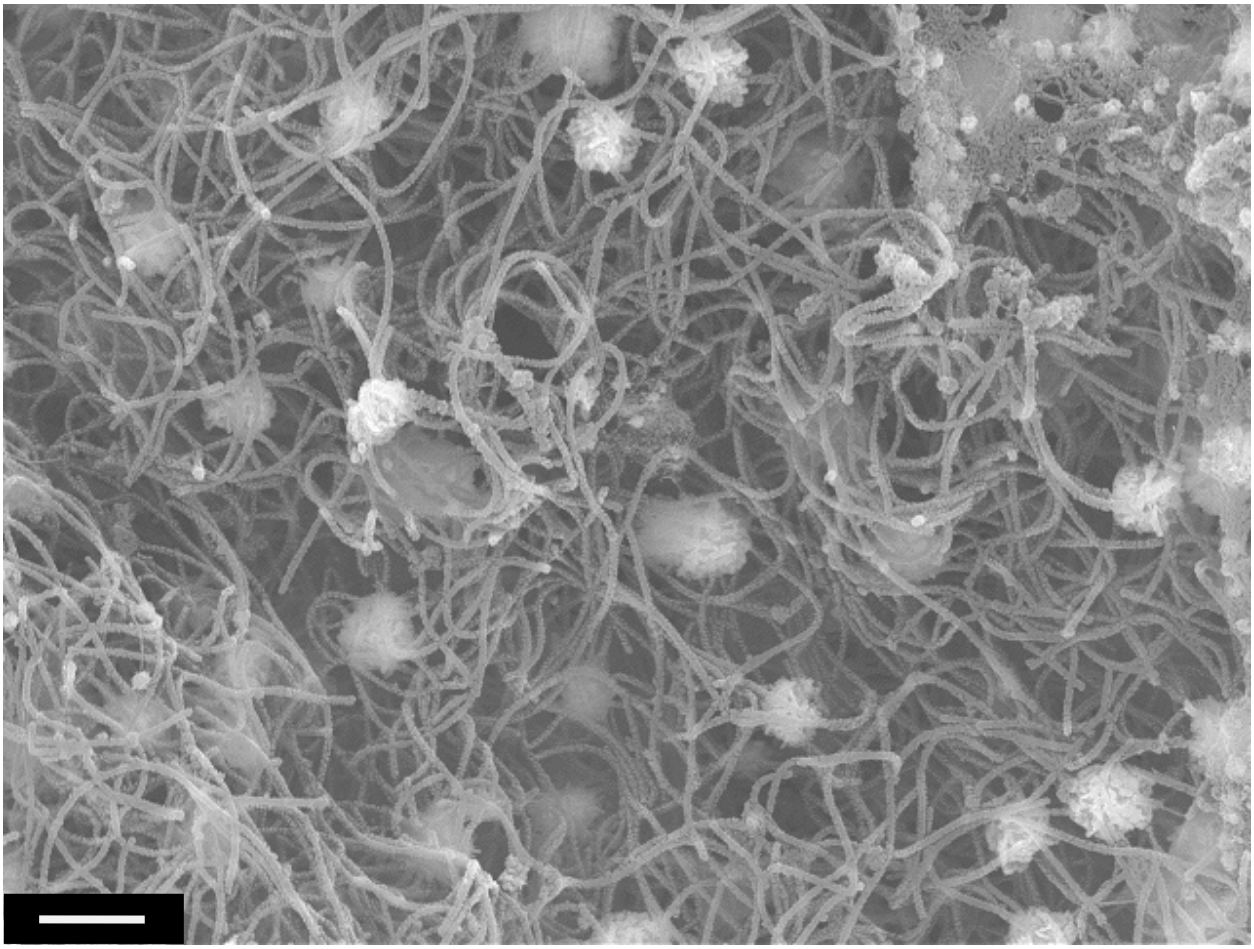

Figure 48 SEM image of PPy/$PtCl_4$ (0.005M) nanocomposite (scale bar: 1μm)

As the solution concentration was decreased to 0.01M a remarkable change in the nanocomposite morphology was observed. Both nanofibers and noble metal nanoparticle aggregates in this structure became more regular and obvious. The dense, web-like characteristic of the nanocomposite matrix left its place to the individual, wrinkled nanofibers and mostly spherical shaped noble metal nanoparticles.

The main reason of this change in the nanocomposite morphology was believed to be directly related with the previously mentioned phenomenon about the red./ox. potentials. At higher concentrations (0.02M) the oxidation potential was also high, that is why monomers were

tending to form bulk and dense, web-like nanofiber structures when they were added to the reaction media under the control of nanofiber seeding templates. At moderate concentrations (0.01M) the oxidation potential was decreased and more balanced formation and distribution of nanofiber structures could be obtained.

However, at low concentrations (0.005M), sometimes the oxidation potential of the solution does not enough to trigger the polymerization reaction to produce nanofibers, as it could clearly be seen from the SEM image. For this nanocomposite, the matrix structure was composed of irregular shaped and uniformly dispersed conducting polymer nanostructures that were covering the mostly spherical shaped noble metal nanoparticle aggregates whose surface silhouettes could be observed on and under the nanocomposite matrix. On the average, conducting polymer nanostructures (fibers, particles) having 23nm, 26nm and 70nm diameters and 261nm, 276nm and 847nm surface areas were detected at the SEM images of nanocomposites obtained from three different concentrated noble metal salt solutions of $PtCl_2$.

When the SEM images of the nanocomposites obtained from three different $PtCl_4$ salt solutions were investigated; the similar web-like and dense nanofiber formation was clearly observed for higher concentration (0.02M). Nanofiber formation was uniform and composed of continuous long fibers, which were mostly stacked together, with the average diameters of 21nm. Noble metal nanoparticle aggregates with 98nm average sizes and uniform spherical morphologies were well dispersed among those nanofibers.

As the noble metal salt solution concentration was decreased to 0.01M there was an increasing trend observed for the formation of irregularly shaped and more stacked nanofibers. It was hard to define certain diameter values for these nanofibers but they were obviously thicker than the previous ones (averagely ~24nm). However, the noble metal nanoparticles with

spherical shapes were still well dispersed among these nanofibers. Their sizes were slightly larger than the previous ones (~103nm).

In contrast, nanocomposites from the lowest concentration (0.005M) solution were exhibiting more individualized nanofiber formation rather than web-like with larger diameters of ~74nm. However, these nanofibers were not seemed solid like the ones from higher concentrated solutions. It was postulated that this situation was again directly related with the redox phenomenon mentioned before. The lower oxidation potential of lower concentrated noble metal salt solution could barely trigger the polymerization of pyrrole and caused to form this type of individual nanofibers that were not solid and not stacked together. Noble metal nanoparticle aggregations were again well dispersed among those nanofibers by exhibiting mostly spherical morphologies in a wide range of particle sizes (~770nm average).

Morphologically controlled, bulk PPy nanofibers' and different noble metals' nanoparticle aggregations formation were explained, according to the SEM images of nanocomposite samples obtained from different concentrated noble metal salt solutions, through the oxidation/reduction phenomenon and the interactions between the two major compounds of these structures.

In summary, the overall SEM characterization of as-prepared nanocomposites was conforming the success of the mechanism of this novel, one-step, and nanofiber seeding-template-assisted chemical oxidative polymerization of pyrrole monomers in different aqueous noble metal salt solutions to obtain PPy nanofibers that were decorated with noble metal nanoparticles. The phenomenon of controlling the morphology of conducting polymers from nanospheres to nanofibers, and also the size of the noble metal nanoparticle aggregates was accomplished by changing the noble metal salt (oxidative agent and dopant) solution

concentrations and by using seeding templates exhibiting the targeted morphology, in such reactions.

### 3.2.2 TEM Characterization Results

To be able to obtain advanced morphological characterization results of different nanocomposite structures and to verify the noble metal aggregations within them; additional TEM images, which were taken with PPy/$PtCl_2$ and PPy/$PtCl_4$ nanocomposites obtained from 0.01M reaction solutions, were utilized due to their better representation of nanocomposite structures.

According to the TEM image of PPy/$PtCl_2$ (0.01M) nanocomposite; the web-like, dense nanofiber formation among the irregularly shaped noble metal nanoparticle aggregates was clearly observed. Long and individual nanofibers could also easily be noticed besides their traditional web-like formation. These two general results were matching the ones obtained from the SEM characterization of the same nanocomposite samples. Even very small sized noble metal nanoparticles (whose surfaces could only be visualized as silhouettes in the SEM images) that were aggregated among the densely packed nanofibers, could clearly be seen in the TEM images below.

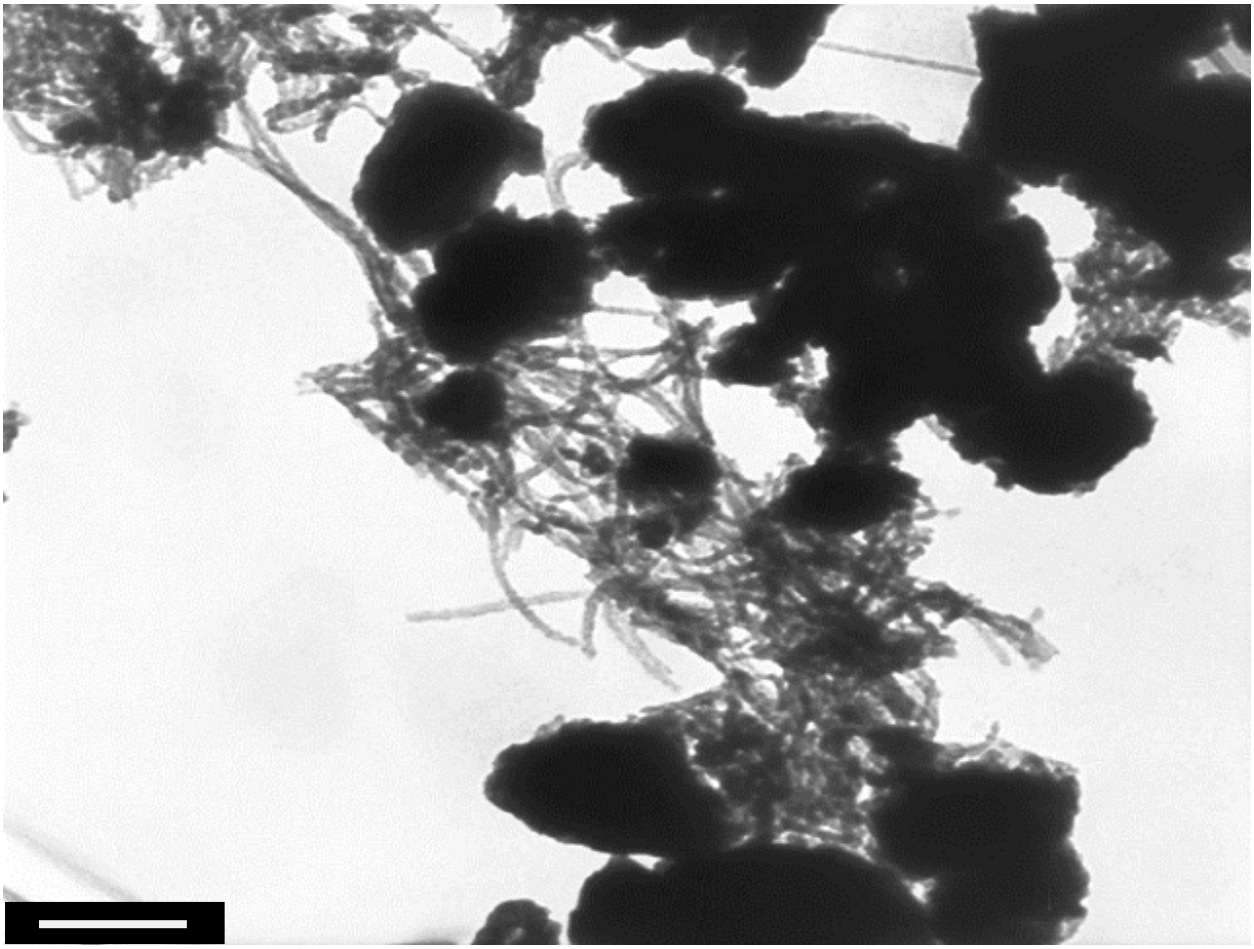

Figure 49 TEM image of PPy/$PtCl_2$ (0.01M) nanocomposite (scale bar: 200nm)

Secondly, the TEM images taken from the PPy/$PtCl_4$ nanocomposites were investigated to be able to understand the morphological characteristics of the nanocomposite structure better. The images were clearly exhibiting the individual rod-like nanofiber formations that were uniformly dispersed among the irregularly aggregated noble metal nanoparticles in different sizes.

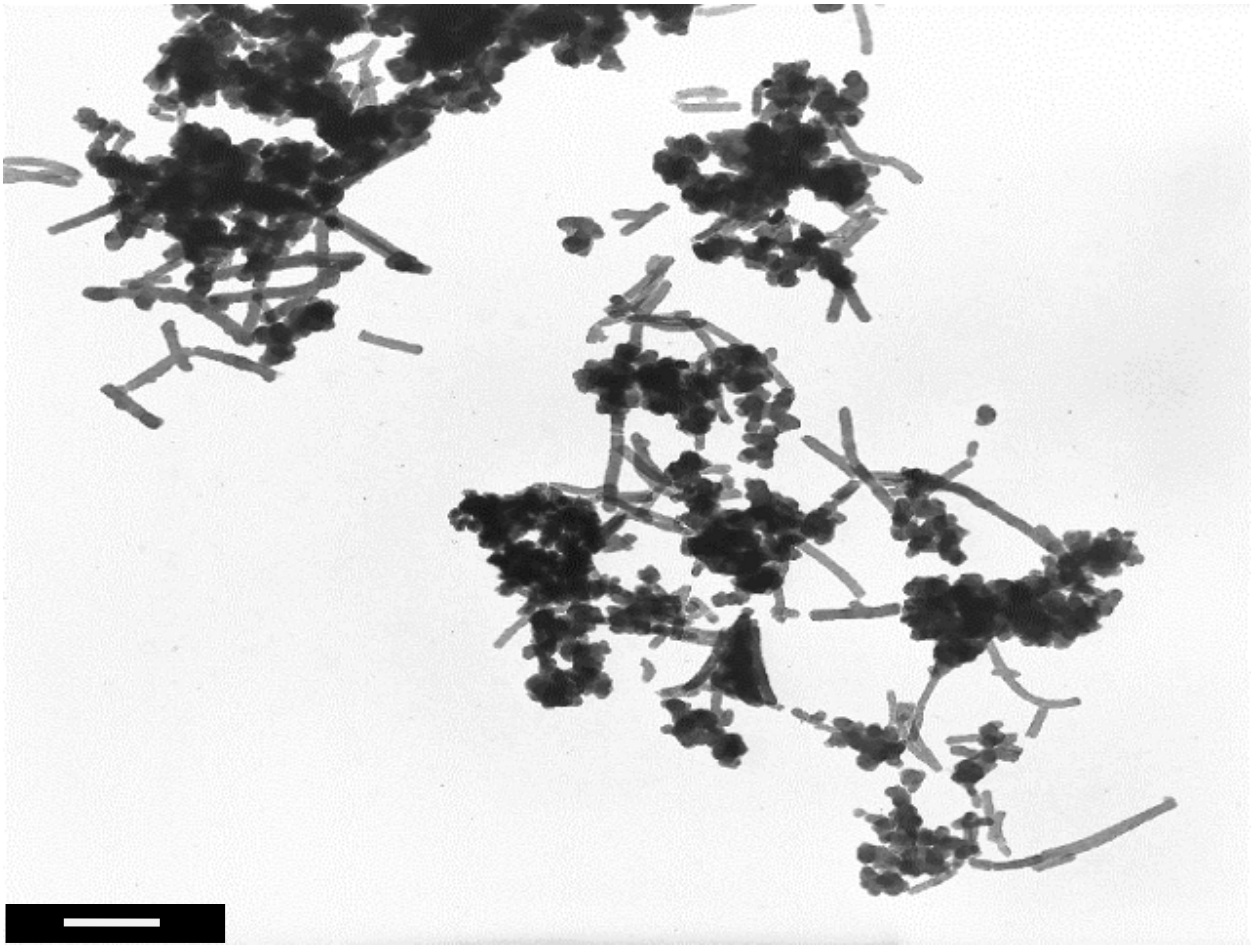

Figure 50 TEM image of PPy/$PtCl_4$ (0.01M) nanocomposite (scale bar: 250nm)

The TEM images of the same nanocomposite structure that were taken at higher magnifications were helped to comprehend the morphological properties better. Uniform and individual nanofibers that were stacked together among the aggregated, mostly spherical, noble metal nanoparticles could clearly be observed from the TEM image below.

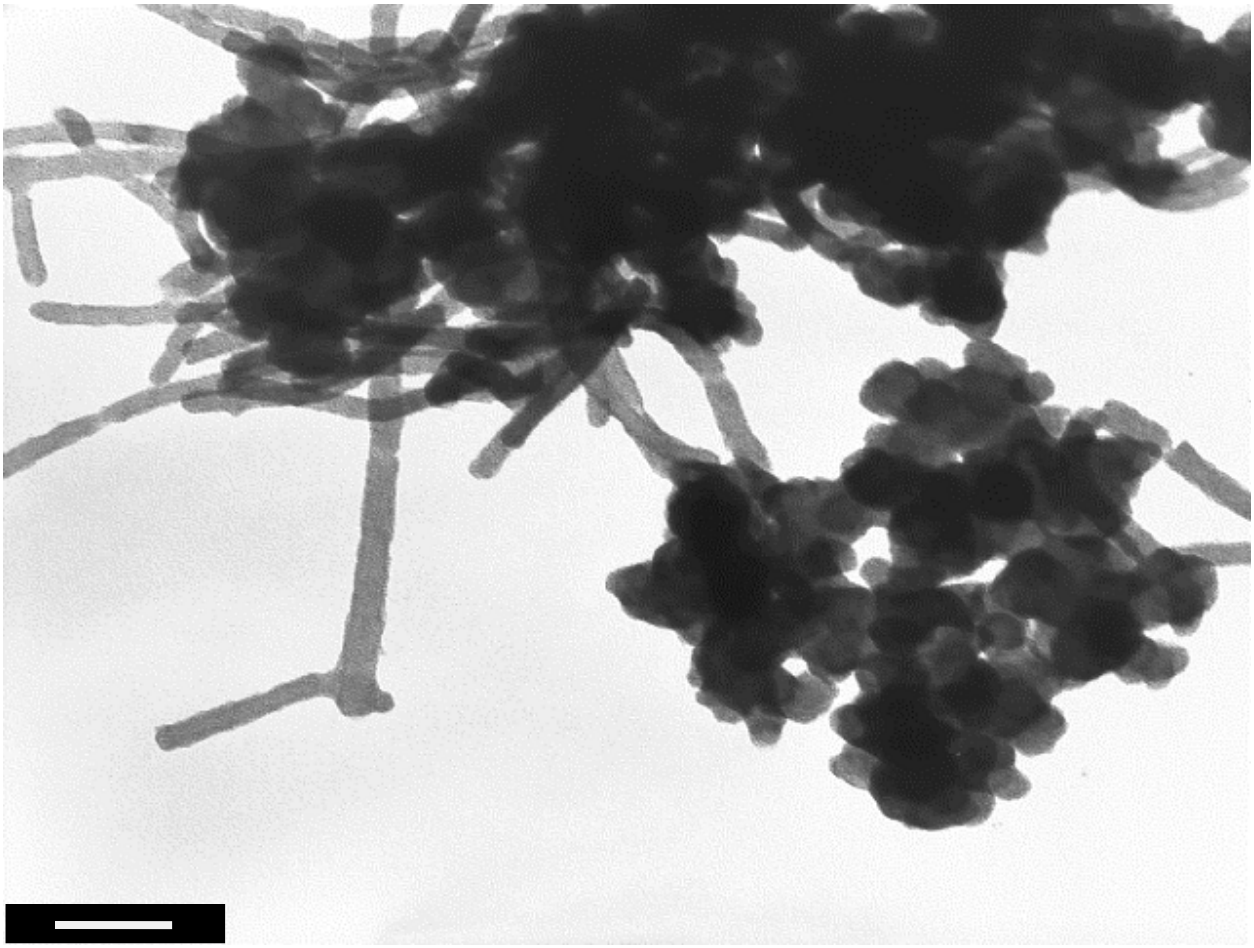

Figure 51 TEM image of PPy/$PtCl_4$ (0.01M) nanocomposite (scale bar: 100nm)

Similar morphological characteristics of the same nanocomposite structure was represented, in a more compatible manner by benefiting the measurements taken from the TEM images, at the higher magnification TEM image below. As a result of their web-like stacking characteristics conducting polymer nanofibers were filling the spaces between the noble metal nanoparticles that were composed of mostly spherical aggregates in different sizes.

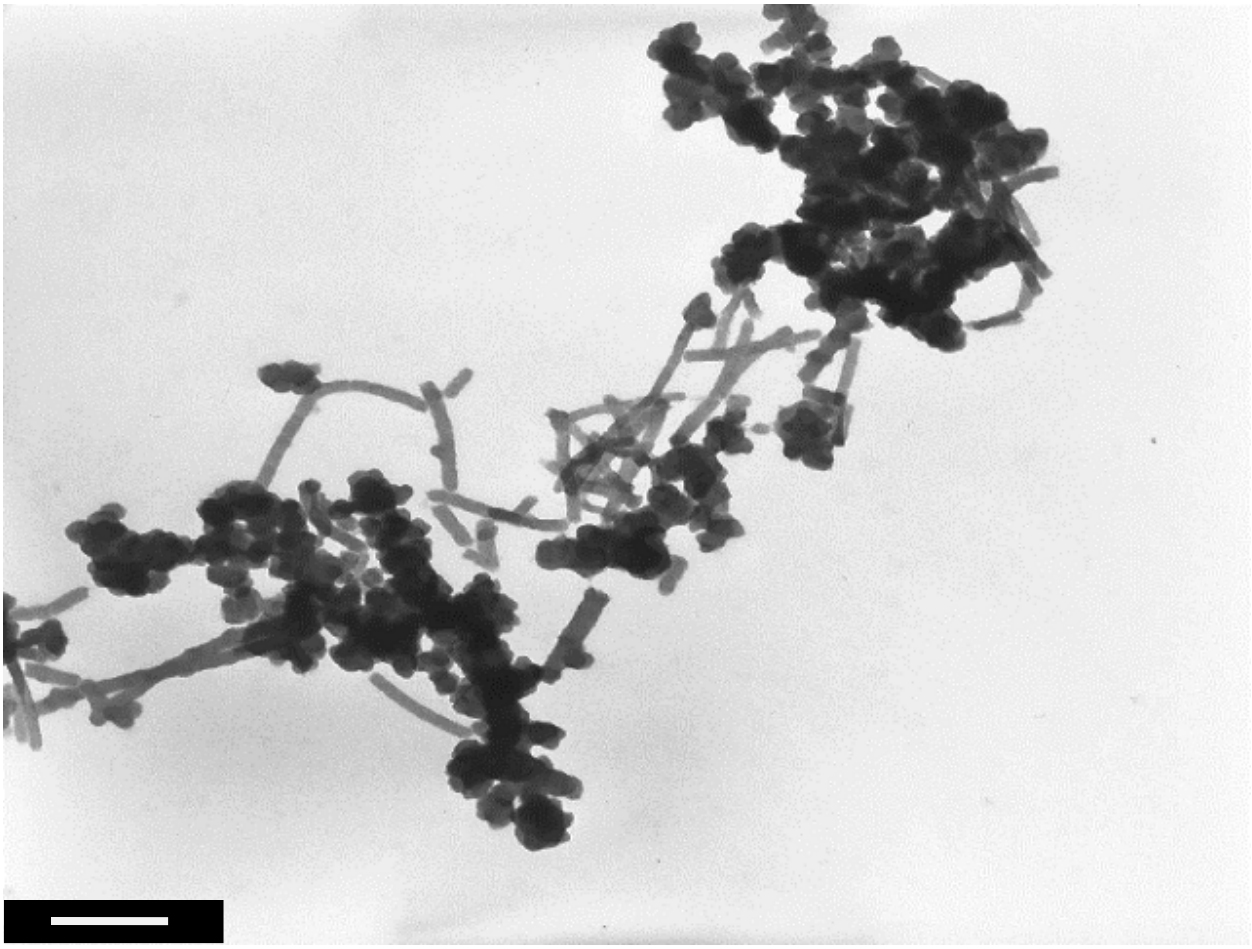

Figure 52 TEM image of PPy/$PtCl_4$ (0.01M) nanocomposite (scale bar: 250nm)

It can be summarized, according to the arbitrary measurements taken from the TEM images of different nanocomposites, that the SEM and TEM results were compatible and complementary for each other in terms of nanofiber formation, diameter and the noble metal nanoparticle dimensions for different nanocomposite structures.

### 3.2.3 TGA Characterization Results

Albeit the TEM characterization could offer a very detailed information about the overall morphological properties of the as-prepared nanocomposites, this technique still could not able to quantify the bulk noble metal nanoparticles that were located widespread in the

nanocomposite structure[10]. Therefore, in order to quantify those noble metal nanoparticles' content in each and every nanocomposite structure, thermal characterization was applied by using the TGA instrument in a way that was described earlier.

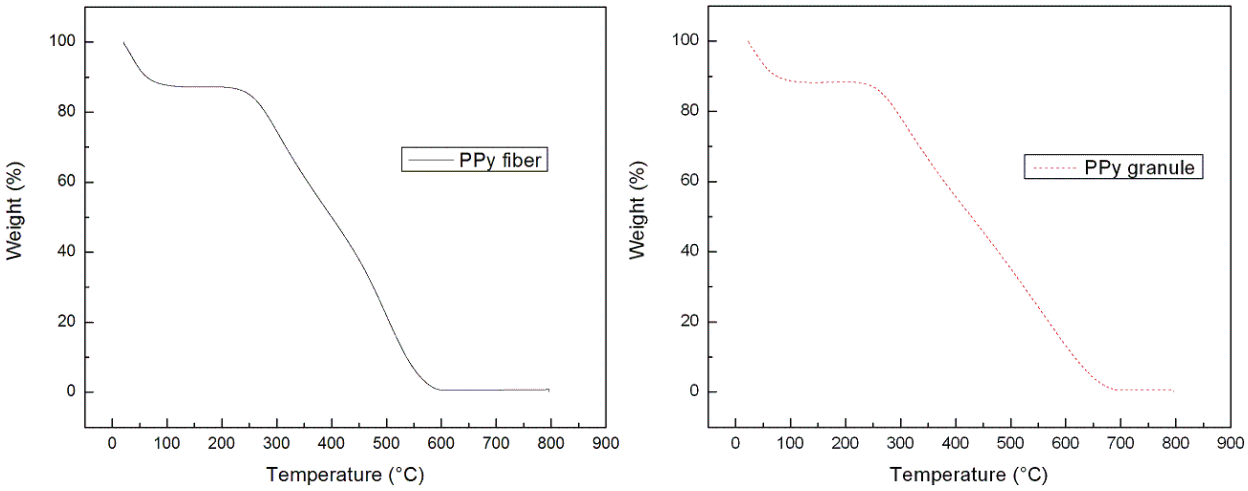


Figure 53 TGA graphics of PPy fiber and PPy granule

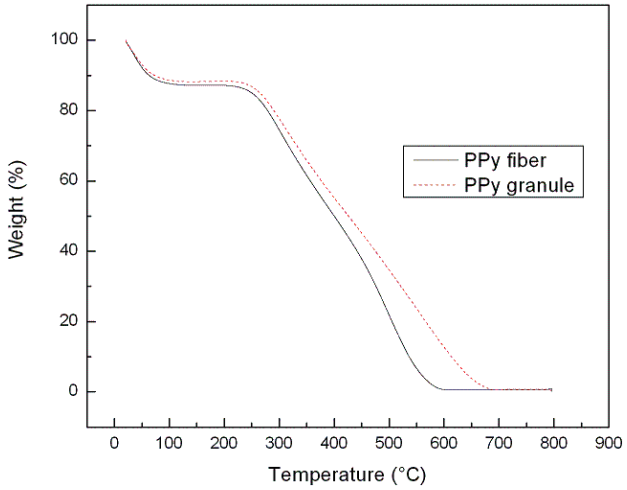


Figure 54 Comparative TGA graphics of PPy fiber and PPy granule

As the control data to be compared with the nanocomposite structures' thermal characterization, PPy fiber and granule samples were also utilized for this study. All the collected thermal characterization results were explained in a comparative way and in details through the following paragraphs of this section.

The first TGA results obtained from the control samples of PPy fiber and granule, respectively. So-called graphics were following a very similar trend with slight differences in their thermal stability and decomposition temperature values. According to the TGA graphic of PPy fiber represented with black color, ~12% of the sample weight was lost during the initial heating between the beginning temperature to 100ºC, which was supposed to be the weight of the moisture that was stored within the polymeric structure. Decomposition of the sample was started around 250ºC and the sample weight was steadily decreased as the temperature was increased up to 600ºC.

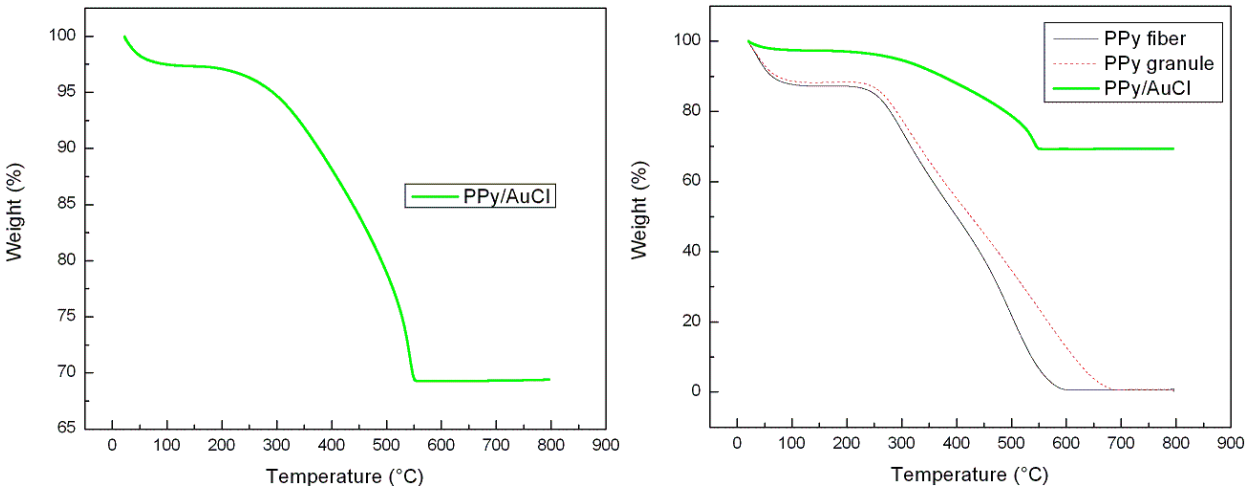


Figure 55 Comparative TGA graphics of PPy/AuCl nanocomposite with PPy fiber and PPy granule

The major weight loss from the sample (~88%) was observed between the temperatures of 200ºC to 600ºC (averagely from 315ºC to 539ºC). Finally, there was no sample left in the TGA pan and the weight % reading from the graphic was showing zero.

When the TGA graphic obtained from the PPy granules (represented with dashed red color) was investigated, less amount of weight loss (~11%) was observed at the beginning, between the initial temperature to 100ºC. It was probably because of the less humidity that was stored within the smaller surface area of PPy granule molecules than fibers. The sample weight became constant for a little while between the temperatures of 100ºC to 250ºC, and then the structure started losing weight at a higher rate than the PPy fiber sample, upon futher heating.

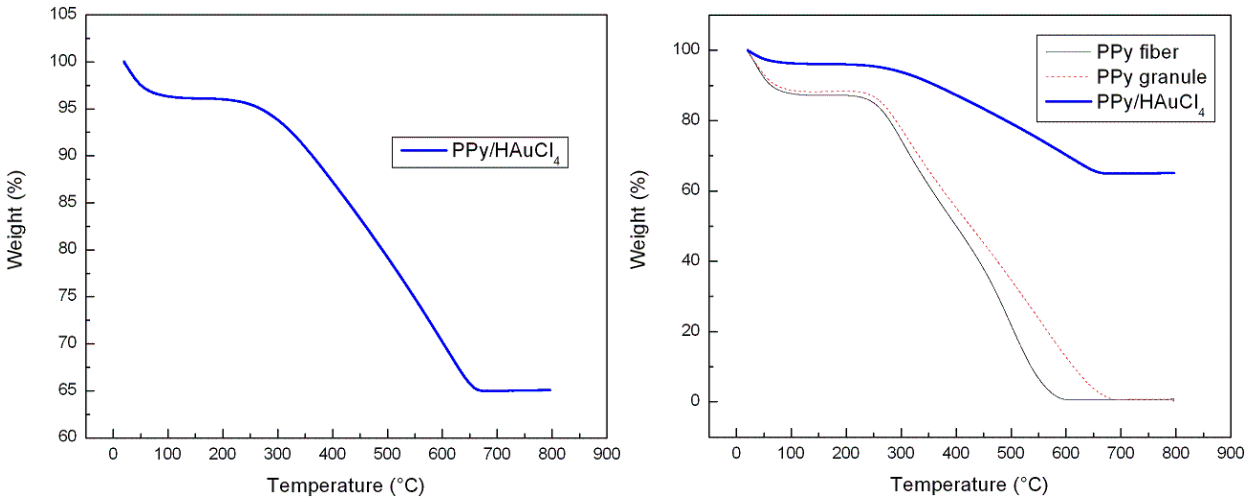


Figure 56 Comparative TGA graphics of $PPy/HAuCl_4$ nanocomposite with PPy fiber and PPy granule

From 200ºC to 700ºC, 89% of the sample weight was gone because of this quick decomposition, between the average temperatures of 260ºC to 573ºC, took place. Finally, same as the PPy fiber, the PPy granule sample's weight % was also reached to zero at the end of the

experiment. By comparing the final decomposition temperatures they last and their rates of decomposition, it could be summarized from these two different morphology polymeric structures' thermal characterization results that PPy fiber samples were exhibiting less thermal stability than the PPy granule samples.

After the thermal characterization of PPy fiber and granule samples, each and every nanocomposite obtained from standard (0.02M) noble metal salt solutions was also thermally characterized in a comparative way with these two different morphology PPy structures.

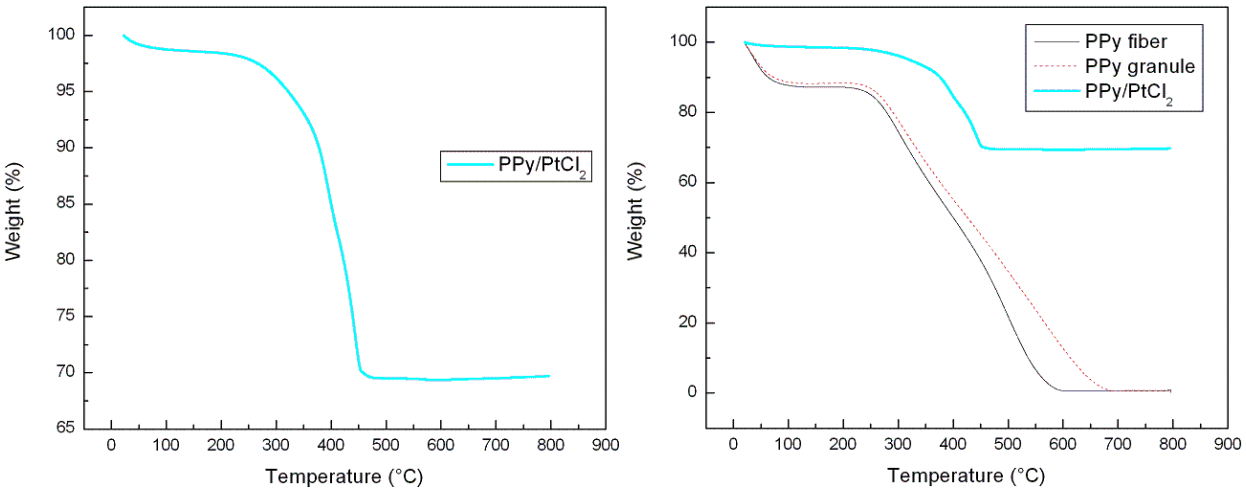


Figure 57 Comparative TGA graphics of $PPy/PtCl_2$ nanocomposite with PPy fiber and PPy granule

First of all, the TGA graphic of the nanocomposite sample obtained from AuCl salt, represented with green color, was investigated. According to the graphic, 2.5% of the sample weight was lost from the beginning temperature up to 100°C indicating the less amount of moisture stored within the structure, than the previous polymeric samples. Supposedly, as a result of the PPy nanofibers characteristic in the nanocompsite structure, this sample started

being decomposed between a temperature range from 200°C to 250°C. Between 100°C to 600°C, especially during the range between 407°C to 555°C, the major weight loss from the nanocomposite sample was observed (28.7%). Finally, the sample weight became constant after 600°C and the leftover weight %, which was believed to be belong to the Au nanoparticles, was showing (~70%) in the TGA pan.

Secondly, when the TGA graphic obtained from the PPy/$HAuCl_4$ nanocomposite was investigated, initially there was a weight loss of ~3.7% from the sample was observed, due to the moisture within the structure. Around 250°C the sample started being decomposed and exhibited a linear and more stable weight loss than the AuCl nanocomposite until 700°C where the weight % value became constant after all. The major weight loss (31.5%) was observed between the temperature values of 345°C to 645°C. Finally, ~65% of the nanocomposite weight was remained in the TGA pan which was indicating the weight % of Au nanoparticles in the structure.

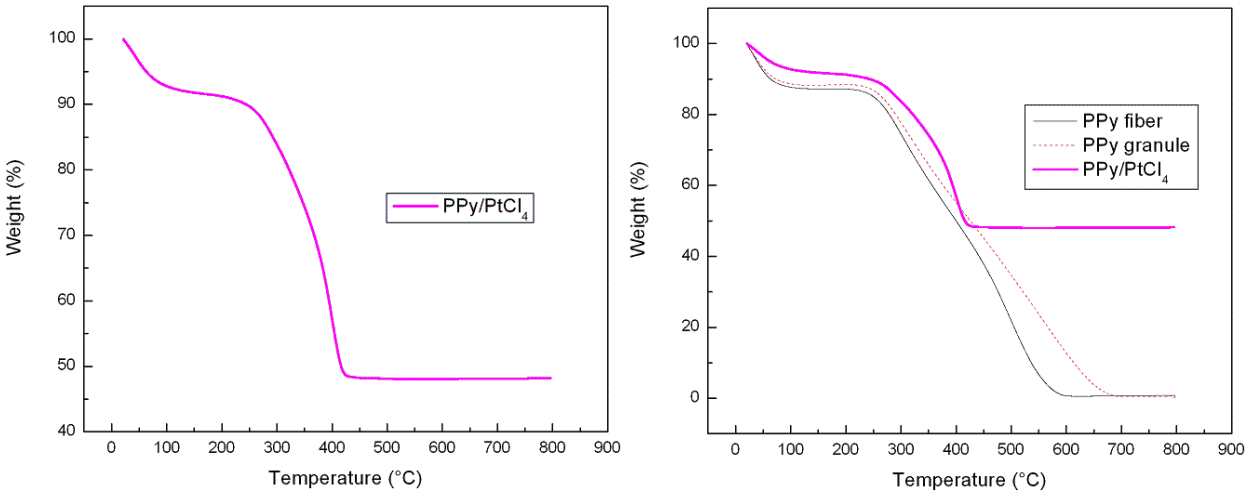


Figure 58 Comparative TGA graphics of PPy/$PtCl_4$ nanocomposite with PPy fiber and PPy granule

After gold nanocomposites, the ones obtained from the platinum salts were thermally characterized at TGA. According to the results of PPy/$PtCl_2$ nanocomposite, there was only 1.2% of the weight was lost at the very beginning because of the moisture inside the sample. Then the sample was started slightly being decomposed around 200°C and exhibited a sharp weight loss (mainly between 377°C to 452°C) of 29.5% until 500°C where the residual weight of the sample became constant. Similarly to the AuCl nanocomposite, this one had also ~70% residual weight of metal nanoparticles within its structure.

The last nanocomposite sample characterized at TGA was from $PtCl_4$. The experimental data was showing a 7.2% of weight loss from the nanocomposite until 100°C due to the moisture content. A bigger weight loss -than the $PtCl_2$ sample- of ~44.6% took place between 100°C to 500°C and the nanocomposite weight became constant, finally at that temperature. The residual metal nanoparticle amount in this structure was 48% according to final readings from the TGA graphic.

In summary, the previously mentioned, one-step, novel synthesis method of conducting polymer nanocomposites within the noble metal salt solutions through a chemical oxidative polymerization reaction of pyrrole was successfully achieved high loading amounts of metal nanoparticles onto PPy nanofibers changing in a range of 48% to 70% based on the affinity and electrochemical interactions between these two compounds. According to the overall TGA data (especially from gold samples) that were indicating higher initial and final decomposition temperatures for nanocomposite structures, it could be suggested that the incorporation of noble metal particles into PPy nanofibers improved their thermal properties and provide more stable characteristics for the nanocomposite structures.

### 3.2.4 EDX Analysis Results

Although, the thermal characterization was applied to obtain more detailed information about the incorporation of noble metal nanoparticles within the nanocomposite structures after the microscopical analysis, a series of supplementary elemental analysis were also conducted sequentially by using all different types of nanocomposites to acquire the most accurate proportions of each different element in nanocomposites.

Despite the EDX is a surface technique, it has a deep penetration depth from the material surface[10] to the measurement point selected inside the structure and can provide more accurate results than the bulk thermal analysis which differs averagely 12.5-31% higher from the EDX results (due to the unburned metal/carbine structures).

Seven different arbitrary measurements were taken from the different points of each and every nanocomposite surface, and then the distributions of different elements within the structures were recorded sequentially. The overall results of seven measurements taken from all different nanocomposite structures, obtained from three different concentrated noble metal salt solutions, were listed in the following table. According to the analysis results, the average distribution of noble metals (Au and Pt) in different nanocomposites were in the range of 35% to 55% -mainly around 40%- of the total nanocomposite weight.

Based on the elemental analysis results represented below, the exact chemical formulas of one nanocomposite structure selected from each different metal salt solutions were determined. Here, since the materials were mounted on a carbon tape, the C% obtained from the EDX characterization may vary (instrument might have also considered the carbon molecules in the tape while taking the measurements) that is why the N% values were taken as the representative for the PPy part of the chemical structure of the nanocomposites.

Table 6 Summary of the EDX analysis results of all different nanocomposite structures

| Sample | C | N | O | Cl | V | Au / Pt | Total |
|---|---|---|---|---|---|---|---|
| PPy/AuCl 0.01M | 36.59 | 9.17 | 5.44 | 0.97 | -0.17 | 47.99 | 100 |
| PPy/AuCl 0.02M | 30.26 | 8.69 | 4.03 | 1.80 | 0.07 | 55.14 | 100 |
| PPy/AuCl 0.005M | 34.98 | 9.93 | 4.96 | 0.69 | -0.10 | 49.54 | 100 |
| PPy/$HAuCl_4$ 0.01M | 39.26 | 10.09 | 2.89 | 2.35 | 0.24 | 45.17 | 100 |
| PPy/$HAuCl_4$ 0.02M | 43.45 | 9.05 | 4.92 | 4.48 | -0.02 | 38.14 | 100 |
| PPy/$HAuCl_4$ 0.005M | 43.42 | 14.50 | 5.08 | 2.00 | 0.16 | 34.83 | 100 |
| PPy/$PtCl_2$ 0.01M | 29.42 | 5.91 | 9.10 | 11.07 | 2.75 | 41.76 | 100 |
| PPy/$PtCl_2$ 0.02M | 27.79 | 4.96 | 5.28 | 12.86 | 0.93 | 48.18 | 100 |
| PPy/$PtCl_2$ 0.005M | 32.44 | 6.73 | 10.78 | 8.61 | 6.22 | 35.21 | 100 |
| PPy/$PtCl_4$ 0.01M | 38.24 | 5.38 | 5.45 | 9.06 | 0.20 | 41.68 | 100 |
| PPy/$PtCl_4$ 0.02M | 33.34 | 9.16 | 5.31 | 9.99 | 0.20 | 41.99 | 100 |
| PPy/$PtCl_4$ 0.005M | 34.39 | 6.37 | 7.19 | 9.37 | 0.18 | 42.50 | 100 |

Similarly, since H% could not be measured by EDX, to be able to represent the $H_2O$ part of the chemical formulas, O% values were used. Selected nanocomposite samples were

PPy/AuCl (0.02M), PPy/$HAuCl_4$ (0.01M), PPy/$PtCl_2$ (0.02M) and PPy/$PtCl_4$ (0.02M). First of all, weight % values of C, N, O, Cl, Au and Pt of each selected nanocomposite sample were divided by the molecular weights of those elements. Next, the reciprocal values of calculated N amounts were taken as the constant to complete other amounts to 1 or 100%.

After all calculations made, the standard chemical formulas of the nanocomposites were represented as; (PPy)(Cl)($H_2O$)(Au or Pt). Chemical formulas of selected nanocomposites were listed according to the calculations as; $(PPy)(Cl)_{0.08}(H_2O)_{0.406}(Au)_{0.451}$, $(PPy)(Cl)_{0.09}(H_2O)_{0.251}(Au)_{0.318}$, $(PPy)(Cl)_{1.022}(H_2O)_{0.93}(Pt)_{0.697}$, $(PPy)(Cl)_{0.43}(H_2O)_{0.51}(Pt)_{0.329}$, respectively for the so-called nanocomposites mentioned above. Same calculations were also made for the microwaved versions of the same samples and the results were discussed in the following paragraphs of this chapter.

Stable dispersions of the noble metal nanoparticles, which was very size dependent, among the conducting polymer nanofibers was achieved through this novel, one-step, seeding-template-assisted chemical oxidative polymerization reaction of pyrrole. EDX results were also consistently unveiling the proportional relation between the noble metal salt solution concentrations and the noble metal nanoparticle ratios in nanocomposites for almost every sample.

Another important information obtained from this analysis was about the fate of the seeding template, $V_2O_5$ nanofibers. The residual % amounts of V element in nanocomposite structures were showing consistency with the previous study results[11] and were almost zero for especially the ones obtained from Au salt solutions. This was actually indicating the advantage of the universal seeding template approach followed for the synthesis of nanocomposites. By using very little amounts (1-3mg) of $V_2O_5$ nanofibers in reactions it was possible to obtain bulk

amounts of nanofibers at the end which were almost free of V (even though the residual V was washed away at the purification step). The ascending V% amount ranking in nanocomposite structures was listed as AuCl, $HAuCl_4$, $PtCl_4$ and $PtCl_2$, respectively.

As a result, it could be suggested that during the reaction the seeding template was quantitatively removed from the final structure without any additional template removal step requirement[11] by following the two possible pathways which were (i) reacting with the pyrrole monomer, and (ii) being dissolved and washed away in $H_2O$[11].

### 3.2.5 FT-IR Characterization Results

To be another complementary and/or supplementary study for EDX and to prove the overall success of our novel, one-step, seeding-template-assisted chemical oxidative polymerization of pyrrole within different concentrated noble metal salt solutions to synthesize conducting polymer nanocomposites decorated with noble metal nanoparticles, additional FT-IR spectroscopy characterizations were applied to all different polymeric and standard (0.02M) nanocomposite structures obtained.

Very similar results, with some slight shiftings and intensity differences in peaks, were obtained from the FT-IR characterization of two different mophology structures of PPy. According to the FT-IR spectrum of PPy fiber (represented with black color) several well-known PPy peaks were clearly observed at the corresponding wave numbers of 2733.3$cm^{-1}$ (C-H stretching vibrations), 1540.1$cm^{-1}$ (C-C and C=C stretching vibrations), 1446.1$cm^{-1}$ (C-N stretching), 1294.9$cm^{-1}$, 1160 $cm^{-1}$, and 1021.1$cm^{-1}$ (C-H and C-H in plane deformation modes) and finally 878.1$cm^{-1}$, 771.9$cm^{-1}$ and 657.4$cm^{-1}$ (C-H outer bending vibrations).

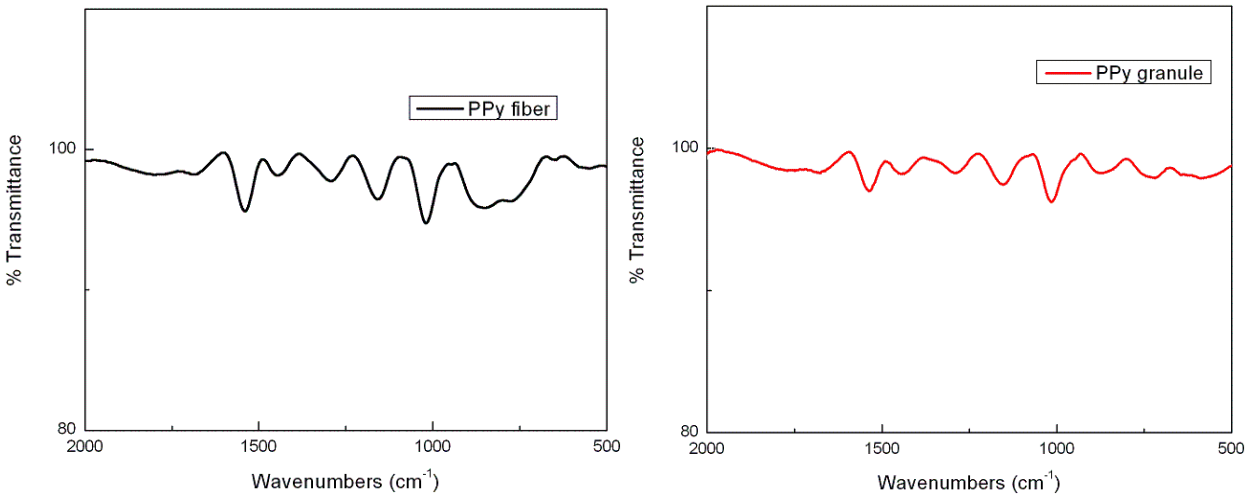


Figure 59 FT-IR spectra of PPy fiber and PPy granule

Likewise, the PPy granule sample was exhibiting very similar FT-IR peaks in its spectrum (represented with red color), by slightly shifting towards shorter wavelengths, at corresponding wave numbers of 2708.7cm$^{-1}$ (C-H stretching vibrations), 1536cm$^{-1}$ (C-C and C=C stretching vibrations), 1446.1 (C-N stretching), 1290.8cm$^{-1}$, 1156cm$^{-1}$, and 1012.9cm$^{-1}$ (C-H and C-H in-plane deformation modes) and finally 882.2cm$^{-1}$ and 706.5cm$^{-1}$ (C-H outer bending vibrations).

FT-IR spectra of the nanocomposites obtained from two different Au salts' standard solutions (0.02M) were both exhibiting smooth and similar graphics whose peak locations were also in a good agreement with the PPy nanofiber characteristics in their structures. The major FT-IR peaks of both Au nanocomposites, especially the ones from AuCl, were located at shorter wavelengths than the different polymeric PPy structure peaks, supposedly due to the higher oxidation of PPy with the ions from AuCl, at the corresponding wave numbers of 1503.3cm$^{-1}$ (C-C and C=C stretching vibrations), 1278.5cm$^{-1}$ (bipolaron band of PPy in doped state), 1147.8cm$^{-}$

[1] (C-N stretching), 1004.8cm$^{-1}$ (C-H in-plane deformation), and finally 886.3cm$^{-1}$ and 706.5cm$^{-1}$ (C-H outer bending vibrations).

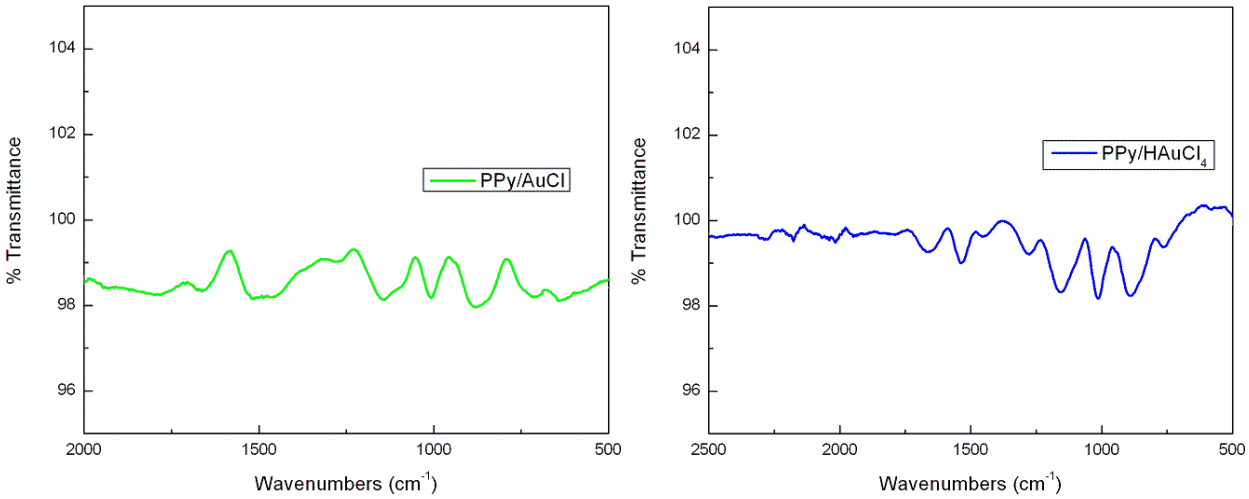


Figure 60 FT-IR spectra of PPy/AuCl and PPy/$HAuCl_4$ nanocomposites

FT-IR spectrum of the nanocompostite obtained from $HAuCl_4$ salt solution (represented in blue color) were also exhibiting almost identically located peaks with AuCl ones, which were slightly shifted to longer wavelengths at the corresponding wave numbers of 1540.1cm$^{-1}$ (C-C and C=C stretching vibrations), 1450.2cm$^{-1}$ (C-H in-plane deformation), 1274.5cm$^{-1}$ (bipolaron band of PPy in doped state), 1156cm$^{-1}$ (C-N stretching), 1017cm$^{-1}$ (C-H in-plane deformation), 886.3cm$^{-1}$ (C-H outer bending vibration) and finally 759.6cm$^{-1}$ (C-H out-of-plane deformation).

FT-IR spectra of the nanocomposites obtained from different Pt salt solutions were quite different from the previously explained ones in terms of peak intensity. However, both spectra of so-called nanocomposites were still exhibiting the characteristic peaks of PPy consistently due to the PPy nanofibers in their structures.

The major peaks in the FT-IR spectrum of $PtCl_2$ nanocomposite were listed as the following; at the corresponding wave numbers of 3284.9$cm^{-1}$ (N-H stretch vibration), 1683.1$cm^{-1}$ (C=C out-of-plane bending), 1589.1$cm^{-1}$ (PPy ring vibration), 1331.7$cm^{-1}$ (=C-H in-plane vibration), 1282.6$cm^{-1}$ (bipolaron PPy band in doped state), 1180.5$cm^{-1}$ (C-N stretching), 1049.7$cm^{-1}$ (C-N vibration) and finally at 939.4$cm^{-1}$ (=C-H out-of-plane bending).

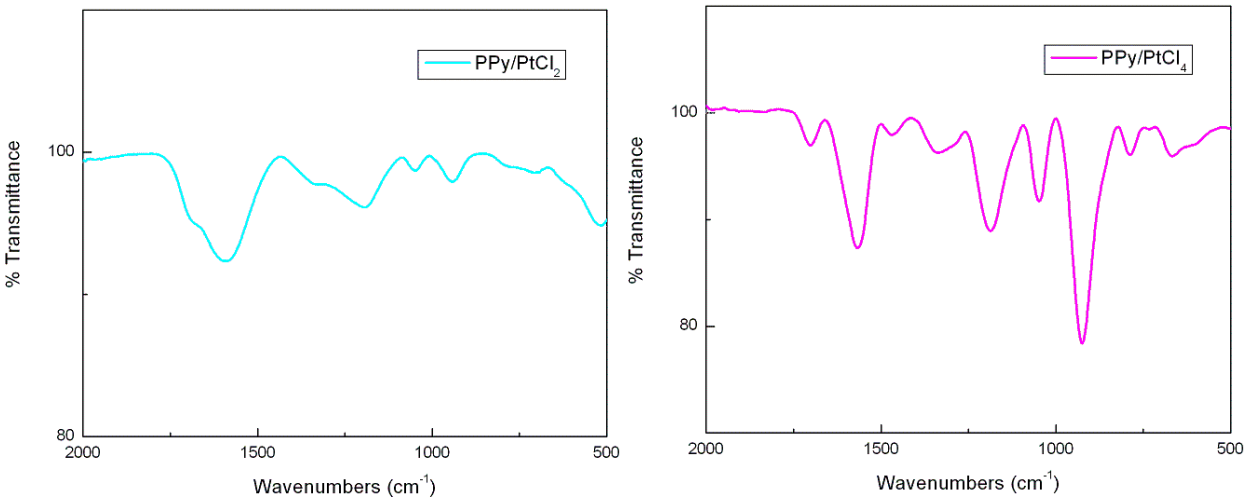


Figure 61 FT-IR spectra of $PPy/PtCl_2$ and $PPy/PtCl_4$ nanocomposites

When the FT-IR spectrum of nanocomposite obtained from $PtCl_4$ salt solution was investigated, a clear observation of increased intensity and slight shiftings of characteristic peaks to shorter wave lengths could be made. Detected characteristic peaks were listed in the following sequence at corresponding wave numbers of; 3227.7$cm^{-1}$ (N-H asymmetric stretching), 3113.3$cm^{-1}$ (little shoulder at the peak represents again N-H stretching), 1560.5$cm^{-1}$ (PPy ring stretching), 1454.3$cm^{-1}$ (PPy ring vibration), 1331.7$cm^{-1}$ (=C-H in-plane vibration), 1180.5$cm^{-1}$ (C-N stretching), 1045.6$cm^{-1}$ (C-N vibration), 923$cm^{-1}$ (C-H bending) and finally at 784.1$cm^{-1}$ (C=C out-of-plane bending).

In summary, the FT-IR characterization of different morphology PPy structures and nanocomposites obtained through the early mentioned, novel, one-step, seeding-template-assisted, chemical oxidative polymerization reaction of pyrrole provided precious information that proves the PPy nanofiber molecules' presence in each nanocomposite. The changing characteristics (spectra) of such structures according to the interactions with different metal salt solutions were clearly observed. Previously published research study results[20-24] were also consistently matching with the overall results that were obtained through the different FT-IR characterizations of these nanocomposite structures. The overall characteristic differences could easily be distinguished after a quick revision of so-called graphics, according to the peak positions (longer-shorter wave numbers) and their intensities (higer/lower).

### 3.2.6 SEM Characterization Results of Microwave Treated Nanocomposites

As it was explained at the end of the previous chapter, as-prepared nanocomposite samples were exposed to microwave irradiation to convert their PPy nanofiber based matrixes in carbon nanofibers coated with noble metal nanoparticles. Different characterization results collected from so-called samples were given and discussed in details, during the following paragraphs.

Again, first of all, to investigate the morphology of as-prepared structures, carbon nanocomposite samples of PPy/AuCl (0.02M), PPy/$HAuCl_4$ (0.01M), PPy/$PtCl_2$ (0.02M) and PPy/$PtCl_4$ (0.02M) after 40s, 70s, 6min. and 2min.15s microwave treatment, respectively, were selected to take the SEM images.

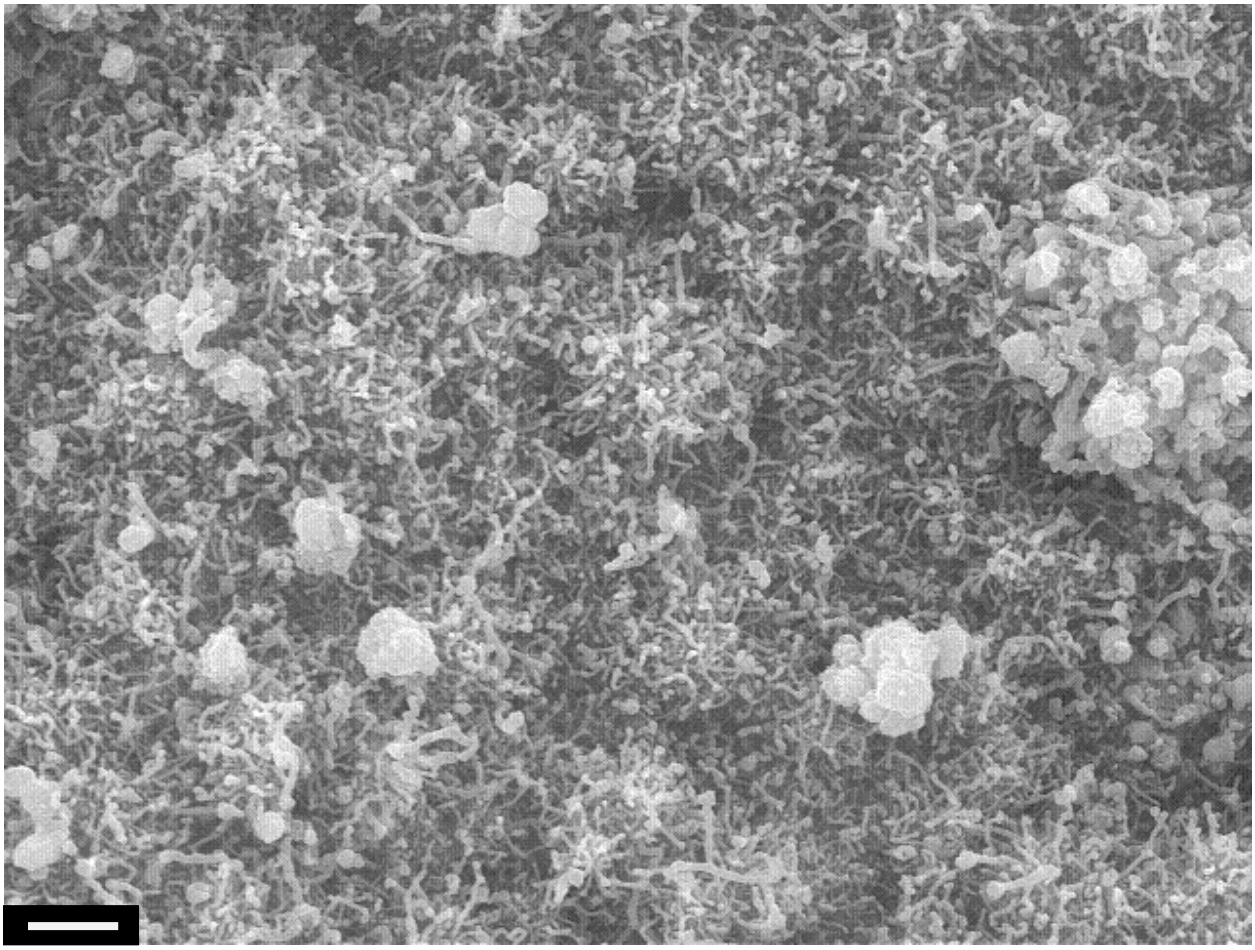

Figure 62 SEM image of microwaved PPy/AuCl nanocomposite (scale bar: 1μm)

From those images, five different measurements were taken to have more clear idea about the possible morphological changes that had taken place after the treatments. Generally, during the tests it was clearly observed that nanocomposites obtained from Au salt solutions exhibited higher reactivity to microwave irradiation than the ones obtained from Pt salt solutions. It was supposedly a kind of reflectance of the specific noble metal characteristics (reactivity/inertness) that were already available in nanocomposite structures.

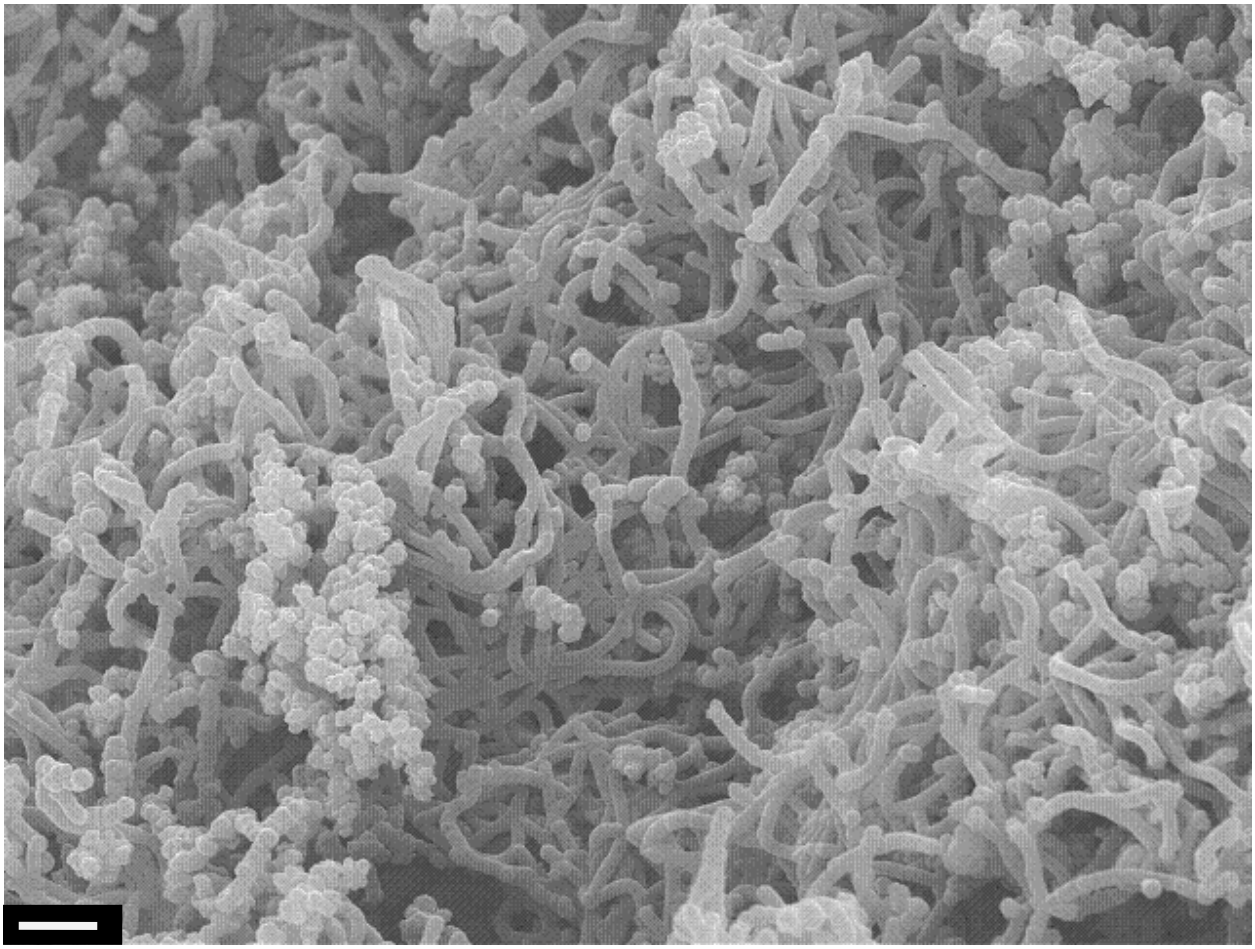

Figure 63 SEM image of microwaved PPy/$HAuCl_4$ nanocomposite (scale bar: 1μm)

When the SEM images of two different nanocomposites obtained from Au salt solutions were investigated; uniformly distributed individual carbon nanofibers could easily be observed among the noble metal nanoparticle aggregates. PPy/AuCl CNC was exhibiting individually bended morphologies, with uniform diameters around 91nm, that were well dispersed among mostly spherical shaped, irregularly aggregated noble metal nanoparticles with several hundred nm (~972.6nm) average particle sizes.

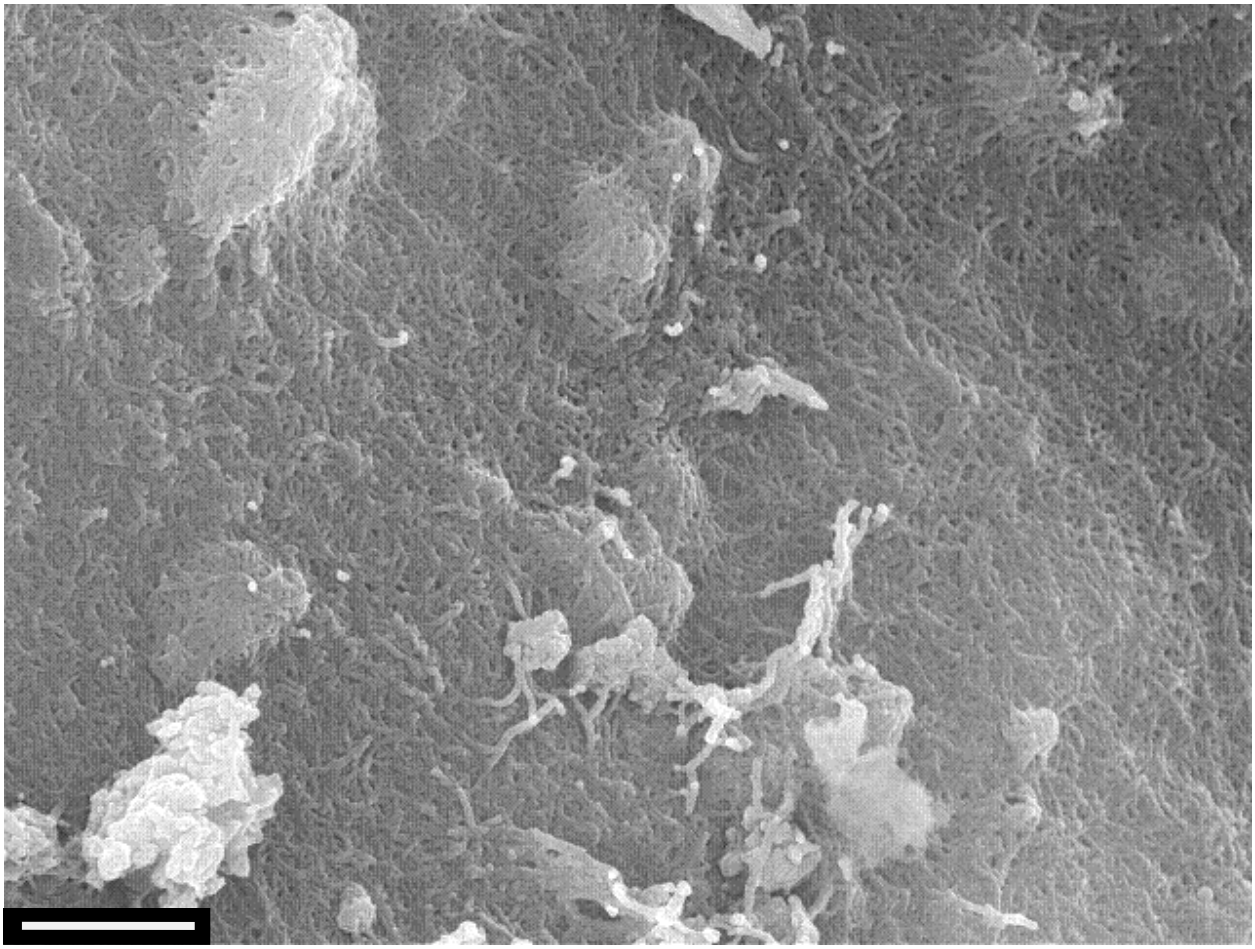

Figure 64 SEM image of microwaved PPy/$PtCl_2$ nanocomposite (scale bar: 1μm)

When the SEM image of microwaved PPy/$HAuCl_4$ nanocomposite sample was investigated, the traditional web-like carbon nanofiber structures that had less smooth surfaces with, averagely, 96nm diameters were clearly observed. Mostly spherical shaped noble metal particle aggregations with more than 1μm particle sizes (averagely 1076.8nm) became more obvious (as a result of burned down and converted PPy nanofiber matrix after being microwaved) through the nanocomposite structure.

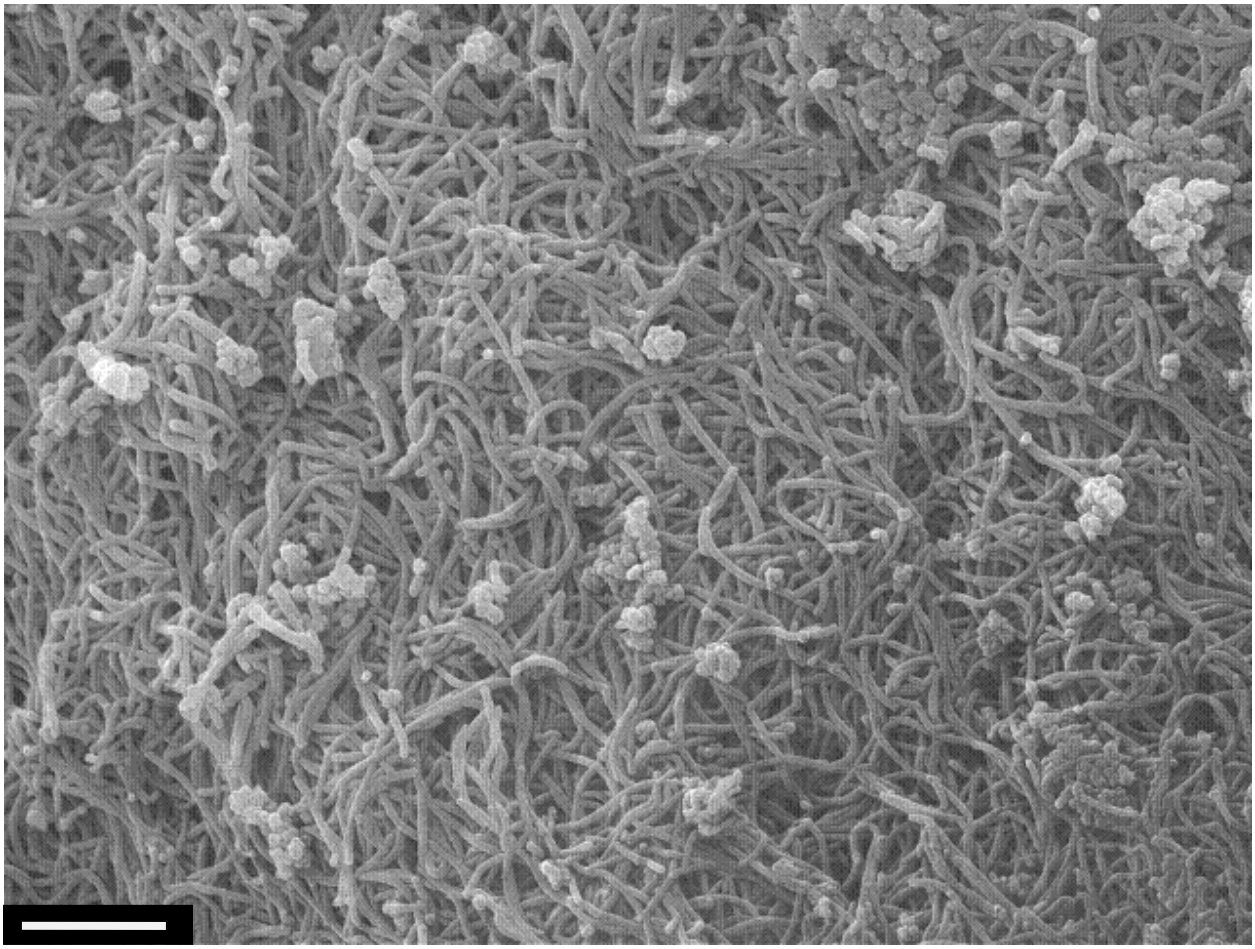

Figure 65 SEM image of microwaved PPy/$PtCl_4$ nanocomposite (scale bar: 1µm)

SEM images of microwaved nanocomposite structures obtained from different Pt salt solutions were exhibiting very similar morphology characteristics with their non-microwaved versions. Intricate, web-like carbon nanofibers that were converted from the PPy/$PtCl_2$ nanocomposite matrix surface (by definitely proving the success of previously explained mechanism) with the diameter averages of 61nm and decorated with averagely 518.5nm sizes irregularly aggregated noble metal nanoparticles, were clearly detected at this samples' SEM image.

Carbon nanofibers formed on the PPy/$PtCl_4$ nanocomposite after microwave treatment were exhibiting individually grown and less smooth morphological properties with a uniform diameter distribution around 87nm which were clearly observed from the last SEM image above. Spherical noble metal nanoparticle aggregates having several hundred nm particle sizes (689.6nm) could also obviously be seen at the final nanocomposite surface after the applied microwave irradiation.

In summary; through a facile,one-step and short term microwave treatment of as-prepared PPy nanofiber based composites it was possible to successfully convert the polymer matrix into carbon nanofibers that had uniform diameter distributions and similar morphological properties like the original PPy nanocomposites.

### 3.2.7 TGA Characterization Results of Microwave Treated Nanocomposites

Thermal characterization was applied to the as-prepared microwaved carbon nanocomposite samples and also to the microwaved PPy structures (fiber/granule) with different morphologies by using TGA instrument to observe the changes that might have happened after the treatment, in terms of thermal stability and the residual material weight of so-called structures. Collected TGA graphics were listed and the results generated from those graphics were discussed in a comparative manner during the following paragraphs.

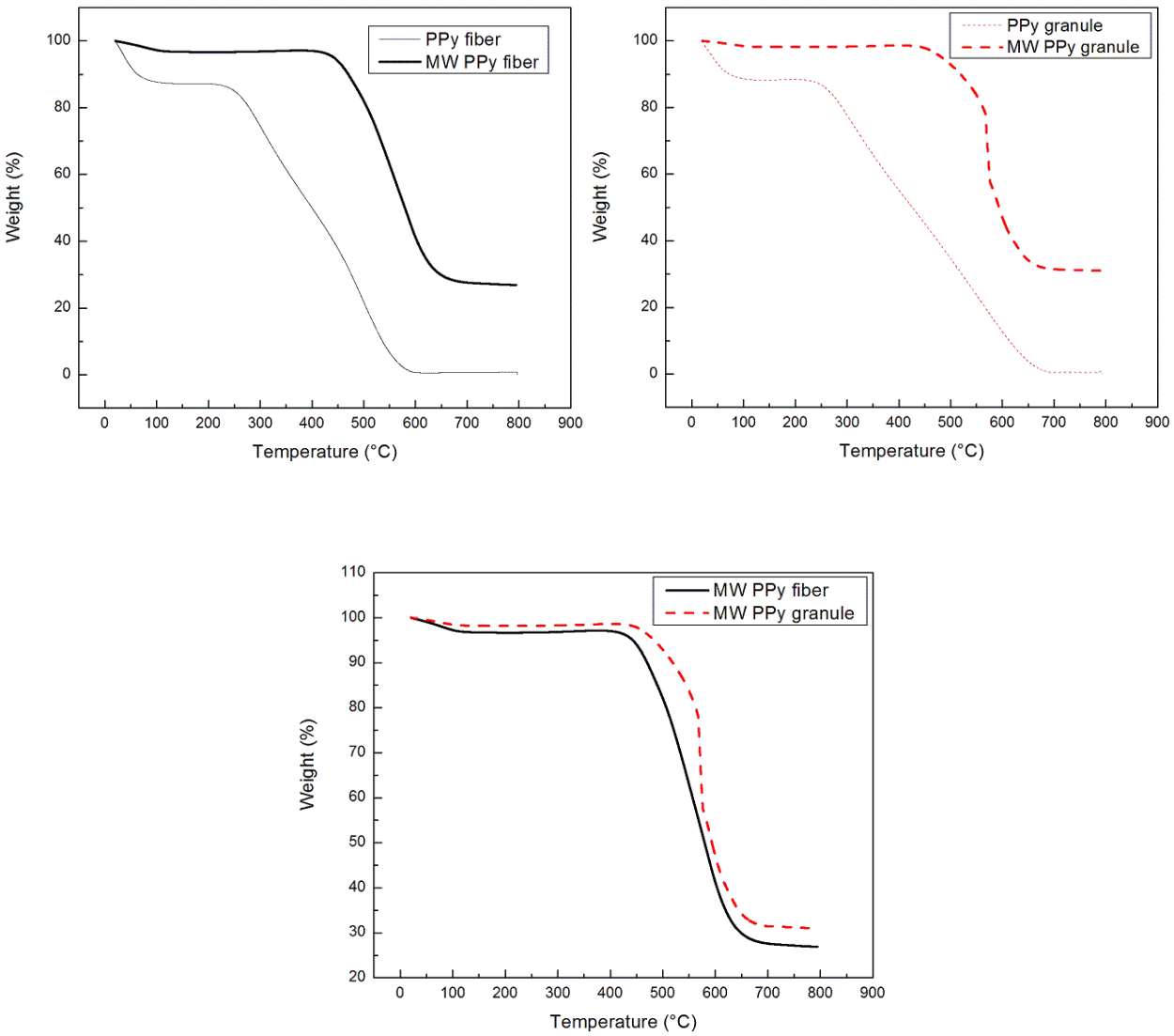


Figure 66 Comparative TGA graphics of non-/microwaved PPy fiber and PPy granule

TGA results of the different morphology PPy structures were firstly investigated in a comparative way with the non-microwaved versions of the same samples. According to the 40s microwaved PPy fibers' TGA graphic (represented in black color) only 2.7% of the sample weight was lost upon heating from the initial temperature up to 400°C where the material was slightly started being decomposed. Initial decomposition temperature range was between 200°C to 250°C for the non-microwaved PPy fiber. The major loss of weight from the sample (~70%)

was observed between the temperatures of 400°C to 770°C (averagely between 480°C to 630°C). After 750°C the weight of the sample became constant and the final readings were showing that ~27% of the sample weight was remained, which was supposedly the weight of CNCs produced in the material structure during the microwave treatment.

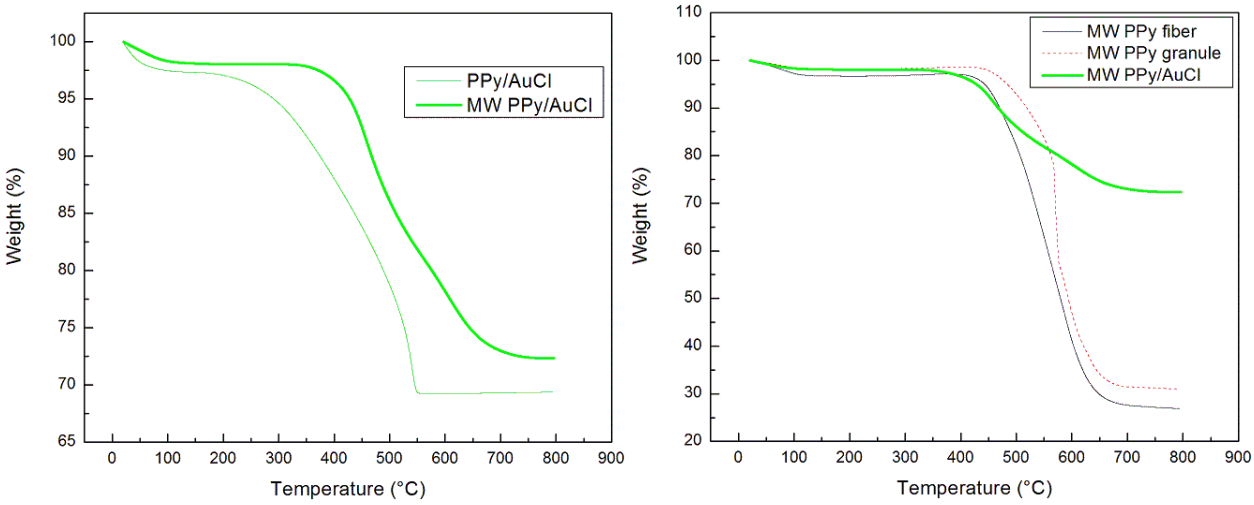


Figure 67 Comparative TGA graphics of non-/microwaved PPy/AuCl with microwaved PPy fiber and PPy granule

Comparatively, non-/microwaved PPy granules' TGA results (represented in dashed red color) were showing better results than PPy fibers. Only ~1.5% of the initial weight was lost as a result of heating from the starting temperature to 450°C where the sample was started being decomposed. 67.3% of the sample was majorly decomposed between the temperatures of 450°C to 750°C (averagely 564°C to 586°C). Finally, after 750°C the sample weight became constant and there was ~31% of the residual sample, which was possibly again the amount of carbon structures converted in the structure, left in the TGA pan.

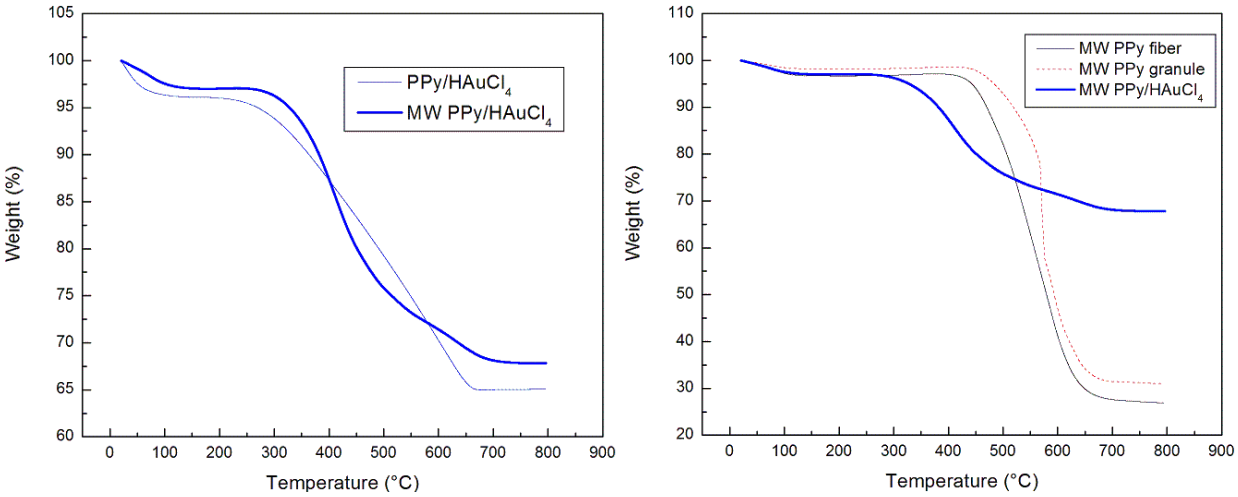


Figure 68 Comparative TGA graphics of non-/microwaved PPy/$HAuCl_4$ with microwaved PPy fiber and PPy granule

After the thermal analysis of microwaved PPy fiber and granules, 40s microwaved and non-microwaved PPy/AuCl (0.02M) nanocomposite samples' TGA results were investigated.

According to the graphics (represented with green color), significant improvements were observed in the thermal stability and the residual amount of samples (due to the converted carbon nanofibers in the structure) after microwave treatment. 1.7% of the sample weight was lost upon heating from the initial temperature up to 350°C, where the major decomposition of the sample was started. From 350°C to 750°C, (averagely between 411°C to 571°C) 26% of the sample was decomposed. Finally, 72.3% (previously 70% for the non-microwaved nanocomposite) of the total sample weight was remained, which was believed to be weight of newly generated CNCs and the noble metal nanoparticles in its structure.

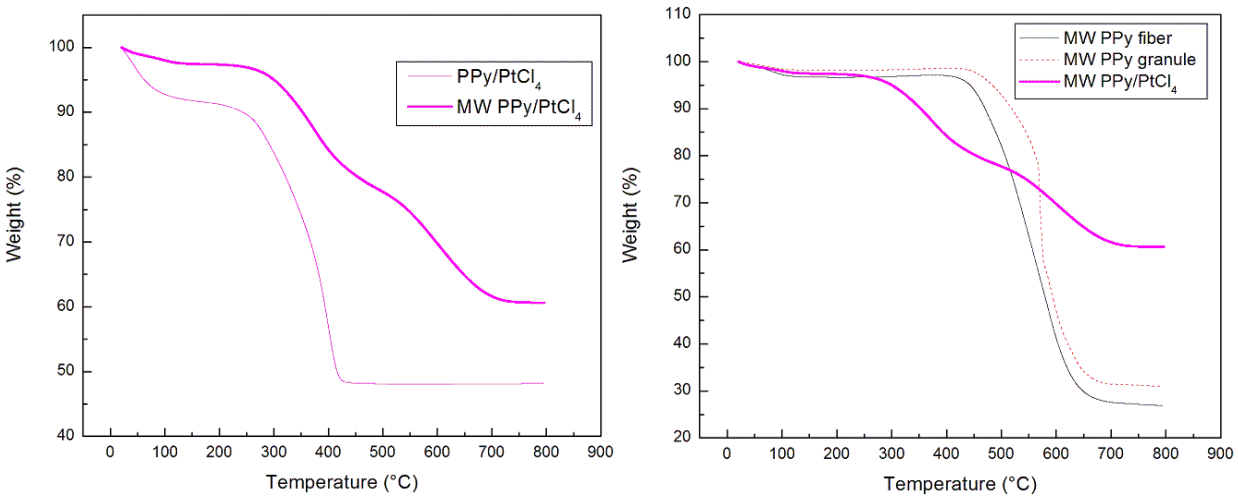


Figure 69 Comparative TGA graphics of non-/microwaved $PPy/PtCl_4$ with microwaved PPy fiber and PPy granule

The thermal analysis of the 70s microwaved $PPy/HAuCl_4$ (0.01M) nanocomposite was also exhibiting superior results in terms of thermal stability and the residual sample weight, than its non-microwaved version. 2.4% of the sample weight was lost during the initial heating of microwaved nanocomposite sample, starting from the initial temperature to 250ºC. The major decomposition of the sample (~29.7%) took place between the temperatures of 250ºC to 750ºC (averagely between 346ºC to 508ºC). Finally, 67.8% of the nanocomposite weight, which could be considered as the weight of as-prepared CNCs and the noble metal nanoparticles in the structure, was remained (previously 65% for the non-microwaved version) in the TGA pan.

Nanocomposites from $PPy/PtCl_2$ (0.02M) was microwaved for 6min. under standard conditions but there was no clear burning (sparkles and/or little flames), indicating the conversion of PPy nanofibers to CNCs at the surface, observed during the treatment. TGA analysis of that sample was not presented here due to this extraordinary situation.

Final thermal characterization result was belong to the 2min.15s microwaved (microwave treatment times were varying due to the relative reactivity of different noble metals) PPy/$PtCl_4$ nanocomposite sample which exhibited the best improvements in terms of thermal stability and the residual amount of weight after thermal heating (indicating the high rate of generation of CNCs in its nanocomposite structure). Only 2% of the sample weight was decomposed upon the initial heating from the starting temperature to 250ºC. Likewise the other nanocomposites, the major decomposition (~37.5%) of this sample also took place between the temperatures from 250ºC to 750ºC (mainly between 300ºC to 537ºC). At the end of the thermal application, 60.6% of the sample weight was remained in the TGA pan, (previously 48% for the non-microwaved version), which considered to be mainly composed of noble metal nanoparticles and as-prepared CNCs in the nanocomposite structure.

In short, this newly developed, simple and one-step microwave treatment method to convert nanocomposite structures to carbon nanocomposites in seconds was obviously successful. CNC conversion rates and the improved thermal properties of so-called nanocomposites were also strongly supporting the success of this rapid and facile mechanism for bulk CNC synthesis.

### 3.2.8 EDX Analysis Results of Microwave Treated Nanocomposites

EDX elemental analysis was the next characterization applied to the microwave treated nanocomposites. Weight % values of C, N, O, Cl, V, Au and Pt elements within these so-called microwaved structures were summarized in the following table.

Table 7 Summary of the EDX analysis results of the microwaved nanocomposite structures

| Sample | C | N | O | Cl | V | Au / Pt | Total |
|---|---|---|---|---|---|---|---|
| PPy/AuCl 0.02M | 10.71 | 4.86 | -0.82 | 0.26 | 0.11 | 84.87 | 100 |
| PPy/$HAuCl_4$ 0.01M | 29.97 | 3.42 | 0.62 | 0.24 | 0.10 | 65.66 | 100 |
| PPy/$PtCl_2$ 0.02M | 24.78 | 5.50 | 5.55 | 11.59 | 0.28 | 52.30 | 100 |
| PPy/$PtCl_4$ 0.02M | 31.19 | 1.09 | 1.29 | 0.14 | 0.14 | 66.14 | 100 |

Based on the EDX analysis results above, calculations were made to find out the exact chemical formulas of microwaved nanocomposite structures by following the previously described method.

Here, again N% values of each sample was considered as the representative for the PPy part of the chemical formulas rather than C% to avoid the possible distractions originated from the supporting carbon tape used. The failure at the microwave treatment of $PPy/PtCl_2$ (0.02M) nanocomposite was negatively effected the EDX analysis results, with the excessive amount of O detected in its structure which was considered as the representative for the $H_2O$ part of the chemical formula and supposed to be very close to/or zero after being microwaved, was proving this failure.

In view of the results listed above and the calculations made based on them, the chemical formulations of microwave treated nanocomposite samples were listed as; $(PPy)(Cl)_{0.021}(Au)_{1.241}$, $(PPy)(Cl)_{0.027}(Au)_{1.366}$, $(PPy)(Cl)_{0.833}(Pt)_{0.684}$, $(PPy)(Cl)_{0.05}(Pt)_{4.358}$, respectively, for the nanocomposites presented in the table.

As a result, the EDX analysis data were also consistently supporting the success of this facile, rapid and one-step microwave treatment technique to convert as-prepared nanocomposites into CNCs. Higher C:N ratios ranging between 5-28 (which were previously around 4-6 for non-microwaved nanocomposites), the absence of $H_2O$ molecules in chemical structure and higer proportions of noble metals (currently ranging between 0.684 to 4.358 and was previously 0.318 to 0.697) in the final nanocomposite structures, were the other important observations made which were also proving the success of this method.

### 3.2.9 FT-IR Characterization Results of Microwave Treated Nanocomposites

After the elemental analysis of as-prepared CNCs by microwave treatments, sequential FT-IR characterizations were also conducted with the same samples and also with the microwaved, different morphology PPy structures to verify the success of this approach.

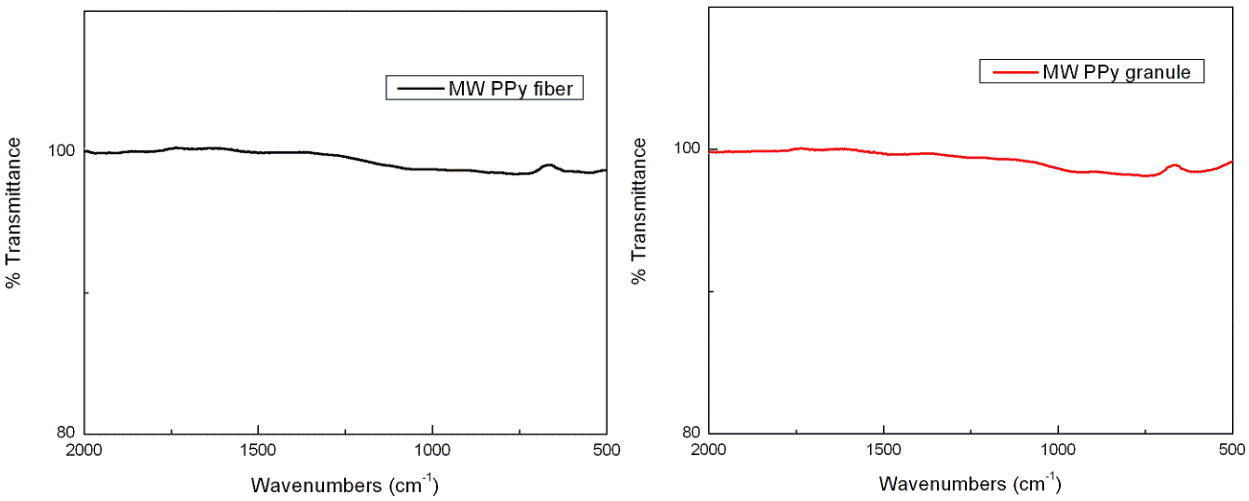


Figure 70 FT-IR spectra of microwaved PPy fiber and microwaved PPy granule

According to the FT-IR graphics listed below, there were not many characteristic peaks detected which could indicate the specific functional groups in those structures, except the ones

recorded from PPy fiber at corresponding wave number of 771.7cm$^{-1}$ (indicating N-H vibrations), from PPy granule at corresponding wavenumbers of 750.1cm$^{-1}$ and 630.4cm$^{-1}$ (both indicating N-H stretchings) and from PPy/$HAuCl_4$ (0.01M) nanocomposite sample at corresponding wavenumber of 1402cm$^{-1}$ (again indicating the N-H bond in the structure).

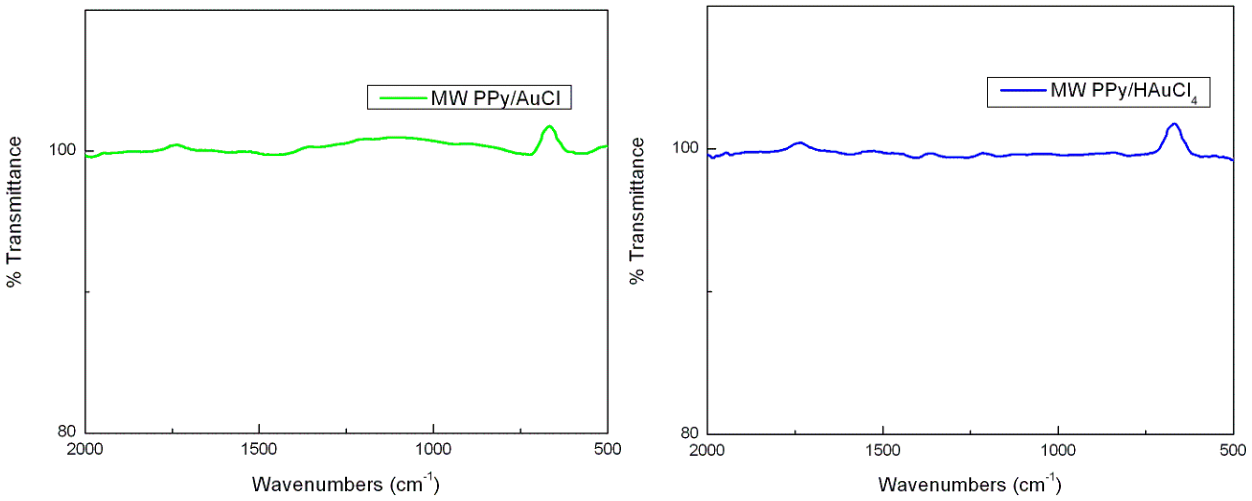


Figure 71 FT-IR spectra of microwaved PPy/AuCl and microwaved PPy/$HAuCl_4$ nanocomposites

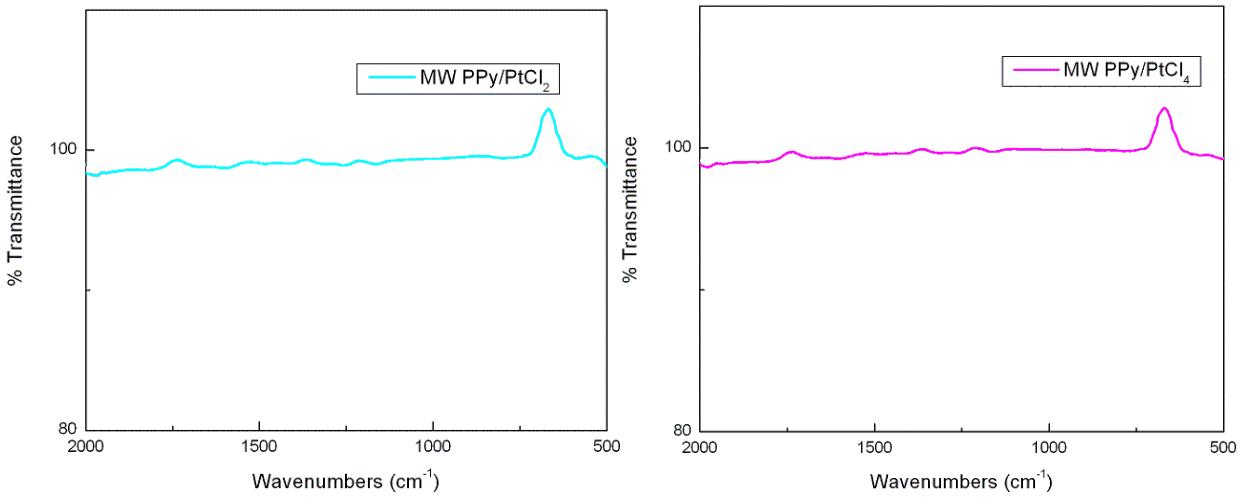


Figure 72 FT-IR spectra of microwaved PPy/$PtCl_2$ and microwaved PPy/$PtCl_4$ nanocomposites

In summary, FT-IR characterization of microwaved nanocomposites were once again proved the success of this facile and one-step technique for CNC production from different nanocomposite structures after very short term microwave treatments, by verfying the high conversion of PPy nanofiber matrix -whose characteristic peaks were hardly been detected in such graphics after the treatments- to CNCs. Seldom characteristic peak values that have been detected in above mentioned microwaved samples' FT-IR graphics were compatible with the previous study results[25-27] found in the literature.

Consistently with the proved success of this simple, rapid and one-step microwave treatment method and its elaborately explained mechanism it was possible to generate bulk quantities of CNCs with uniformly retained morphological properties directly from conducting polymer nanocomposites[18].

This unique method could open new windows in design and development of new-generation fuel-cell membranes (by maintaining the electrochemical properties of conducting polymer/noble metal nanocomposites), energy storage systems and high sensitivity volatile organic molecule sensors based on CNCs[18].

### 3.2.10 Four Probe Conductivity Measurement Results of Different Polymeric and Nanocomposite Structures

One of the major characterizations of as-prepared different morphology PPy structures (fiber/granule) and four different conducting polymer nanocomposites obtained from standard noble metal salt solutions (0.02M) were conducted by using previously described linear four probe conductivity measurement method to gain a deeper knowledge about the electrical properties of so-called structures. Six different samples were prepared by applying high pressure (3500psi) onto them while they were filling a mold cavity with certain dimensions (LxWxH =

1.5cm x 0.2cm x 0.225cm). Specific thickness (heigth) values of each thin film was measured to determine the crossectional area (A) that was necessary to calculate the conductivity of each sample. Since the conductivity (S/cm) is the reciprocal of resistivity (R) and can be calculated with the equation of [$\sigma = L/(R \times A)$][19] it was easy to obtain the required data by simply touching the four probes onto the thin film surfaces to read the specific resistance values from the connected device. Here, L represents the distance (0.52cm) between the two inner probes. A simple representation of the utilizd linear four probe method was shown in the figure below.

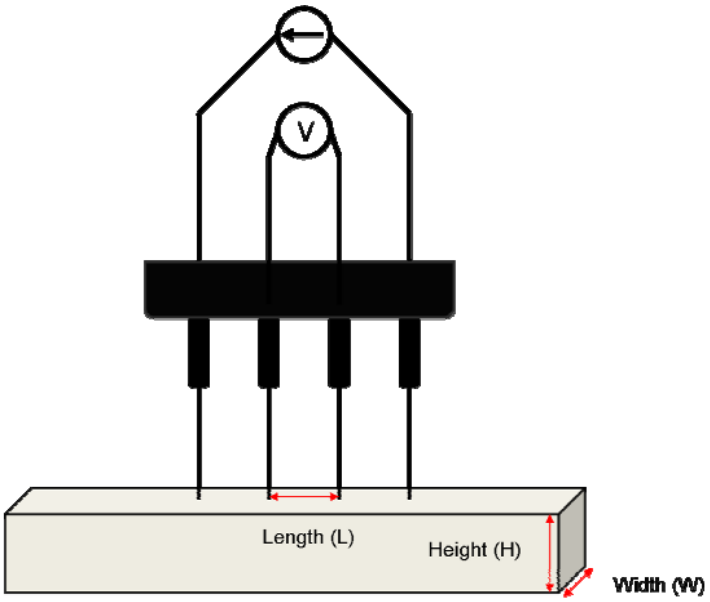


Figure 73 Linear four probes and a representative sample bar[19]

Table 8 Summary of the calculated values of samples used for conductivity measurements

| Sample | Thickness (cm) | Resistance (Ω) | Conductivity (S/cm) |
|---|---|---|---|
| **PPy fiber** | 0.055 | 26 | 1.82 |
| **PPy granule** | 0.08 | 18.9 | 1.72 |
| **PPy/AuCl** | 0.055 | 2420 | 0.0195 |
| **PPy/$HAuCl_4$** | 0.09 | 1260 | 0.023 |
| **PPy/$PtCl_2$** | 0.07 | 2600 | 0.0143 |
| **PPy/$PtCl_4$** | 1 | 2400 | 0.0011 |

In summary, previously described linear four probe conductivity measurement method was successfully utilized to define the specific conductivity values of as-prepared polymeric and nanocomposite structures.

According to the results, PPy fibers exhibited a higher conductivity value than the granule sample, probably because of its higher surface area and more regularly aligned morphology which made easier for electrons to move through. Compared to the conventionally prepared PPy structures (PPy.Cl obtained from HCl)[19], these samples were exhibiting less conductivity due to their less doping level, provided by $Cl^-$ ions, of their structures and the type of the reaction media used ($HCl>H_2O$) for their preparation. Generally, different morphology PPy structures were exhibiting higer conductivity values than the nanocomposite samples. There were three possible main reasons listed as; (i) very low doping levels, provided by $Cl^-$ ions, of their structures (because of using 0.02M, 0.01M and 0.005M concentrated solutions, compared to 1M HCl used in conventional PPy synthesis, of noble metal salts $Cl^-$ amount provided was very less), (ii) the large interfaces (junctions) between the noble metal nanoparticle aggregates

and the PPy nanofiber matrix which were supposed to increase the conductivity but contrastingly decreasing it by being large obstacles against the electrons moving through their structure, (iii) using aqueous system, which has less ionic potential, rather than HCl as the reaction media, causing the above mentioned situation.

### 3.2.11 Cyclic Voltammetry (CV) Application Results of Different Polymeric and Nanocomposite Structures

Four different polymeric and nanocomposite structures (PPy fiber, PPy/$PtCl_2$ (0.02M), PPy/$PtCl_2$ (0.01M), PPy/$PtCl_2$ (0.005M) and microwaved PPy/$PtCl_2$ (0.01M)) were utilized to conduct electrochemical cyclic voltammetry (CV) applications by using Arbin-010 MITS Pro 4-BT 2000 instrument at standard laboratory conditions upon applying a sweeping potential within -0.8V to 0.4V at 20mV/s range vs. SCE used as the reference electrode. A modified pure graphite rod was used as the counter electrode and similar graphite rods with above mentioned polymeric structures pasted at their tips by colloidal carbon, were used as the working electrodes. 76mL of 1M KOH aqueous solution mixed with 4mL methanol -$CH_3OH$- (5% of total volume of 80mL) was used as the electrolyte for these applications.

The purpose of this application was to obtain certain information about the electrochemical behavior of different as-prepared polymeric nano/structures and to verify their applicability in fuel-cells via detecting the oxidation of methanol in their test results. Cyclic voltammograms (CVs) of each sample and related discussions were listed along the following paragraphs.

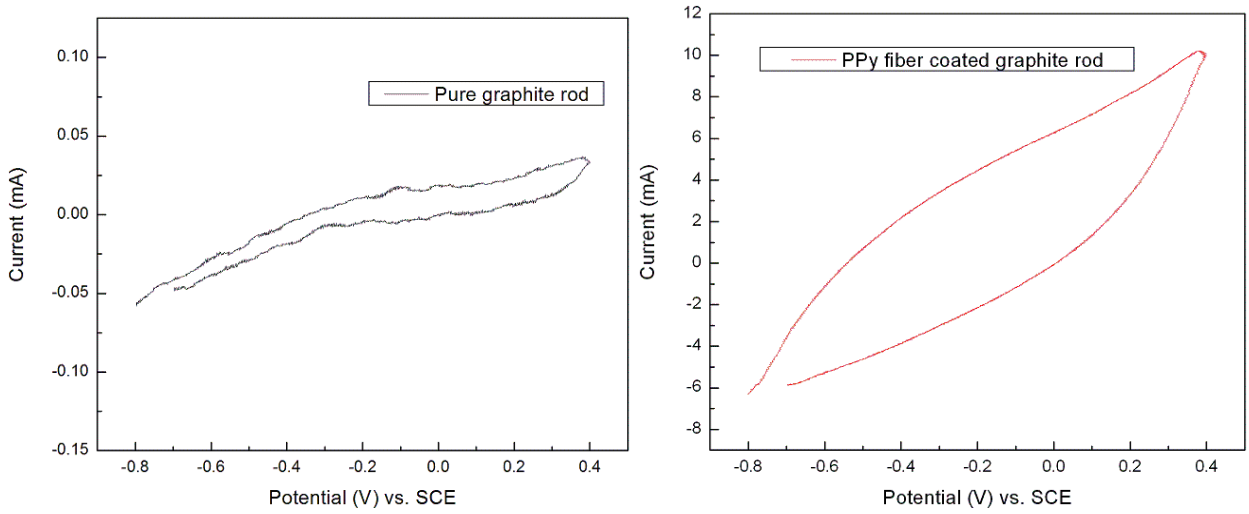


Figure 74 CVs of pure graphite rod and PPy fiber coated graphite rod

The lowest current range readings (-0.05mA to 0.05mA) were obtained from the CV of pure graphite rod as the control sample, whose results was represented in black color, as expected.

Due to the inertness of its pure carbon structure against $CH_3OH$ it was not easy detect any significant peaks referring the oxidation of $CH_3OH$. Characteristic oxidation peaks that were supposedly belong to the $CH_3OH$ (during charging around -0.1V) and CO (the by product of slightly oxidized methanol according to the reactions of ($CH_3OH + Pt \longrightarrow Pt\text{-}CO + 4Pt\text{-}H$ and $4Pt\text{-}H \longrightarrow 4Pt + 4H^+ + 4e^-$ and $Pt\text{-}CO + H_2O \longrightarrow CO_2 + 2H^+ + 2e^-$) during discharge around -0.3V could barely be seen from the CV of the pure graphite rod verfying a very weak oxidation reaction that might have happened.

The CV of PPy fiber coated graphite rod, which was represented in red color, was exhibiting the largest current range readings (-6mA to 10mA) without any peak indicating the oxidation of $CH_3OH$ due to the lack of elements that could catalyze the so-called reaction, in its polymeric structure.

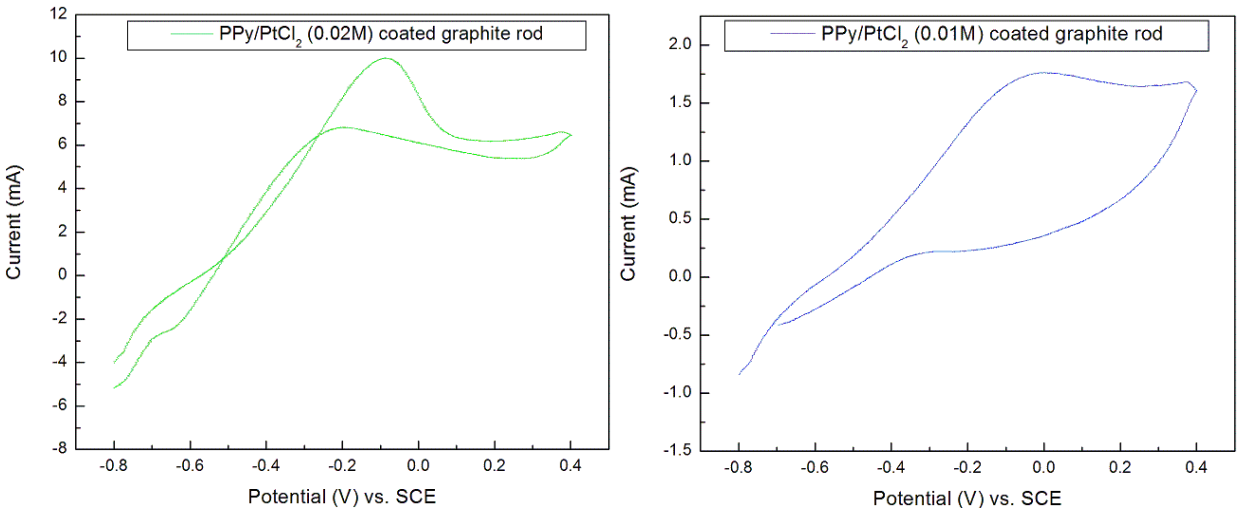


Figure 75 CVs of $PPy/PtCl_2$ (0.02M) and $PPy/PtCl_2$ (0.01M) nanocomposite coated graphite rods

CVs of $PPy/PtCl_2$ nanocomposites (represented in green and blue colors) obtained from different concentrated solutions were clearly proving the accrued oxidation reactions of $CH_3OH$ upon the applied potential during the tests. The largest current range readings (from -5mA to 10mA) were obtained from the CV of $PPy/PtCl_2$ (0.02M) nanocomposite coated graphite rod, represented in green color. A sharp oxidation peak of $CH_3OH$ around -0.1V, and another very broad oxidation peak, located between -0.3V and -0.2V (indicating the oxidation of CO) during discharge could be observed from the voltammogram. The CV of $PPy/PtCl_2$ (0.01M) nanocomposite coated graphite rod had a narrower current range between -0.75mA to 1.75mA supposedly indicating a milder oxidation reaction of $CH_3OH$. A broad oxidation peak of $CH_3OH$ located between -0.1V and 0V and another very weak oxidation peak of CO placed between -0.4V to -0.3V were both proving the success of the electrochemical oxidation of $CH_3OH$ catalyzed by noble Pt elements in such nanocomposite structures.

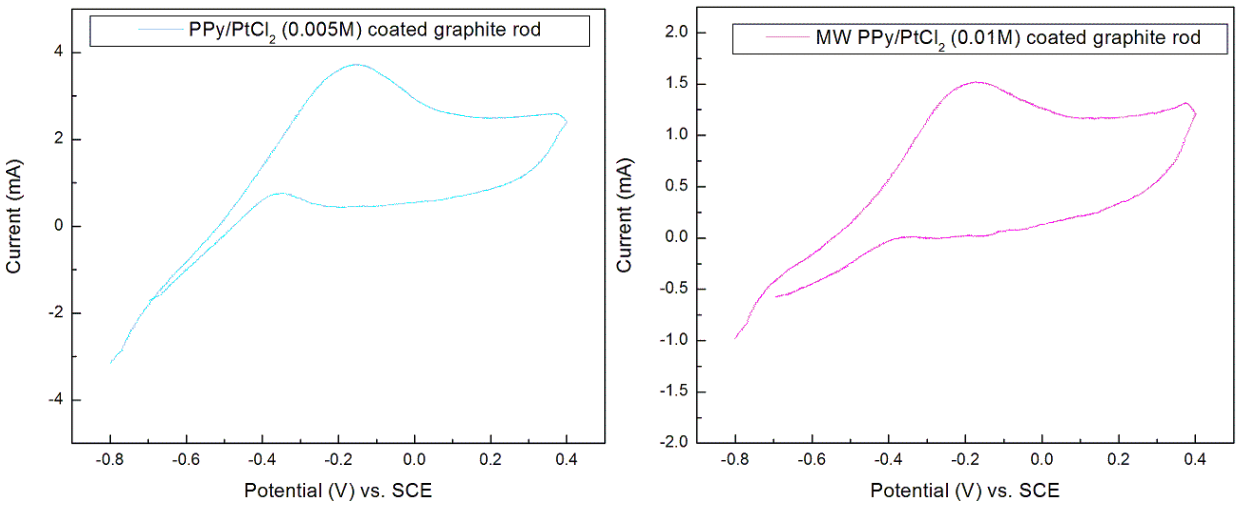


Figure 76 CVs of $PPy/PtCl_2$ (0.005M) and microwaved $PPy/PtCl_2$ (0.01M) nanocomposite coated graphite rods

The last two voltammograms, represented in cyan and magenta colors, were belong to the $PPy/PtCl_2$ (0.005M) and microwaved $PPy/PtCl_2$ (0.001M) nanocomposites coated graphite rods, respectively.

The one belong to the $PPy/PtCl_2$ (0.005M) nanocomposite coated graphite rod was exhibiting the second largest current range (between -3mA to 3.5mA) among all nanocomposite structures. There were again two oxidation peaks clearly be seen at this voltammogram. A wide and sharp $CH_3OH$ oxidation peak located around -0.2V and another weaker one indicating the CO oxidation located around -0.4V were still in good agreement with the already taken place oxidation reaction of $CH_3OH$. Lastly, the CV of microwaved $PPy/PtCl_2$ nanocomposite obtained from 0.01M salt solution was investigated. The results were also indicating a similar current capacity (-1mA to 1.5mA) for this nanocomposite likely to its non-microwaved verison. A very broad $CH_3OH$ oxidation peak located around -0.2V and another very weak and broad one,

located around -0.4V at this sample's CV once again proved the success of the electrochemical application even after the microwave treatment.

In summary, the overall CV applications of non-/microwaved PPy/$PtCl_2$ nanocomposites from different concentrated noble metal salt solutions were consistently able to catalyze the oxidation of methanol through a series of electrochemical reactions.

Here, concentrations of the noble metal salt solutions, which directly determine the metal amount incorporated in the nanocomposite structure, were playing a vital role for the fate of so-called reactions. The direct relationship between the amount of noble metals in the structure and the current capacity of the oxidation reactions could also be observed from the comparative CVs of different samples above. As a result, our novel, one-step, seeding-template-assisted chemical oxidative polymerization of pyrrole, conducted in different concentrated aqueous solutions of various noble metal salts, was able to produce nanocomposite structures that were composed of PPy nanofibers decorated with noble metal nanoparticles which could catalyze the oxidation reaction of $CH_3OH$ witin its traditional fuel-cell solution with KOH via applying sweeping potential.

Increased surface area of so-called, non-/microwaved, nanocomposites helped both to improve the electrochemical properties and also the distributions of noble metal nanoparticles in a fuel-cell membrane. It was believed that this kind of nanocomposite structures would play an important role in the development of highly efficient, next-generation fuel-cell devices[12, 15].

# CHAPTER 4

# CONCLUSIONS AND THE FUTURE WORK

## 4.1 Conclusions

To control, investigate, improve and characterize the several properties of conducting polymer based different nanocomposites and to find out the effects of the noble metal salt solution concentrations besides the other reaction and application parameters (the use of $V_2O_5$ sol-gel nanofibers, microwave treatment…etc.) on the final nanocomposite morphologies and properties, this project was undertaken in details throughout this Master's thesis.

In this study; (i) a novel, one-step, seeding-template-assisted chemical oxidative polymerization of pyrrole monomers in different concentrated four types of aqueous Au and Pt salt solutions to produce PPy nanofiber (with 25-70nm diameters) based nanocomposites decorated with well dispersed noble metal nanoparticles, (ii) another facile, one-step and rapid microwave treatment approach with different as-prepared nanocomposites to convert their structures into CNCs by retaining their morphologies, (iii) effectively use of noble metal salts as the dopant and the oxidative agent for pyrrole monomers in stead of large, toxic oxidants (like APS) to initiate their polymerization reaction, and (v) according to a previously mentioned approach[11], i.e., the use of degradable, oxidative-reactive $V_2O_5$ sol-gel nanofibers as the seeding templates to initiate and maintain bulk nanofibrillar morphology during the polymerization reaction of pyrrole, were "for the first time" described in details.

Also, with the intrinsic catalysis property provided by noble metal particles in their structure of so-called non-/microwaved nanocomposites were proven to be promising infrastructure materials for the design and development of new-generation fuel-cell membranes in the future.

**4.2 Future Work**

All those unique knowledge, gained from the overall experimental and applied studies, would be canalized to perform similar research activities by utilizing other intrinsic conducting polymers like PANI and/or PEDOT with different noble metal salts like silver nitrate ($AgNO_3$) and copper chloride ($CuCl_2$) to produce well-defined nanocomposites with superior properties, which will also be promising candidates for the different industrial applications, in the future.

**References**


1. Pratt, C. Essay on conducting polymers **1996**, 1-7
2. Ramakrishnan, S. *Resonance* **1997**, 48-58
3. Conducting polymers, 1-17
4. Zhang, X.; Manohar, S. K. *J. Am. Chem. Soc.* **2005**, 127, 14156-14157
5. Zhang, X. PFEN 7970 Conductive polymer materials - Lecture 1 **2010**, Auburn University, Auburn, Alabama
6. Lai, E. K. W. Conducting polymer composite films for the electrocatalytic reduction of oxygen, Thesis, **1994**, Simon Fraser University, British Columbia, Canada
7. Zhang, X. PFEN 7970 Conductive polymer materials - Lecture 2 **2010**, Auburn University, Auburn, Alabama
8. Wallace, G. G.; Spinks, G. M.; Kane-Maguire, L. A. P.; Teasdale, P. R *Handbook of Conductive Polymers*, 3rd edition, CRC Press Taylor & Francis Group, Florida, **2009**
9. Skotheim, T.A.; Reynolds, J. R. *Conjugated polymers processing and applications*, 3rd edition, CRC Press Taylor & Francis Group, Florida, **2007**
10. Pringle, J. M.; Winther-Jensen, O.; Lynam, C.; Wallace, G. G.; Forsyth, M.; MacFarlane, D. R. *Adv. Funct. Mater.* **2008**, 18, 2031-2040
11. Zhang, X.; Manohar, S. K. *J. Am. Chem. Soc.* **2004**, 126, 12714-12715

12. Xu, P.; Han, X.; Zhang, B.; Mack, N. H.; Jeon, S. H.; Wang, H. L. *Polymer* **2009**, 50, 2624-2629

13. Huang, H.; Feng, X.; Zhu, J. J. *Nanotechnology*, **2008**, 19, 145607-145613

14. Smith, J. A.; Josowicz, M.; Janata, J. *Journal of The Electrochemical Society*, **2003**, 150, (8), 384-388

15. Zhang, X.; Goux, W. J.; Manohar, S. K. *J. Am. Chem. Soc.* **2004**, 126, 4502-4503

16. Zhang, X. Synthesis and characterization of high surface area polyaniline nanofibers, Master's thesis, **2003**, The University of Texas at Dallas, Dallas, Texas

17. Zhang, X. Synthesis of nanostructured polymers, Dissertation, **2005**, The University of Texas at Dallas, Dallas, Texas

18. Zhang, X.; Manohar, S. K. *Chem. Commun.* **2006**, 2477-2479

19. Liu, Z.; Zhang, X.; Poyraz, S.; Surwade, S. P.; Manohar, S. K. *J. Am. Chem. Soc.* **2010**, 132, (38), 13158-13159

20. Xu, J.; Hu, J.; Quan, B.; Wei, Z. *Macromol. Rapid Commun.*, **2009**, 30, 936-940

21. Lu, X.; Chao, D.; Chen, J.; Zhang, W.; Wei, Y. *Materials Letters*, **2006**, 60, 2851-2854

22. Pillalamarri, S. K.; Blum, F. D.; Bertino, M. F. *Polymer Preprints*, **2005**, 46, (1), 483-484

23. Martínez, M. W.; Thompson, T. T.; Smit, M. A. *Int. J. Electrochem. Sci.,* **2010**, (5), 931 - 943

24. Jiwei, L.; Jingxia, Q.; Miao, Y.; Chen, J. *J. Mater. Sci.*, 2008, 43, 6285–6288

25. Price, Jr., D. W.; Dirk, S. M.; Maya, F.; Tour, J. M. Improved and new syntheses of potential molecular electronics devices, Review, Rice University, Houston, Texas

26. Moreno, R. B. The Design and Synthesis of Complexes for the Activation of Carbon Dioxide, Dissertation **2010**, University College London, London, UK

27. Andrews, L.; Wang, X. *J. Phys. Chem. A*, **2001**, 105, 6420-6429

28. Fincher, Jr., C. R.; Ozaki, M.; Tanaka, M.; Peebles, D.; Lauchlan, L.; Heeger, A. J. *Physical Review B* **1979**, 20, (4), 1589-1602

29. Goto, H.; Yoneyama, H.; Togashi, F.; Ohta, R.; Tsujimoto, A.; Kita, E.; Ohshima, K. *Journal of Chemical Education* **2008**, 85, (8), 1067-1070

30. http://www.ebeijing.gov.cn/feature_2/Noble_Forum_2008/Nobel_History/Nobel_Prize_Chemistry/t999486.htm,

31. http://oledbuild.com/

32. Dennler, G.; Bereznev, S.; Fichou, D.; Holl, K.; Ilic, D.; Koeppe, R.; Krebs, M.; Labouret, A.; Lungenschmied, C.; Marchenko, A.; Meissner, D.; Mellikov, E.; Meot, J.; Meyer, A.; Meyer, T.; Neugebauer, H.; Opik, A.; Sariciftci, N.S.; Taillemite, S.; Wohrle, T. *Solar Energy* **2007**, (81), 947–957

33. http://newt.phys.unsw.edu.au/~arh/background/Organic%20Electronics/Organics.html

34. http://en.wikipedia.org/wiki/Dehydrohalogenation

35. http://en.wikipedia.org/wiki/Saturated_calomel_electrode